TARGETING NUCLEIC ACIDS FOR PANCREATIC CANCER: DISEASE MODELING AND THERAPY

by

JUSTIN HAN-JE LO

B.S. Biological Engineering,
Massachusetts Institute of Technology, 2008

Submitted to the Harvard-MIT Division of Health Sciences and Technology
in Partial Fulfillment of the Requirements for the Degree of

DOCTOR OF PHILOSOPHY IN HEALTH SCIENCES AND TECHNOLOGY
at the
MASSACHUSETTS INSTITUTE OF TECHNOLOGY

June 2015

Signature of Author:_____
Harvard-MIT Program in Health Sciences and Technology
May 18, 2015

Certified by:_____
Sangeeta N. Bhatia, MD, PhD
John J. and Dorothy Wilson Professor of Health Sciences and Technology &
Electrical Engineering and Computer Science
Thesis Supervisor

Accepted by:_____
Emery N. Brown, MD, PhD
Director, Harvard-MIT Program in Health Sciences and Technology
Professor of Computational Neuroscience & Health Sciences and Technology

Abstract

Pancreatic cancer is responsible for nearly 40,000 deaths in the U.S. annually, with a dismal 5-year survival rate below 7%. The poor therapeutic outcomes reflect a paucity of new approaches targeting the genomic underpinnings of pancreatic ductal adenocarcinomas (PDAC, the vast majority of pancreatic cancers) as well as our inability to overcome the desmoplastic stromal barrier characteristic of PDAC. RNA interference through siRNA holds promise in targeting key mutations driving PDAC, such as oncogenic *KRAS*; however, a nucleic acid delivery vehicle that homes to PDAC and breaches the stroma does not yet exist. Noting that the novel cyclic peptide iRGD mediates tumor targeting and penetration through interactions with $\alpha_v\beta_{3/5}$ integrins and neuropilin-1, we hypothesized that "tandem" peptides combining a cell-penetrating peptide and iRGD can complex with siRNA to form tumor-penetrating nanocomplexes (TPNs) effective in delivering siRNA to PDAC. Such a nanoscale carrier could provide a practical means of bridging our understanding of PDAC as a genetic disease to the clinic. Furthermore, the modular aspect of these self-assembled particles permits them to accommodate alternate cargoes or targeting domains, and we have proposed that tandem peptide complexes could be extended to applications outside of RNA interference, particularly for the delivery of components for CRISPR/Cas9-mediated gene editing. This delivery system could be applied to generate improved animal models of pancreatic cancer.

In this work, we first designed, characterized, and optimized iRGD-based TPNs for RNAi in pancreatic cancer cells *in vitro*, showing robust knockdown of single and multiple targets. In order to stabilize these nanoparticles for systemic administration, we then devised and compared diverse, non-covalent materials for formulating TPNs with polyethylene glycol (PEG). The best material in this capacity, a peptide-PEG conjugate, reduced accumulation of TPNs in off-target organs and improved circulation kinetics, while preserving functional knockdown capacity. Incorporating this approach with the iRGD tandem peptides, we studied the translational potential of PEGylated iRGD TPNs to deliver siRNA to various models of pancreatic cancer and have begun therapeutic testing with siRNA targeting *KRAS*. Finally, we have adapted the tandem peptide platform to mediate delivery of CRISPR/Cas9 components. Particle configurations to deliver guide RNA alone, guide RNA with a DNA template for homology-directed repair, and guide RNA with Cas9 protein have all shown efficacy in gene editing *in vitro*, important steps toward creating sporadic mutations to model PDAC. Thus, we have established a versatile approach to the delivery of nucleic acids for studying and treating pancreatic cancer.

Acknowledgments

I would first and foremost like to thank Sangeeta, who has been an incredible mentor, teacher, and role model throughout my experiences in graduate and medical school. She has encouraged me to follow my passions, not only allowing me to pursue the research projects and directions that interested me the most, but also being supportive of my more ancillary interests such as creating scientific artwork and animations. Through all these years, she's been dedicated to my growth and improvement in all aspects of research – experimental design, presentations, writing, working with collaborators, and more. Beyond that, she's been invested in my growth on the larger scale, helping me to navigate the MD-PhD big picture, meeting with me longitudinally starting when I was an undergraduate, and even gracing my wedding with her presence.

Next, I would like to thank my thesis committee members: Professor Dan Anderson, renowned for his innovations in drug delivery and tissue engineering, has provided so many spot-on insights on how to study and troubleshoot vehicles for siRNA and CRISPR delivery. He has never hestitated to share his lab's resources to help with new techniques and ideas. Professor Bill Hahn, a physician-scientist and pre-eminent expert in cancer genomics, has lent so much of his time and expertise to guiding my thesis projects, in addition to being a longstanding scientific collaborator and an inspiring role model.

Working in the Laboratory for Multiscale Regenerative Technologies has been a rich and ceaselessly exciting experience. I've had the unique opportunity of first working with the group as a collaborator and UROP while an undergraduate student, doing a rotation during my first year of medical school, and finally joining as a PhD candidate in 2010. Through these phases, I have had the honor of working with several "generations" of phenomenal scientists, engineers, and clinicians whose visions, perspectives, experimental expertise, and support have been so influential and enriching:

I cannot thank Ester Kwon enough for all her advice, support, feedback, mentorship over the last three years of my PhD. She has been a veritable beacon providing guidance, good ideas, and reassurance during the darkest hours of my journey through graduate school. I am in plenty of company when I say that her witty sense of humor, creativity, and thoughtful generosity have reinforced and defined the positive, uplifting atmosphere in the lab. I also would like to extend my deepest gratitude to Kevin Lin, who has been a remarkable collaborator, benchmate, and roommate, and moreover, an unwavering friend. I can't imagine how I would have navigated through all the tricky nuances of the PhD experience without his expert guidance. I have also had the privilege of working with, mentoring, and learning from two extremely bright MIT undergraduates, Angela Zhang and Felicia Hsu, who have put in so many hours in lab helping with key experiments. With their extraordinary maturity and obvious scientific talent in the lab, I can only wait with excitement to see what they accomplish next.

I am extremely indebted to Sue Kangiser, who has helped so much at every turn, from computer/software/server help to working on making sure I received funding to gathering people and reserving rooms for meetings. I have learnt so much from Heather Fleming, who has taken the time to give insightful feedback on my papers, presentations, and grants that I have taken to heart for all my current and future scientific endeavors. I also have only the deepest gratitude for the lab managers I've had to pleasure of working with in this lab: Lian-Ee Ch'ng, Lia Ingaharro, and Steve Katz.

I would like to thank the current members of LMRT: Andrew Warren, for all the conversations where I benefited from his profound scientific and cultural knowledge as well as his no-nonsense feedback; Jaideep Dudani, for his unending generosity, insightful discussions, chill attitude, and shared love of actually great music and questionably great food; Vyas Ramanan, who seemingly knows everything and who now shares the brethren honor of being the TA for HST.500; Piyush Jain, who has helped me so much in lab and outside of lab; Tal Danino, whose adventurous and imaginative scientific world I was briefly able to dabble in on a fun project some years ago; and all the wonderful lab members I get to talk and work with every day – Matt Skalak, Simone Schürle, Alex Albanese, Colin Buss, Arnout Schepers, Kelly Stevens, Sandra March-Riera, Arnav Chhabra, Nil Gural, Ani Galstian, Chelsea Fortin, Ben Tsuchudy

Seney, Candice Gurbatri, Justin Voog, Liangliang Hao, and all the awesome undergrads, past (especially my fellow UROPs in the good old days – Renuka, Jayanthi, Mary, Daniel, Luvena, and everyone) and present.

And as one of the most senior members of the lab now, I have even more alums who I would be remiss not to thank with my sincerest gratitude. Yin Ren was the mastermind behind tumor-penetrating siRNA delivery, and his mentorship as I embarked on the continuation of his legacy was instrumental in my early years in the lab. Nate Reticker-Flynn is a reliable friend, impressive engineer, even more impressive biologist, talented musician and rapper, and all-around amazing guy who, when he graduated, left behind a meticulously organized trove of cell lines and antibodies, and a legacy of top-notch science that we should all aspire to. I haven't forgotten that we're still due to perform his song one day, if we can ever get a band together. Kartik Trehan, who lives on long after his graduation through the wonders of LMRT lore (it would be far too boring if the only traditions were passing down lab notebooks and cell stocks), was a great benchmate and labmate with whom I have shared many a post-midnight meal and continue to have entertaining discussions on all matters serious or trivial … mostly trivial. Alex Bagley has been a compatriot for the long haul: a classmate at MIT as an undergrad and through the Harvard MD-PhD program, and I couldn't ask for a kinder, more inspiring companion through it all. Cheri Li continues to be the pinnacle of the creative mind empowered by science, and when I'm stumped by a challenge requiring a quirky solution, I just tell myself to think about what she would've done. I will also not let her thesis be the only one in MIT history to include the word "purr," so there you go. This section will go on forever, so I must unfortunately be brief: I'd like to thank Dave Wood, who was a great collaborator when I was an undergraduate in the Engelward lab and who connected me with Geoff for my first Bhatia lab project; Geoff von Maltzahn – the man, the legend – who taught me so much about the wonders of nanomedicine during my brief UROP months; Sabine Hauert, who conjured up the NanoDoc project that I am so happy to have been a part of, because through it I was able to realize my dream of working on a scientifically-informed game to teach people about cancer and cancer therapy; Salil Desai, an engineering whiz whose world travels ought to become a national bestseller; Rob Schwartz, a genius with such breadth of knowledge that he must have a thirty-minute talk stored in each neuron; and Shengyong Ng, Gabe Kwong, Meghan Shan, Kathleen Christine, Mythili Prabhu, Alice Chen, David Braga Malta, Amit Agrawal, Gaya Murugappan, Neetu Singh, and Greg Underhill.

I have also been blessed with wonderful collaborators from many local labs. I would particularly like to thank my amazing collaborators in the lab of Tyler Jacks: Mandar Muzumdar, an expert in pancreatic cancer who has lent me so much expertise, knowledge, and experimental support; David Canner, without whom there would be no Chapter 5 of this thesis; and Wen Xue and Leilani Chirino, who taught me so much about treating preclinical models of cancer. I would also like to thank the Hahn lab, particularly Andrew Aguirre and Belinda Wang, whose knowledge and skills in cancer genetics have been invaluable to the RNAi efforts in our lab, for obvious reasons. Lastly, Omar Khan from the Anderson lab has generously shared new and exciting techniques for RNAi analysis.

I would not have even considered graduate school if not for two astounding mentors who have guided me along the way: Professor Darrel Stafford, who stimulated my interest in biomedical research when I was a high school student and who gifted me my first animation software; and Professor Bevin Engelward, who let me join her lab as an undergraduate researcher with only my scant animation experience as a qualification, and thus set me on firm footing towards becoming a biological engineer.

I am also indebted to the many programs and schools I have been affiliated with. On HST's MIT side, I am grateful for the guidance I've received from my advisor, Richard Cohen, as well as all the help from the HST office: Laurie Ward, Traci Anderson, Joseph Stein, and Julie Greenberg. On HST's HMS side, I've had the great pleasure of being advised by Lee Gehrke, and I cannot thank Patty Cunningham enough for her dedication to keeping all the HST students up-to-speed, somehow always having the answers when everyone else hasn't got a clue, and warmly welcoming me back on the HMS campus whenever I start questioning whether I still belong there. The MD-PhD program has been a vital common thread throughout this long journey through medicine and medical research. I thank the current MD-PhD director, Loren Walensky, as well as Stephen Blacklow, who led the program for many years before that, for all their valuable advice. I also would like to thank my MD-PhD advisor, David Frank, with whom I've had great discussions about research as well as navigating the MD-PhD track. And finally, the MD-PhD office has always been there, seemingly always able to surmount the largest of unexpected hurdles, from keeping the

same health insurance as I changed schools, to understanding how taxes are supposed to work for MSTP grants, to figuring out how to transition back to medical school after the PhD; for all that and more, I would particularly like to thank Yi Shen, Amy Cohen, Robin Lichtenstein, and Jennifer DeAngelo.

Of course, no work would have gotten done if not for all the wonderful friends who have supported and cheered for me. I extended warm thanks to all my MD-PhD classmates, and I would especially like to thank Billy Hwang, Katie Lee Hwang, Laura Jacox, Rishi Puram, Jennifer Yeh and Shuyu Wang for all their support and friendship. I've also been part of a great HST MEMP class, and I wanted to especially mention Jean-Philippe ("JP") Coutu, Luvena Ong, and Stephanie Yaung, who have been unwavering friends through our journey through HST together, and whose unfailing support of my musical performances always brings the widest smile to my face.

In my free time – which I've probably savored a bit too fervently – I've been fortunate to have the opportunities to enrich my artistic experiences. It's been a joy being able to remain an active amateur musician and an even greater joy to have encountered fellow musicians who have gone on to become such great friends. I would first like to thank my friends comprising the Goldfish Quartet – Jon Epstein (viola), Mikiko Fujiwara (cello), and Aaron Kuan (first violin). I never tire of Jon's creativity and self-deprecating humor and appreciate the millions of rides he's given me. Mikiko is a ridiculous riot to be with who puts up with my absurd (but true!) tales, and if I could capture a tenth of her flair for writing in this thesis, I would be satisfied. And I have no idea how Aaron has simultaneously pursued a productive Applied Physics graduate career while conducting and directing the Dudley House Orchestra full-time, but he is needless to say a remarkable inspiration. From the HMS Chamber Music Society, I would especially like to thank Sherman Jia, Andrew Noll, and Alvin Chen, who have set formidable examples as stupendous musicians, budding clinicians, and great leaders, as well as Grace Yuen and Hattie Chung, fellow biomedical graduate students, MIT alums, and wonderful chamber musicians to perform with. From the Longwood Symphony and Mercury Orchestra, two groups I have been playing with for many years now and that feel like second homes, I wanted to recognize Psyche Loui, Richard West, Jenny Smythe, and Lisa Wong for the fun experiences pushing the frontiers in the intersection of music, medicine, and science. From the Dudley House Orchestra, I wanted to thank Jennifer Hsiao, who has been a wonderful and dependable friend since elementary school and fellow chamber musician on piano and violin in countless groups (not to mention the organist at my wedding), as well as Eric Tai and Julia Liu.

I have also been so lucky to have kept in touch with my undergraduate classmates, and I wanted to particularly mention Kenny Yan, who has proven that it is possible to keep participating in the MIT Mystery Hunt throughout one's MD-PhD career, in addition to the many others who have already been mentioned elsewhere in this list. And my friends from high school, with whom it seems like times never change (even though they're all so incredibly accomplished now) – Teddy, Yeufann, Charles, Stanley, and John.

Last but of course not least, I would like to thank my family: all my relatives in the states and overseas, my parents-in-law and brother-in-law, Alan, and of course my immediate family. I could not ask for better, more loving parents. My mother has tirelessly given me support, wisdom, and care packages – and has so selflessly ensured that I have a warm and happy life. I can assure her that she has 100% made that happy life happen. My father's practical advice and magical ability to get things to work out have saved me time and time again. And both being scientists themselves, my parents have instilled in me an endless curiosity about the workings of the world around me. My brother, Michael, is still the same fun-loving, hilarious, athletic, video game-dominating, food-appreciating guy I grew up with, but he's also become such a brilliant person who I look up to and know I can turn to for help when I need it most. Finally, I thank my wife, Sharon, with all my heart. Having earned her PhD before me, she has been a great motivation and guide, without whom I'd be lost. And I can't begin to count all the selfless ways she's cared for me throughout graduate school, like giving me rides back from lab when it gets very late, sitting beside me to keep me company as I analyze data, and tolerating my bizarre sleep schedules as I write this thesis. Most of all, the reassuring warmth of her unconditional support and love have brightened each and every day.

Table of Contents

Abstract iii

Acknowledgments v

List of Figures and Tables xi

Chapter 1: Motivation and background **1**

1.1 Overview 1

1.2 Pancreatic cancer: clinical profile, genetics, & the potential of nucleic acid therapies. 2

1.2.1 Epidemiology and clinical features 2

1.2.2 Shortcomings of pancreatic cancer treatment 4

1.2.3 Targeting the genetic basis of pancreatic cancer 6

1.2.4 Murine models of pancreatic cancer 9

1.3 Nucleic acid therapies 12

1.3.1 RNA interference (RNAi) and the utility of RNAi in cancer therapy 12

1.3.2 RNA-guided endonuclease gene editing 15

1.4 Nanotechnology & nucleic acid delivery: challenges and progress 18

1.4.1 Rationale for the use of nanoparticles in therapy 18

1.4.2 Tumor targeting and penetration 20

1.4.3 RNAi nanoparticle carriers 22

1.4.4 Tumor-penetrating nanocomplexes 25

1.4.5 CRISPR/Cas9 delivery 28

1.5 Summary of thesis aims 30

Chapter 2: Development of iRGD-targeted tumor-penetrating nanocomplexes 32

2.1 Introduction 32

2.2 Results 34

2.3 Discussion 40

2.4 Methods 42

Chapter 3: Modular strategies for stabilizing self-assembled nanoparticles 46

3.1 Introduction 46

3.2 Results 49
3.3 Discussion 57
3.4 Methods 61

Chapter 4: PEGylated iRGD TPNs for siRNA delivery to pancreatic cancer 65
4.1 Introduction 65
4.2 Results 66
4.3 Discussion 74
4.4 Methods 77

Chapter 5: CRISPR/Cas9 delivery using tandem peptides 81
5.1 Introduction 81
5.2 Results 84
5.3 Discussion 94
5.4 Methods 97

Chapter 6: Discussion and Perspectives 100
6.1 Summary and future work 100
6.2 The modularity of tandem peptide systems 101
6.3 The future of tandem peptides as self-assembled nanosystems 104
6.4 Nanoparticle systems 108
6.5 Conclusion 109

Chapter 7: References 111
Chapter 8: Appendix 128
8.1 Preliminary Results 128
8.2 Author Contributions 130
8.3 Curriculum Vitae 131

List of Figures

Figure 1-1: Pancreatic Cancer Statistics 3
Figure 1-2: Mechanism of iRGD 20
Figure 1-3: Barriers to Nucleic Acid Delivery 23
Figure 1-4: CPP Selection 26
Figure 1-5: Outline of Aims 30

Figure 2-1: Schematic of iRGD tandem peptides and TPNs 34
Figure 2-2: iRGD receptor expression on PDAC cell lines and delivery of siRNA into receptor-positive cells 35
Figure 2-3: Optimization of iRGD TPNs *in vitro* 37
Figure 2-4: Knockdown of Kras using iRGD TPNs 39
Figure 2-5: Dual gene knockdown using TPNs 40

Figure 3-1: Schematic of approach to formulate PEGylated TPNs 50
Figure 3-2: Physical properties of PEGylated TPNs 51
Figure 3-3: Cryo-TEM micrographs of PEGylated TPNs 52
Figure 3-4: Serum stability of PEGylated TPNs 53
Figure 3-5: *In vitro* functionality of PEGylated TPNs 54
Figure 3-6: *In vivo* properties of PEGylated TPNs 56

Figure 4-1: Physical properties of PEGylated iRGD TPNs 67
Figure 4-2: Capacity of PEGylated iRGD tandem peptides and TPNs to mediate endosomal escape 68
Figure 4-3: Impact of PEGylation on iRGD TPN-mediated knockdown 69
Figure 4-4: Comparison between iRGD tandem peptides bearing different N-terminal lipid tails 70
Figure 4-5: Pharmacokinetic properties of PEGylated iRGD TPNs 71
Figure 4-6: iRGD TPN-mediated delivery of siRNA in models of pancreatic cancer 72

Figure 5-1: Overview of CRISPR/Cas9 tandem peptide particles 85
Figure 5-2: Encapsulation and delivery of sgRNA by tandem peptides..... 88
Figure 5-3: Delivery of sgRNA and DNA templates 91
Figure 5-4: Delivery of sgRNA-Cas9 complexes 93

Figure 6-1: Therapeutic gene knockdown by iRGD TPNs *in vitro* 101

Figure 8-1: mRNA delivery with tandem peptides 128
Figure 8-2: pTP-SWCEPGWCR delivery to the pancreas 128
Figure 8-3: microRNA delivery *in vivo* 129

List of Tables

Table 1-1: Pancreatic Cancer Statistics 7
Table 3-1: Summary of results comparing three modular strategies for siRNA nanoparticle stabilization in non-targeted and targeted forms 57

Chapter 1: Motivation and Background [^]

1.1 Overview [^]

Pancreatic cancer is a devastating disease that kills over 40,000 people in the U.S. annually, with less than 7% of patients surviving five years past their initial diagnosis [1]. Traditional chemotherapy is rarely effective at managing the disease and results in considerable toxicity. Two important factors contributing to the failure of current treatment regimens are the dense stromal layers surrounding pancreatic cancers, which block the entry of therapeutics [2], and the lack of therapeutic agents targeted specifically at important genetic drivers of pancreatic cancer progression. As such, there is a need for new approaches that incorporate mechanisms for overcoming delivery barriers and that deliver therapeutics with the capacity to potently address commonly mutated genes, such as the *KRAS* oncogene activated in over 95% of pancreatic ductal adenocarcinomas (PDACs) [3], which in turn comprise over 85% of pancreatic cancers [4]. Thus, the overall goal of this thesis is to develop and formulate peptide-based tumor-penetrating nanocomplexes for the systemic delivery of nucleic acid therapies targeted to PDAC-specific genetic abnormalities. We additionally show that the modularity of this delivery platform allows it to be further adapted to mediate genomic editing, an important tool in generating new animal models of pancreatic cancer that can contribute a better understanding of the disease process and treatment.

1.2 Pancreatic Cancer: Clinical Profile, Genetics, and the Potential of Nucleic Acid Therapies [^]

1.2.1 Epidemiology and Clinical Features

Pancreatic cancer is one of the deadliest types of cancer, with overall five-year survival of only 6.7% in the United States for cases first diagnosed in 2006 [5] (**Fig. 1-1A**). Indeed, while considerable inroads have been made in reducing mortality associated with many of the most common forms of cancer – lung, colorectal, prostate, and breast among them – no such improvement has been seen for pancreatic cancer over the last three decades (**Fig. 1-1B**). The poor prognosis and persistent mortality rate of pancreatic cancer reflect several clinically challenging aspects of the disease: the frequently asymptomatic progression of the disease until the disease is too advanced to treat surgically, the lack of a pre-emptive diagnostic screen, high rates (~80%) of recurrence following surgical resection, and a very poor response to standard chemotherapy regimens [3, 6]. This explains why a cancer originating from the pancreas – an organ that a patient could live entirely without, given appropriate enzymatic and hormonal supplementation – can become such a severe and incurable disease.

Efforts to mitigate risk factors have been a crucial centerpiece in bringing down mortality in many forms of cancer, but in the case of pancreatic cancer, few preventable risk factors have been identified – conclusive evidence of causation exists only for tobacco use, with a risk ratio of 2.5-3.6 (notably much less impactful than in lung cancer) [3]. Furthermore, efforts to screen for pancreatic cancer have stalled, as no screening markers possess the needed sensitivity and specificity to reliably detect disease before it reaches advanced stages. For instance, CA19-9, a useful marker for tracking therapeutic response in advanced pancreatic

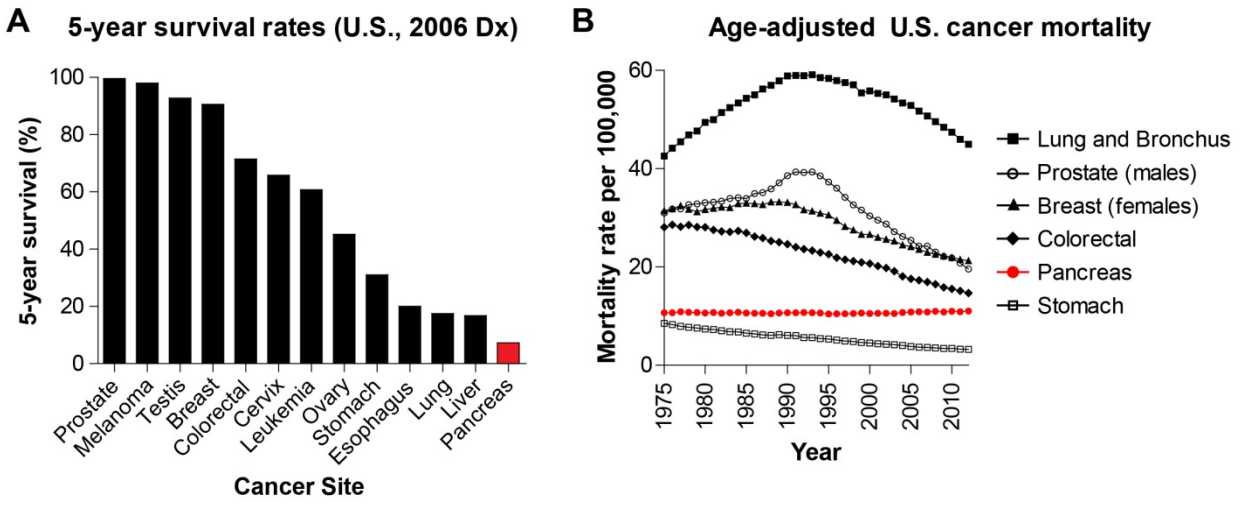

Figure 1-1: Pancreatic cancer statistics. (A) Comparison of U.S. five-year survival rates for primary cancers of different sites for cancers diagnosed in 2006, with the survival rate of pancreatic cancer highlhighted. (B) Age-adjusted U.S. cancer mortality for selected cancer sites from 1975-2012. Mortality rates for prostate cancer and breast cancer pertain to male and female populations only, respectively. Data from the NCI Surveillance, Epidemiology, and End Results (SEER) Program [1].

cancer, is only elevated in 40% of early-stage pancreatic cancer and may also be elevated in a number of unrelated, benign hepatobiliary conditions. As such, its use in screening is discouraged by the ASCO [7, 8].

The lack of preventable risk factors and diagnostic screening tools leaves diagnosis up to symptomatology. Unfortunately, symptoms that patients might present with, such as weight loss, fatigue, cholestasis, abdominal (epigastric) pain, jaundice and pruritis, steatorrhea, clay-colored stools, or new-onset diabetes mellitus are either non-specific or likely to arise only when the cancer is quite advanced, as many of these phenomena require the tumor to be large enough to obstruct the common, bile, or pancreatic ducts, to have metastasized to the liver, or to substantially interfere with islet function in both physical and hormonal manners [9]. At advanced stages of disease, surgical resection of the primary tumor or the entire pancreas is no longer therapeutically beneficial, and most patients will eventually die from complications of

metastasis such as liver failure. Even when surgery is an option, patients rarely live 5 years past the procedure, with only ~12% 5-year survival following pancreatic head resection (the exact rate varies considerably by site and study) [10]. Thus, there is a present and persisting need for new strategies for treating advanced pancreatic cancer.

1.2.2 Shortcomings of Pancreatic Cancer Treatment

Current standard-of-care first-line chemotherapy for locally advanced, unresectable pancreatic cancer is a regimen of the nucleoside analogue gemcitabine, with a median survival of only 5.5 to 6 months [11]. In the setting of metastatic pancreatic cancer, several recent clinical trials have identified alternative regimens that show improvement in survival over gemcitabine alone. Combination therapy of gemcitabine with nab-paclitaxel (albumin-bound paclitaxel) has recently shown a significant survival benefit of 1.8 months over gemcitabine monotherapy, though accompanied by increased rates of peripheral neuropathy and myelosuppression [12]. FOLFIRINOX, a combination of 5-fluorouracil, leucovorin, irinotecan, and oxaliplatin, is a more aggressive treatment option that has impressively extended survival to 11.1 months versus gemcitabine monotherapy at 6.8 months, and thus is the preferred first-line therapy for metastatic disease [13]. While the benefit of combination therapies has not yet been proven in clinical trials on unresectable but non-metastatic disease, many treatment centers now employ them as first-line therapy, particularly in patients with good performance status (i.e. ECOG scale 0-1 [14]) and serum total bilirubin <1.5 over the upper limit of normal (an indicator of liver function), who are able to tolerate the increased toxicity [15]. However, the severity of the toxic side-effects as well as a median survival of less than a year in the best treatment scenario clearly

provides impetus for seeking out new "cancer-targeted" therapeutic options rather than piling on additional indiscriminate chemotherapeutics.

In a first step towards this goal, many clinical trials have striven to treat pancreatic cancer with new targeted molecular therapies that have found success in other types of cancer, including anti-VEGF (bevacizumab [16], aflibercept [17]), anti-VEGFR/PDGFR/cKit (axitinib) [18], and anti-EGFR (cetuximab [19], erlotinib [20]). Unfortunately, these therapies have all failed to significantly extend survival with the exception of erlotinib, which prolonged survival by the statistically significant but clinically underwhelming margin of 0.3 months [11, 21].

These dismal results emphasize the need to tailor therapeutic strategies to the complexities of pancreatic cancer, which presents both a unique delivery challenge as well as a unique genetic landscape. Ninety-five percent of pancreatic cancers involve the exocrine pancreas, most often giving rise to pancreatic ductal adenocarcinomas (PDACs), which generate a characteristic thick and poorly vascularized desmoplastic stroma that prevents penetration of even small molecules [22]. Strategies for dismantling or reorganizing the stroma, such as hedgehog inhibition (IPI-926, also called saridegib, a SMO inhibitor) [22] or PEGylated hyaluronidase (PEGPH20) [2, 23] have demonstrated improved delivery to PDAC animal models, though resistance and restoration of the stromal barrier eventually occurs. Saridegib has unfortunately not shown any therapeutic benefit in Phase II clinical trials for pancreatic cancer [24], but this is perhaps less surprising in the context of recent evidence that while stromal cells may abet tumor cells in some capacities, long-term hedgehog inhibition and stromal depletion can actually *accelerate* pancreatic cancer growth [25] – likely on account of increased vascularity – and furthermore, cancer-associated fibroblast depletion can lead to

immunosuppression [26]. These findings suggest that perhaps a better approach would be to transiently penetrate the stromal barrier – as will be discussed in Section 1.4.2 – rather than frankly abolish it. Beyond tackling the stromal barrier, the ideal approach to therapy must also consider the key signaling pathways and mutations that drive PDAC (discussed in the following Section 1.2.3), rather than simply importing targets that have worked in other cancers. *Therefore, the approach to therapy in this thesis combines both a tumor-penetrating peptide carrier and RNAi therapies against key PDAC pathways.*

1.2.3 Targeting the Genetic Basis of Pancreatic Cancer

Progress in unraveling the complex genetic basis of cancer has been proceeding at a rapid pace. At the core of PDAC as a genetic disease are two key mutations: *KRAS* oncogenic activation and loss-of-function mutations in the cell-cycle checkpoint gene *CDKN2A* (encoding both *P16-INK4A* and *P14ARF*), both found to occur in over 90% of cases [3]. The ubiquity of *KRAS* mutations is a unique feature to PDAC, though these mutations are also relevant to lung cancer and colorectal cancer in particular. Interestingly, virtually all (99%) *KRAS* mutations in PDAC involve Glycine-12, which leads to constitutive Ras signaling through conformational changes. The preferential downstream signaling pathways depend somewhat on the resulting amino acid in the 12^{th} position; for instance, G12D mutations (by far the most common amino acid-level substitution at 50% of all *KRAS* mutations in PDAC [27]) activate PI3 kinase and Mek signaling, while G12C mutations preferentially activate Ral signaling [28]. These preferences are of relevance to the design of inhibitors to K-Ras signaling, as discussed later in this section.

A large proportion of pancreatic adenocarcinomas also harbor mutations in the tumor suppressors *TP53* and *SMAD4/DPC4* [29, 30]. The causative role of the four most common mutations – *KRAS*, *CDKN2A*, *TP53*, and *SMAD4* – in driving pancreatic cancer has been exhaustively borne out in genetically-engineered mouse models, in which combinations of these mutations in the pancreas lead to highly aggressive PDAC [31, 32]. A brief summary of common genetic abnormalities in PDAC, as well as less common mutations in PDAC of relevance to current targeted therapies, is presented in **Table 1**. Importantly, there are countless supporting mutations that occur at lower frequencies, whose role and importance in tumor formation and growth have yet to be delineated in pancreatic cancer due to the difficulty of generating new animal models. Many of these mutations are important players in the complex

Gene	Protein	Type	Frequency	Mutation Types / Locations
KRAS	K-Ras	Oncogene	95%	99% involve Glycine-12 (G12D, 50%; G12V; G12R, 12%; G12S; G12C; G12A), G13 mutations rare in PDAC
CDKN2A	p16-Ink4A, p19Arf	Tumor Suppressor	98%	Homozygous deletion, intragenic missense mutations, epigenetic promoter silencing
TP53	p53	Tumor Suppressor	70%	Missense mutations, dominant negative mutations; rarely homozygous deletion
SMAD4 (DPC4)	Smad4	Tumor Suppressor	45%	Missense mutations
NCOA3	AIB1, NCOA3	Oncogene	37-44%	Copy-number gains
RB1	pRb	Tumor Suppressor	<6%	
ERBB2	HER2/neu	Oncogene	<27%	
EGFR (ERBB1)	EGFR	Oncogene	0-4%	

Table 1-1: Selected mutations in exocrine pancreatic cancer. Adapted with significant alterations from [27]

dialogue between pancreatic tumor cells and the surrounding stromal elements, impacting therapies in often uncharacterized ways [33]. New methods for creating custom animal models containing these mutations, perhaps on a background of the "big four" mutations, would be of benefit in providing a more complete understanding of the genetic underpinnings of the disease; this topic is discussed at greater length in Sections 1.2.4, 1.3.2, and Chapter 5.

While translation of genetic targets into new therapies has begun over the last two decades, current targeted therapies have been limited to druggable proteins such as HER2/neu (by trastuzumab) and EGFR (by gefitinib and erlotinib), with the therapeutic being either an antibody or small molecule tailor-made for the target [34]. Mutations in these genes occur relatively infrequently in PDAC, which is in essence a *KRAS*-driven disease. Unfortunately, it has proven difficult to inhibit K-Ras function or post-translational modification with small molecules, despite over 30 years of research directed at this challenge. Inhibiting critical post-translational modification of Ras proteins using farnesyltransferase inhibitors (FTIs) showed encouraging preclinical efficacy, yet failed in clinical trials due to molecular evasion involving redundant pathways (e.g. geranylgeranyltransferases) – and attempts to concomitantly block these pathways led to unacceptable toxicity [35]. More recently, the pan-Ras inhibitor farnesylthiosalicylic acid (salirasib), acting as a competitor for Ras-escort proteins, made it to phase II clinical trials but failed to meet target survival criteria in lung cancer patients with tumors known to harbor KRAS mutations [36]. Researchers have thus shifted focus to other members of the Ras signaling pathways, with MEK and PI3K inhibitors enjoying the most success [37]. However, the preclinical and clinical experience with MEK [38] and PI3K inhibitors [39] has suggested that they are more likely to be useful as combination therapies than acting

alone. *Thus, there remains a need for potent therapeutic strategies to strike at driving mutations, such as RNAi, which prevents cancer-driving proteins from being made in the first place rather than trying to block function after they have already been translated and assembled. Strategies like RNAi could potentially complement existing small molecule inhibitors and chemotherapies in the clinic, especially as we consider ways to address redundant, compensatory, and synthetic lethal pathways in the context of pancreatic cancer.*

1.2.4 Murine models of human cancer

Validation of new cancer therapies requires accurate animal models of human disease, especially as sophisticated therapies are being optimized for delivery via specific targeting, penetrating, and deployment pathways and their cargoes take action via specific molecular pathways.

Transplant models, in which tumor cells are introduced into a host animal, are simple to establish and allow the use of human cells (xenografts) in immunosuppressed animals or mouse cells (allografts) in immunosuppressed or syngeneic immunocompetent animals. Heterotopic grafts, where tumor cells are injected in a convenient location unrelated to the primary organ of origin, simplify tracking of tumor growth but necessarily overlook the complex host organ-tumor interactions, the gradual mutation of tumor cells leading to polyclonality, and the role of the immune system if immunosuppressed animals are employed [40, 41]. Unfortunately, there have been several cases in which therapeutics demonstrating efficacy in xenograft models failed to show any clinical efficacy [40, 42, 43]. Orthotopic grafts into the appropriate primary organ [44, 45] or into representative organs of metastatic disease (e.g. via intrasplenic or intracardiac

injection) better replicate the proper microenvironment and therefore are important first steps in validating delivery vehicles, but still exhibit rapid growth and monoclonality, features that influence tumor responses.

Genetically-engineered mouse models (GEM models) have been shown to closely replicate clinical pathology in humans, including critical components of the vasculature, microenvironment, and immune system. In these models, initiating mutations drive tumorigenesis based on site-specific promoters, as in the KPC (Kras-p53) model of PDAC [31], or site-specific delivery of a recombinase, as in a $Kras^{G12D}$-$Trp53^{-/-}$ model of lung adenocarcinoma [46]. Specifically, the KPC model of pancreatic cancer is based on triple-mutant LSL-$Kras^{G12D/+}$;LSL-$Trp53^{R172H/+}$;Pdx-1-Cre or LSL-$Kras^{G12D/+}$;LSL-$Trp53^{fl/fl}$;Pdx-1-Cre mice, which develop invasive pancreatic tumors as a result of pancreas-specific (Pdx-1 promoter) Cre recombinase activity. Pancreatic Cre-mediated recombination leads to expression of the oncogenic $Kras^{G12D}$ allele and either homozygous loss of p53 or activation of the dominant-negative $Trp53^{R172H}$ allele [31, 47, 48]. The $Kras^{G12D}$ mutant is frequently seen in human pancreatic cancer, and the $Trp53^{R172H}$ allele, homologous to human R175H mutations, is present in both the hereditary Li-Fraumeni cancer syndrome and spontaneous mutations. This mutated variant of p53 not only acts as a dominant negative through aberrant tetramer formation with wildtype p53 but also contributes to pro-metastatic signaling in pancreatic cancer [49]. Tumors from this model have been documented to metastasize widely to sites such as the liver, which represents 58% of PDAC metastases in humans [50]. Models based on *KRAS* and *CDKN2A* mutations [32] or *KRAS* and *SMAD4* mutations [51], among others, have also been described. Extensive insights into the roles of these mutations in PDAC have been gleaned from these

models, yet because they all rely upon pan-pancreatic gene mutations, the resulting simultaneous transformation of nearly the entire pancreas makes these models incredibly difficult to treat with new therapies, whether for the purposes of validating new drugs or new genetic targets. This comes on top of the challenge and time involved in the development of new transgenic models – usually a process requiring years for each genotype – limiting the number and combinations of mutations that may be studied.

CRISPR/Cas9-mediated genetic manipulation for the purposes of cancer model development presents an opportunity to generate a myriad of mutations – in a more sporadic manner and much more quickly. The basis and delivery of CRISPR/Cas9 technology is introduced in Sections 1.3.2 and 1.4.5, respectively.

In the larger picture, these genetic models of pancreatic cancer represent the first half of the "preclinical testing pipeline," in which cancers are created to closely replicate the genetic, morphological, and contextual properties of the disease. The second half, then, is the capacity to treat these models in hopes that such treatments would also translate to human therapy. As mentioned in Section 1.2.3, the challenges in developing effective conventional small molecule drugs for key protein targets in pancreatic cancer necessitates the development of other therapeutic paradigms such as RNAi for addressing specific genetic mutations that cause disease.

1.3 Nucleic Acid Therapies [^]

1.3.1 RNA Interference (RNAi) and the Utility of RNAi in Cancer Therapy

RNA interference is a technique for silencing gene expression via the introduction of double-stranded RNA (dsRNA) complementary to a portion of the gene of interest, a strategy first described in *C. elegans* by Andrew Fire et al. in 1998 [52]. The precise mechanism of RNAi has since been elucidated and relies upon a host of endogenous machinery that orchestrates the suppressed translation or frank cleavage of mRNA complementary to the antisense strand of the dsRNA in a catalytic fashion. In the natural setting, RNAi is effected by microRNAs (miRNAs), which originate as long primary-microRNAs (pri-miRNAs) transcribed from the genome and are subsequently processed by the Drosha ribonuclease and Pasha into pre-microRNAs [53]. These pre-microRNAs are in turn cleaved by the Dicer ribonuclease into 19-23 base pair (bp) dsRNAs that can be loaded into the RNA-induced silencing complex (RISC) [53]. In the RISC, the inactive strand of miRNA is removed, leaving only the active (antisense) strand, which binds to one of many mRNA targets through the seed sequence located approximately from base pairs 2 through 8. This binding encumbers mRNA translation, promotes deadenylation of the mRNA, or leads to cleavage of the mRNA [54-57]. The fate of the mRNA depends on the degree of complementarity – stronger binding is more likely to result in cleavage [58].

Non-endogenous short interfering RNAs (siRNAs) have been designed to harness the miRNA/RISC machinery so as to exert control over gene expression in a potent yet reversible manner. siRNA is structurally identical to mature miRNA except for three subtle yet critical differences: (1) the two strands are perfectly complementary to each other, (2) the antisense

sequence is perfectly complementary to the target mRNA, and (3) the seed sequence is optimally designed to have minimal off-target binding [59]. Thus, miRNA-like effects are minimized and the target mRNA is efficiently cleaved.

The adaptation of RNA interference (RNAi) to mammalian cells in 2001 has opened the possibility of knocking down or modulating expression of virtually any protein in the cell, requiring only knowledge of the target's mRNA sequence to rationally design the therapeutic molecule, in contrast to small molecules or antibodies, which require chemical screens or immunizations, respectively [59]. In this respect, RNAi resembles the phenomenon of suppressed translation by antisense oligonucleotides (ASOs), first described in the contexts of virology [60] and plant biology [61] more than decade before the discovery of RNAi. However, there are several key differences: ASOs are single-stranded while RNAi depends on double-stranded RNA; naked ASOs are taken up at low efficiency into cells, while siRNA/miRNA require extensive modification or carriers for uptake [62]. And probably most importantly, ASOs function by either stoichiometrically binding mRNA partners and impeding translation or through cleavage of target mRNA by RNase H (if phosphorothioate oligonucleotides are used) [63], whereas RNAi uses the RISC machinery. As a consequence of these distinct mechanisms, the superior technology in a specific situation depends on the application and the types of functional modifications made to the base molecules; however, the preexisting machinery for RNAi and more developed delivery mechanisms generally result in greater efficiency. Though it is difficult to directly compare, this is borne out in practice, as the first FDA-approved ASO, Kynamro (mipomersen sodium), is dosed at 200 mg per person [64], while

the siRNA-based ALN-TTR02 (patisiran) mediates efficient knockdown at 0.15 mg/kg (~10 mg for a typical 70 kg patient) [65].

The breadth of genetic manipulation afforded by RNAi technology extends beyond "knocking down" genes, which is important because knockdown alone cannot address the genetic loss of tumor suppressor function. In addition to targeting oncogenic pathways with siRNA or antagomiRs (which oppose complementary miRNA), miRNAs such as miR-34a can be delivered that restore tumor suppressor functions [66, 67]. Because the mRNA degradation mechanism of siRNA binding depends upon essentially perfect complementarity – as opposed to the partial binding exhibited by miRNAs that modulates but rarely completely knocks out gene expression – it is possible to design siRNA sequences that distinguish mutated mRNAs from their wildtype counterparts [68].

Dozens of siRNA targets have been proposed for cancer therapy, including oncogenes such as EGFR, Her-2, K-Ras, n-Myc, c-Myc, as well as regulators of apoptosis, senescence, cell cycle checkpoints, and protein stability [69]. siRNA therapies for cancer have shown promise in clinical translation: Alnylam recently completed Phase I trials for a combination of siRNA against VEGF and KSP delivered to liver cancers via PEGylated liposomes [70]. Additionally, replacement of miRNAs involved in key cancer pathways such as the p53 pathway (miRNA-34 family [71, 72] and Ras signaling (let-7 family [73, 74] have been shown to slow tumor progression and may synergize with siRNA approaches.

High-throughput technologies have enabled the large-scale screening of specific gene targets. In one approach, lentiviral transfection of plasmids encoding an extensive library of shRNAs covering all human genes [75] has been applied to sets of tumor cells lines in order to,

for instance, identify particular susceptibilities common to ovarian cancer [76]. Cell lines virally transduced with a library of shRNAs have been transplanted into animals, constituting a smaller-scale *in vivo* RNAi screen, although this approach represents a best-case scenario free from the intricacies of systemic dosing regimens and, in addition, limits the animal models to allografts or xenografts [77]. The rapid development of CRISPR/Cas9 technology for genomic editing, introduced more fully in Section 1.3.2, has enabled the use of sgRNA screens in a similar fashion to shRNA screens, but with the potential benefits of complete, permanent knockdown of genes as well as reduced off-target effects [78]. Regardless of the method used to identify key mutations that show potential as therapeutic targets, there remains a need for a systematic platform for the validation of targets *in vivo* that accounts for systemic distribution and delivery, allows high-throughput testing, recapitulates the therapeutic scenario (where tumors are established and *then* subsequently treated), and is compatible with more realistic genetically engineered models of cancer. *The systemically-administered nucleic acid delivery platform developed in this thesis could fulfill these important criteria.*

1.3.2 RNA-Guided Endonuclease Gene Editing

In contrast to RNAi, which leads to suppression or modulation of gene function at the mRNA level, genome editing seeks to make permanent changes in genomic DNA, making it a useful strategy for the facile creation of genetic models and an alluring permanent therapy for correcting hereditary genetic conditions. Several sequence-specific gene editing techniques have been devised, including zinc-finger nucleases (ZFNs) [79] and transcription activator-like effector nucleases (TALENs) [80], which encode target DNA sequence specificity through the

correspondence of DNA bases to protein domains, at ratios of one ~20-amino acid peptide domain per three bases or two amino acid residues per two bases for ZFNs and TALENs, respectively. Despite the elegance of these technologies, their reliance upon proteins necessitates the cumbersome process of creating a new protein for every new target, limiting throughput.

The discovery of the bacterial clustered regularly interspaced short palindromic repeat (CRISPR) system revealed a mechanism for targeting nucleases with RNA guides rather than protein guides. This system is employed by many species of bacteria as an adaptive immune system, in which a library of known pathogenic DNA sequences is used to create crRNA that, in combination with a CRISPR-associated (Cas) nuclease, leads to cleavage of instances of cognate DNA outside of the genome [81]. Three types of CRISPR/Cas systems have been described (termed Types I-III). Of these, the Type II system, featuring the Cas9 nuclease, has received the most interest as a genome editing tool because it depends solely on a complex containing Cas9, a constant tracrRNA, and the variable crRNA [82]; the two RNAs can additionally be synthesized as a single guide RNA (sgRNA) [83]. This stands in contrast with the other CRISPR/Cas types that require crRNA processing and formation of large complexes.

The Cas9 nuclease will only cleave DNA when its paired guide RNA binds perfectly or near-perfectly *and* there is a protospacer adjacent motif (PAM) on the non-bound DNA strand immediately 3' to the guide sequence, thus natively enforcing considerable specificity while imposing a relatively minor constraint on eligible guide sequences [82]. The PAM requirement arises from the source bacteria's mechanism of distinguishing self and non-self, the PAM sequence being present on the foreign sequences but not in the host's genomic library. Studies

on specificity have shown that most of the specificity is encoded in the 10-12 base pairs immediately 5′ from the PAM [84], and that specificity can be enhanced by carefully titrating dose or through clever engineering of the Cas9 nuclease itself. For instance, taking a cue from an earlier ZFN innovation, nickase variants of Cas9 have been developed that induce single-strand breaks (SSBs) rather than double-strand breaks (DSBs), such that the full DSB only occurs when a pair of nickases relying upon guideRNA binding on either side of the target site cleave simultaneously. This can reduce spurious cutting by 50-1000 times, though at the expense of efficiency [85, 86]. Alternatively, breaking Cas9 into two complementary protein fragments that only function when united, termed a split-Cas9 architecture, has also been shown to reduce off-target cutting [87, 88]. Finally, catalytically inactive forms of Cas9 have been designed to either mediate transcriptional repression (dCas9) or activation (dCas9-VP64) [89], extending the gene-modulating repertoire beyond permanent gene inactivation.

With the development of resources for the rapid design of sgRNAs against just about any gene, the proof-of-concept correction of many genetic diseases caused by a single mutation has been reported, including beta-thalassemia (*HBB*) [90], Cystic Fibrosis (*CFTR*) [91], and Type 1 Hereditary Tyrosinemia (*FAH*) [92]. Unlike gene therapy, in which an exogenous "corrected" gene is delivered and integrates, there is far less opportunity for potentially harmful random integrations, though risk still exists because of the invocation of DNA DSB repair pathways, potentially mitigated by the use of SSB-based methods instead, *e.g.* nickases.

Cancer stands as one of the most complex yet indisputably genetically-driven diseases. While there is potential for CRISPR/Cas9 in cancer therapy far in the future, *e.g.* targeting oncogenes in a similar fashion as RNAi, such technology would have to overcome hurdles such

as low rates of cutting *in vivo*, the rapid selection for cells that escape editing, the potential for creating unintended and potentially dangerous mutations such as NHEJ-mediated translocations, and the need for exquisitely specific delivery or mutation-specific strategies so that editing in normal cells does not lead to unwanted side-effects.

Thus, at present, a more accessible avenue for CRISPR/Cas9 to benefit efforts to treat cancer is to use such gene editing technology to rapidly develop new models of cancer that comprehensively catalogue and permutate the mutations discovered through sequencing, screening, and biological investigation. As with RNAi, delivery of CRISPR/Cas9 components presents considerable delivery challenges, compounded by the increased number of heterogeneous cargoes that must be delivered. This topic is discussed at greater length in Section 1.4.5, and our efforts in developing *targeted* technology for CRISPR/Cas9 delivery is presented in Chapter 5.

1.4 Nanoparticle Drug Delivery: Challenges and Progress [^]

1.4.1 Rationale for the use of nanoparticles in therapy

Nanoparticles carriers are promising platforms for drug delivery to cancer because of their potential to actively and/or passively seek out sites of disease while avoiding unwanted side-effects elsewhere in the body and shielding cargo from being tampered with prior to delivery. There are three chief considerations in designing nanoparticle carriers, based on the sequence of environments that nanoparticles must pass through in order to reach their destinations.

First, one must devise mechanisms for evading the many "traps" of the body – uptake by the reticuloendothelial system (RES) such as Kupffer cells and splenic phagocytes, dismantling and excretion via renal filtration, and interactions with blood components or the endothelium which lead to deposition or accumulation. For instance, coating nanoparticles with poly(ethylene glycol) (PEG) can reduce macrophage uptake [93, 94]. Particles >6 nm in diameter (>4 nm if anionic and >8 nm if cationic) are typically retained from entering the glomerular ultrafiltrate [95], although recent work has suggested that larger charge-associated assemblies may be dismantled into filterable components in the glomerulus by highly anionic heparan sulfate [96]. Certain guidelines for primary organ targeting have been empirically established, such as the tendency of cationic or large particles (>200 nm) to nestle in the pulmonary capillaries and for lipophilic, neutral particles to home to the brain [97]. Such considerations must be accounted for when designing particles that must arrive at the tumor in spite of systemic exposure; thus, Chapter 3 of this thesis centers on engineering formulations to reduce non-specific loss and off-target side-effects of siRNA particles.

Second, the nanoparticle must be able to target and penetrate into tumors. Small particles (<100 nm) may take advantage of the enhanced permeability/retention effect (EPR) resulting from defects and fenestrations in tumor vasculature and abnormal interstitial fluid pressure [98-101], and additional mechanisms of active targeting to angiogenic endothelium may help "address" payloads to the specific tumor vasculature [102]. As this is frequently the rate-limiting step in accumulation, targeting is discussed in greater detail in Section 1.4.2 [103].

Third, for payloads which do not natively cross cell membranes, such as siRNA and most other nucleic acids, there must be a mechanism of cell penetration, e.g. fusing with the cell

membrane, triggering endocytosis and endosomal escape or forming pores in the cell surface, as described in Section 1.4.3.

1.4.2 Tumor targeting and penetration

While targeting nanoparticles to particular *organs* may be accomplished by controlling physical and chemical parameters such as size, charge, and hydrophobicity as described above, targeting to tumors – particularly tumors that are disseminated into a variety of host organs and which may not have undergone the angiogenic switch – requires additional strategies. Tumor-targeting domains aimed at high-affinity interactions have been described, including antibodies [104, 105] or RNA-based aptamers (e.g. A10, which binds to prostate-specific PSMA [106, 107]. These moieties display impressive specificity, but have the drawbacks of targeting only a subset of any given type of cancer due to receptor heterogeneity, being relatively large in terms of molecular weight, and encountering binding-site barriers, where excess presentation of the target precludes deep penetration of a high-affinity therapeutic [108-110]. Broader strategies considering more universal tumor targets have included using transferrin protein to target upregulated transferrin receptor in many tumor types [111]. However, in addition to its overexpression in cancers, transferrin receptor is also expressed on the surface of many normal cell types such as the hepatocytes and Kupffer cells, [112, 113].

Short peptides representing the relevant motif needed for target binding are preferable over whole proteins, as they allow increased avidity and are less likely to elicit MHC-derived immune responses. Peptide sequences NGR, RGD, and *iso*DGR, uncovered by phage screens, are effective at targeting $\alpha_v\beta_{3/5}$ integrins in angiogenic blood vessels, and are easier to synthesize

and functionalize than fibronectin, the parental 450 kDa protein that natively contains related peptide motifs [102, 114].

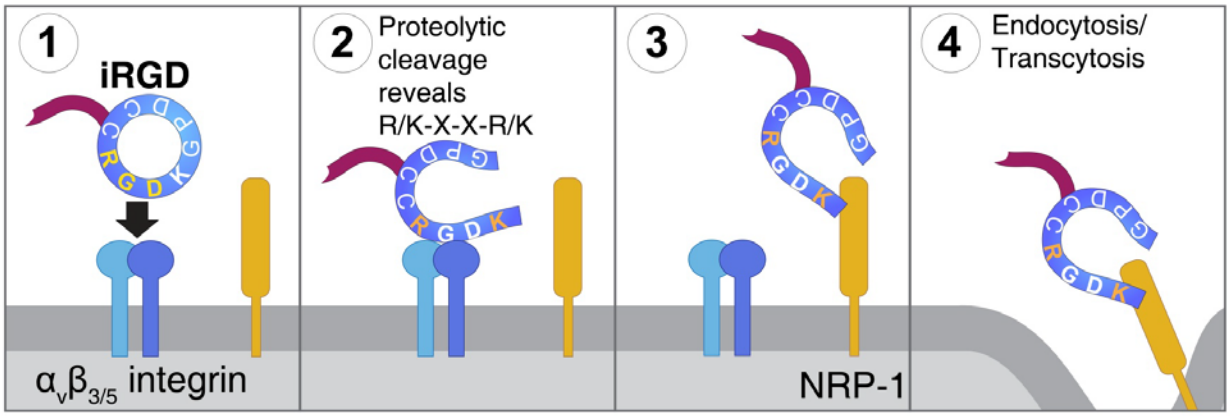

Figure 1-2. Mechanism of iRGD: (**A**) binding to α_v integrins, (**B**) proteolytic cleavage unveiling CendR motif, (**C**) binding to NRP-1, (**D**) endo/transcytosis. *Loosely based on an illustration in [110]*

More recent phage screens *in vivo* have yielded a new class of internalizing peptides that share a consensus C-terminal R/K-X-X-R/K ("C-end rule" or CendR peptides), with homology to VEGF-165A and some semaphorins [115]. Unlike classical cell-penetrating peptides (described in greater detail in Section 1.4.3), which are universally internalizing, these peptides penetrate through tissues by binding to neuropilin-1 (NRP-1) to activate transcytosis, vessel permeability, and cell internalization [116]. Because NRP-1 itself is commonly expressed on many cell types (though often upregulated in tumor cells or tumor-associated stroma), tumor *targeting*, in contrast to penetration, can be achieved by incorporating veiled CendR sequences into longer cyclic peptides that first bind to tumor-specific receptors and then are cleaved by proteases to reveal the CendR motif. Prototypical cyclic peptides possessing this two-step tumor-targeting and tumor-penetrating function include LyP-1 (CGNKRTRGC) and the more recently discovered internalizing RGD peptide (iRGD, CRGDKGPDC, **Fig. 1-2**). Lyp-1's tumor target is p32 (gC1qBP), a mitochondrial oxidative phosphorylation protein, which is aberrantly

presented on the surface of many tumor cells and tumor-associated lymphatics [117, 118]. iRGD operates by first binding $\alpha_v\beta_3$ and $\alpha_v\beta_5$ integrins located on angiogenic vessels and additionally upon tumor cells [119]. Upon cleavage, both peptides reveal CendR domains with NRP-1 specificity. *We are particularly interested in employing iRGD for guiding siRNA delivery due to its ability to mediate increased penetration and accumulation of small molecule dyes to genetically-engineered mouse models of PDAC [116] as well as enhancement of gemcitabine therapy in NRP-1-overexpressing PDAC models [120] when co-administered as a free peptide.*

1.4.3 RNAi nanoparticle carriers

The delivery of small RNAs and other nucleic acids poses additional challenges on top of those general to nanoscale drug delivery: (1) prior to arrival at the tumor, naked RNA is readily compromised by serum nucleases and also serves as a substrate that activates Toll-like receptors of the innate immune system, and (2) unlike many small molecule therapies, RNA is strongly polar and large (~13 kDa molecular weight), and is therefore excluded from crossing the cell membrane [98]. Work on strategies to deal with these challenges in fact predates the discovery of siRNA itself. Early approaches were aimed at gene delivery, beginning with viral approaches exploiting the success of virions at inserting genomes into mammalian cells [121]. While viral approaches are still employed – for instance, to transfect short hairpin (shRNA)-expressing plasmids into cell lines – the robust antiviral response *in vivo* and difficulty of functionalizing and customizing whole viruses have encouraged development of alternative carriers for RNAi therapeutics [122].

Chemical modifications to the siRNA molecule itself can increase stability, including methylation [93], locked nucleic acids (LNAs) [123], and oligomeric or polymeric shRNA assemblies such as RNA microsponges [124]. Further modifications have been employed to enhance specificity, for instance by incorporating unlocked nucleic acids (UNAs) into the sense strand of the siRNA [125] or through methylation of the seed region of the guide strand [126]. However, these types of modifications alone do not efficiently deliver or target the RNAi molecules.

Numerous non-viral carriers for siRNA delivery have been described to date, including cationic lipids [98], lipidoids and lipid-like nanoparticles [127, 128], spherical nucleic acids (gold core) [129], DNA tetrahedrons [130], and a variety of linear and dendritic polymers (polyfectins) such as polyethylenimine (PEI) [131], cyclodextrin-containing polymers (CDPs) [132], and the endothelial cell-targeting 7C1 polymer, which has also successfully delivered siRNA and miRNA to models of lung cancer [67, 128]. Our group has designed iron oxide-based nanoparticles decorated with PAMAM dendrimers which complex with siRNA, improving over the performance of the dendrimers alone and doubling as both an MRI diagnostic and therapeutic [133].

Most present siRNA therapeutics that have advanced along the drug-development pipeline to Phase III trials use direct siRNA modification rather than a separate carrier, including the multivalent GalNAc construction employed by several of Alnylam's siRNA conjugates to broadly target ASGPR-expressing hepatocytes [134]. However, such approaches have not yet seen application in cancer, partially owing to the more involved and bulky structures required to specifically target cancer, as discussed previously in Section 1.4.2.

In addition to the aforementioned siRNA delivery vehicles, cationic cell-penetrating peptides (CPPs) have been explored as promising transfection agents, including HIV-derived TAT [135], HSV-1-derived VP22 [136], and generic polycationic sequences such as poly-L/D-lysine and poly-L/D-arginine [137]. For instance, nona-D-arginine (9R) has been used for T-

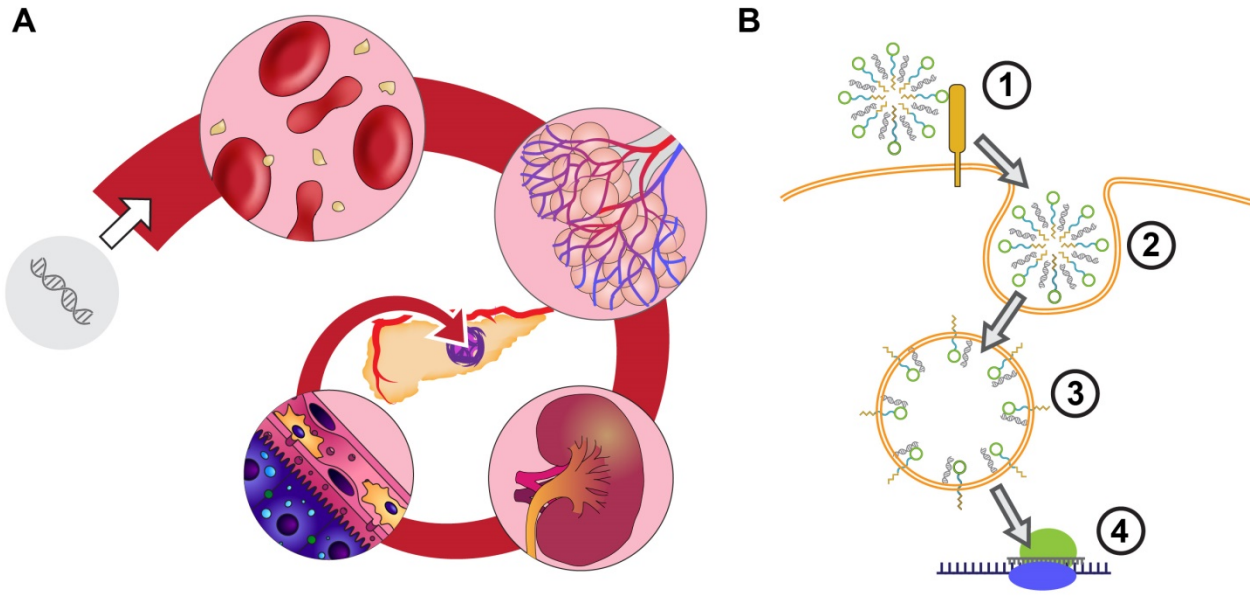

Figure 1-3: Barriers to Nucleic Acid Delivery. (A) Systemically-delivered nucleic acid particles to tumor cells must overcome aggregation, binding, disruption, or degradation by blood components, avoid capillary bed entrapment in organs such as the lung, avert dismantling or filtration in the glomeruli of the kidney, evade uptake by the reticuloendothelial system, and surpass barriers associated with the tumor itself. **(B)** Once a nucleic acid carrier reaches the cell, it must (1) interact with receptors or induce uptake mechanisms to mediate cellular uptake, (2) be endocytosed, (3) escape the endosome, and (4) be freed from the carrier in the cytoplasm to then be processed by Dicer and loaded into RISC.

cell siRNA delivery *in vivo* [138]. Like many siRNA transfection agents, these cationic CPPs condense cargo and attach to cells based on their extremely high densities of positive charge, frequently resulting in toxicity, as in the case of PEI, poly-lysine, and early generation PAMAM dendrimers [122], or robust immune responses in the case of unmodified cationic liposomes [139]. Thus, it may be preferable to instead employ amphipathic CPPs, which include transportan and its truncated form, transportan 10 [140, 141], penetratin [142], CADY and

CADY2 [143], and Pep-1, Pep-2, and Pep-3 (tested *in vivo* in tumor models) [144], which may induce fewer of these polycation-mediated effects.

Excellent *in vivo* delivery to hepatocytes [145] and endothelial cells [128] has been achieved using lipopeptide and polymeric nanoparticles, respectively. Indeed, Phase II trials of Alnylam's LNP-encapsulated anti-TTR siRNA therapy for familial amyloidotic polyneuropathy has shown sustained >80% knockdown and stabilization of neuropathy scores over 6 months [146], and Phase III trials have been initiated. However, the applications of RNAi have thus far been limited by the fact that siRNA delivery to other organs is challenging, and most clinical success has been seen in relatively rare diseases (TTR-mediated FAP affects 10,000 people in the world).

Only a few siRNA delivery vehicles have actively targeted the tumor itself, particularly PEGylated cyclodextrin-containing polymers with a transferrin-based targeting domain, which has recently entered Phase I clinical trials [132], and a cRGD-targeted TAT-based micelle [147]. Noting the considerable unexploited potential of utilizing active targeting mechanisms, our group has developed a new platform that packages the nucleic acid cargo into "tumor-penetrating nanocomplexes," seeking to deliver siRNA in a tumor-penetrating fashion by incorporating CendR peptides into an siRNA delivery vehicle.

1.4.4 Tumor-penetrating nanocomplexes

Our group's approach herein of employing cyclic CendR peptides represents the first use of a multifunctional targeting motif in siRNA delivery in which that motif not only binds a tumor-specific surface target but also has secondary tumor and vessel-penetrating capacity to

enhance distribution. This objective has been realized through the tandem peptide platform, where an N-terminal cell-penetrating peptide is fused to a C-terminal CendR peptide, LyP-1. Yin Ren et al. designed the inaugural library of such materials by synthesizing fused peptides including a wide range of cationic and amphipathic CPPs (**Fig. 1-4A**). We showed that these peptides spontaneously complex with siRNA to form tumor-penetrating complexes (**TPNs**) (**Fig. 1-4B**), efficiently packaging the siRNA cargo (**Fig. 1-4C**). Endosomal escape properties were improved through addition of an N-terminal saturated fatty acid. Finally, after constructing a model of tandem peptide "fitness," a metric encompassing both knockdown capacity of a reporter cell line (**Fig. 1-4D**) and receptor specificity (**Fig. 1-4E**) of each peptide in the library, it became evident that transportan-LyP1 showed the greatest fitness (**Fig. 1-4F**, top right) [148]. Indeed, transportan-LyP1 TPNs were subsequently used to validate the novel ovarian cancer target *ID4* through siRNA delivery in an intraperitoneal model of disseminated ovarian cancer [149]. Thus, in our present work on iRGD-targeted tandem peptides, we have decided to focus on fatty acid-transportan as the N-terminal portion of the peptide construct. This thesis builds upon these first-generation TPNs, with technological focus on employing new targeting groups, stabilizing the particles with non-covalent PEG compounds, and generalizing the cargo to many types of nucleic acids of relevance to therapy and genetic modeling.

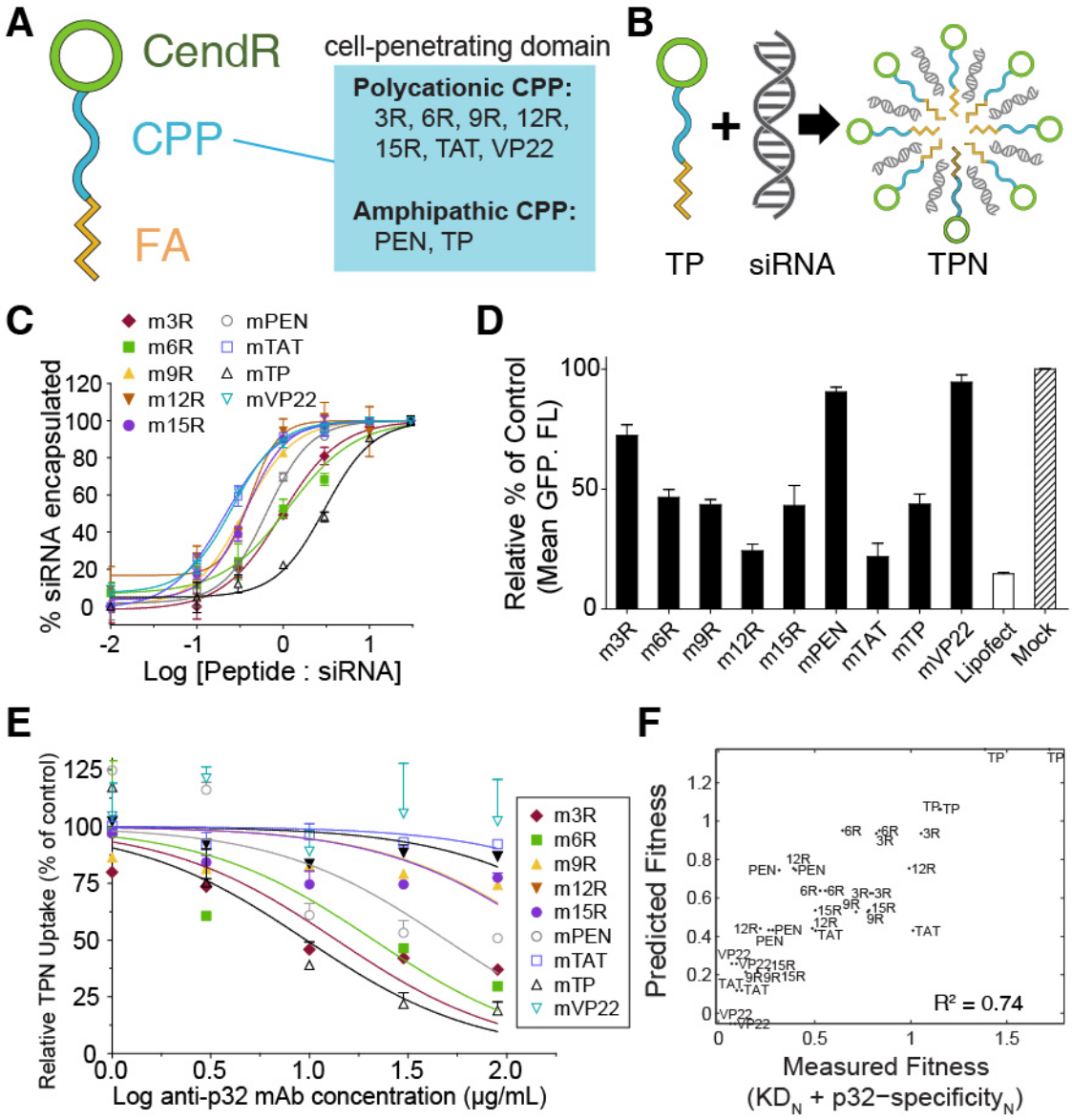

Figure 1-4: Tandem peptides for siRNA delivery. (A) Schematic structure of a tandem peptide; inset: cell-penetrating peptide candidates used in the original screen of LyP-1 tandem peptides. **(B)** Formation of tumor-penetrating nanocomplexes. **(C)** Encapsulation of siRNA cargo by tandem peptides, measured by TO-PRO-3 intercalating dye quenching assay (full incorporation quenches the dye, while labeled free siRNA is unquenched). **(D)** Knockdown of destabilized GFP in a HeLa dGFP cell line at 24 hours. **(E)** Competitive binding assay demonstrating receptor-specific TPN uptake based on inhibition of binding by anti-p32 antibody. **(F)** Model of tandem peptide fitness, a metric that encompasses both knockdown and p32 specificity. Higher values represent better fitness. Figures adapted from [148].

1.4.5 CRISPR/Cas9 Delivery

Though still in its nascent stages, development of delivery vehicles for CRISPR/Cas9 components has proceeded at a rapid pace over the last few years, in response to the voracious interest in realizing the full potential of the technological platform. In contrast to RNAi delivery, genomic editing with CRISPR requires multiple exogenous components, namely the crRNA(s), tracrRNA(s), Cas9, and any DNA templates required for homologous recombination [83]. Re-engineering the crRNA and tracrRNA as the chimeric single guide RNA (sgRNA) has helped to simplify the dossier of components [150], but efficacious delivery remains challenging. In animal models, it has been possible to effect CRISPR activity by injecting large quantities of plasmids containing the genes for sgRNA, Cas9, and template via high-volume hydrodynamic injection [92]. However, this process is inefficient, restricted to the liver, and not extensible to use in humans.

As with RNAi delivery, viral vehicles have shown great potential in delivering guide RNA and Cas9 DNA. Efficient gene editing has been seen *in vitro* via adenoviral and lentiviral vectors, and recently, adenoviruses have been used to mediate cutting of the Cebpα gene in the mouse liver in over 90% of copies of the gene (consistent with e.g. 80% homozygous knockout and 20% heterozygous knockout) [151]. Despite the obvious utility of virally-delivered CRISPR/Cas9 as a potent research tool, these approaches face several shortcomings in the *in vivo* setting. First, viruses are limited in organ selectivity – lentiviruses administered systemically will primarily infect the liver while adenoviruses broadly infect any cell expressing the coxsackievirus and adenovirus receptor (CAR). Adeno-associated viruses possess more refined tropism [152], but customized targeting remains difficult. Furthermore, (1) viruses cannot

deliver large quantities of DNA templates for homologous recombination; (2) viruses raise a robust immune response; and (3) viral delivery of CRISPR/Cas9 components may result in permanent integration and expression of guide RNA and Cas9, which increases the time-integrated risk of off-target cutting. For these reasons, development of alternative delivery methods is warranted.

To this end, researchers have reappropriated delivery platforms for RNAi for CRISPR/Cas9, including cell-penetrating peptides [153] and cationic lipids [154]. To avoid the inherent risks of delivering plasmids such as random integration and longterm expression, efforts have been made to delivery mature guide RNA, which in many ways resembles siRNA, though with a molecular weight ~2.5 larger and being single-stranded. Delivery of guide RNA alone is useful in systems where constitutive or selective Cas9 expression in the host is reasonable, but therapeutic applications as well as rapid generation of animal models strongly favor methods that can deliver Cas9 as well.

Thus, recent work has investigated whether mature sgRNA may be delivered alongside Cas9 in mRNA or protein form. Due to the sheer size and instability of Cas9 mRNA, protein delivery has seen greater interest. Ramakrishna et al. have used a combination of nonarginine-Cas9 fusion proteins and nonarginine-sgRNA conjugates to form complexes for delivery; however, the overall efficiency of this approach was low, with ~6% indel rates *in vitro* based on a GFP reporter assay [153]. More recently, David Liu's laboratory has identified that sgRNA and Cas9 may be delivered simultaneously by commercial lipid transfection reagents (Lipofectamine 2000 and Lipofectamine RNAiMax) at high efficiency *in vitro* as well as in the inner ear *in vivo* [154]. However, instability of such lipid formulations in the *in vivo* setting as

well as their lack of targeting capacity limit their use as systemic agents of gene editing in the living animal. Thus, there remains a need for CRISPR/Cas9 delivery platforms that can target specific cell types of interest to enable disease-specific gene editing while delivering all key components of the CRISPR/Cas9 system: Cas9, guide RNA, and DNA templates. In Chapter 5, we present progress towards adapting the tandem peptide platform for CRISPR/Cas9 component delivery, with focus on developing a framework for the generation of new animal models of pancreatic cancer.

1.5 Summary of Thesis Aims [^]

Pancreatic cancer is a deadly disease for which present therapeutic options are woefully inadequate. Two major factors contributing to our inability to extend survival in patients with pancreatic cancer are the physical barriers present in these tumors and the difficulty in drugging the relevant central mutations driving the disease process. These factors create a pressing need for novel delivery strategies, genetically-informed therapies such as RNAi, and new preclinical models for better understanding and better treating pancreatic cancer. Thus, in this work, we have striven to engineer tumor-penetrating nanocomplexes (TPNs) that incorporate the multifunctional iRGD domain for siRNA delivery to pancreatic cancer. Expanding the modularity of the tandem peptide platform, we then extend the use of TPNs for systemic delivery through and furthermore demonstrate generalizable nucleic acid delivery with the delivery of CRISPR/Cas9 components towards the development of new models of pancreatic cancer.

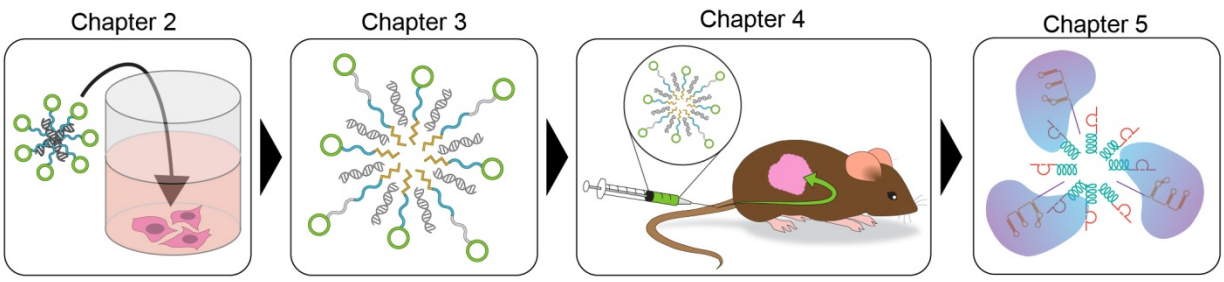

Figure 1-5: Overview of thesis aims and breakdown into chapters.

The specific aims of thesis have been as follows **(Fig. 1-5)**: First, to design, characterize, and optimize modular iRGD-based TPNs for gene knockdown in pancreatic cancer *in vitro*, presented in Chapter 2. Second, to develop modular formulations TPNs for systemic delivery, presented in Chapter 3; and to subsequently apply the preferred formulation to the preferred iRGD-based siRNA delivery vehicle to create "second-generation" TPNs, employed for delivery of siRNA in animal models of pancreatic cancer, presented in Chapter 4. Lastly, to adapt the tandem peptide delivery platform for genomic editing through the CRISPR/Cas9 system, presented in Chapter 5.

Chapter 2: Development of iRGD-targeted tumor-penetrating nanocomplexes [^]

2.1 Introduction

Pancreatic cancer is an extremely deadly disease, with an overall 5-year survival rate below 7% [1]. Poor therapeutic outcomes reflect two key shortcomings of current treatment regimens: a lack of new approaches targeting the genomic changes stereotypically seen in PDAC, and an inability to overcome the formidable physical delivery barriers posed by the desmoplastic stromal reaction incited by the tumor.

RNA interference holds promise in striking at the heart of tumor progression by specifically eliminating expression of essential oncogenes, such as mutated Kras seen in over 90% of PDACs, or modulating expression of tumor suppressor genes [3]. However, the use of RNAi in cancer therapy has been obstructed by the challenge of achieving specific and potent delivery of siRNA and miRNA to sites of disease. This is especially true in the case of PDACs, which are typically surrounded by dense, fibrous, and poorly vascularized tissue [4] and highly metastatic to sites such as the liver and abdominal cavity.

Nanoparticles are well-poised to address these challenges. However, while many nanomaterials have been successfully developed for siRNA delivery in general, including non-specific cell-penetrating peptides, they typically have limited translational potential for PDAC due to (a) lack of a mechanism for tumor targeting, (b) failure to penetrate deep into the tumor, especially in poorly vascularized settings, or (c) an affinity for single organs or tissues, preventing use in metastatic disease.

Recently, phage display screening in tumors performed by collaborators in the lab of Erkki Ruoslahti have identified a class of peptides known as CendR peptides, which have the

unique dual-function capacity to both target and penetrate through tissue including tumors and their associated stroma. The first such peptide to be discovered was LyP-1, which binds p32 and, following cleavage, revealing a cryptic CendR domain (K/R-X-X-K/R on the C terminus) that allows neuropilin-1-based transcytosis and endocytosis. To exploit this mechanism for siRNA delivery, a team led by Yin Ren in our group developed "tandem peptides," comprising a cell-penetrating peptide and LyP-1 as the tumor-penetrating peptide. Such tandem peptides self-assemble with siRNA and have been shown to be effective in treating models of disseminated ovarian cancer by targeting a novel genetic target identified through shRNA screening, *ID4*. This platform is introduced in detail in Section 1.4.4.

In contrast to cancers such as breast cancer, ovarian cancer, and endometrial cancer, which exhibit profound upregulation of p32 in carcinomas and the virtual absence of p32 in healthy tissues, such selectivity from differential p32 expression does not exist for pancreatic cancer *versus* the healthy pancreas [117]. Furthermore, we have found that p32 expression is not very high in several pancreatic cancer cell lines. Thus, to develop tandem peptides for pancreatic cancer, we instead looked to iRGD, a new cyclic peptide that mediates tumor targeting and penetration by binding $\alpha_v\beta_{3/5}$ integrins while cyclized, again signaling through neuropilin-1 after proteolytic cleavage reveals a cryptic CendR domain [7,8]. iRGD's integrin targets are commonly overexpressed in angiogenic tumor vasculature and on tumor cells themselves, while neuropilin-1 is commonly overexpressed in tumor-associated stromal tissue [155] as well as the tumor as a whole, where increased neuropilin-1 expression correlates with worse outcomes in patients [120, 156]. Indeed, iRGD as a free peptide has been shown to mediate uptake of dyes and therapeutics into models of pancreatic cancer [116].

Thus, we hypothesized that tandem peptides combining a cell-penetrating peptide (CPP) and iRGD can complex with siRNA to form tumor-penetrating nanocomplexes (TPNs) effective in delivering therapeutic siRNA to PDAC. A tumor-targeted and penetrating nanoscale carrier could address many of the delivery constraints inherent to this disease as well as provide a practical means for bridging the extensive compendia of *in vitro* RNAi hits to clinical translation by serving as a platform for validating genetic targets in realistic animal models of PDAC. In this chapter, we present the development of iRGD TPNs and their activity within *in vitro* models of PDAC, with particular focus on knocking down *KRAS* as a starting point for RNAi therapy.

2.2 Results

2.2.1 Design of iRGD tandem peptides to form tumor-penetrating nanocomplexes

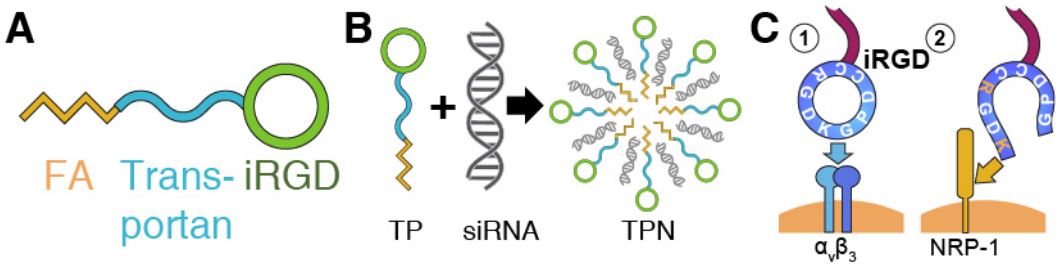

Figure 2-1: Schematic of iRGD tandem peptides and TPNs. (A) Tandem peptides consist of a cell-penetrating peptide, here transportan (light blue), fused to a C-terminal targeting peptide, here iRGD (green), and capped on the N-terminus by a fatty acid (yellow) to aid with endosomal escape. **(B)** Addition of tandem peptides to siRNA solutions spontaneously forms tumor-penetrating nanocomplexes (TPNs). **(C)** iRGD functions by binding to $\alpha_v\beta_{3/5}$ integrins when cyclized and by binding neuropilin-1 (NRP-1) following proteolytic cleavage.

To develop tandem peptides for RNAi delivery to PDAC, we built upon the tumor-penetrating nanocomplex platform developed in our group, where siRNA is complexed with a tandem peptide containing both a C-terminal tumor-penetrating domain and N-terminal cell-

penetrating peptide (CPP), as introduced in Section 1.4.4 (**Fig. 2-1A**) [9,10]. Harnessing the modularity of the platform, we replaced the original LyP-1 targeting peptide with iRGD. Informed by *in vitro* modeling that compared the different cell-penetrating peptides on the basis of their function and the degree to which they subsumed their universal penetrating function to the control of the targeting ligand, we selected transportan (TP)-iRGD tandem peptides to move forward with in the remainder of these studies (see also Section 1.4.4). Additionally, we appended a saturated fatty acid (C_{14}, myristic acid) to the N-terminus of transportan, as this was

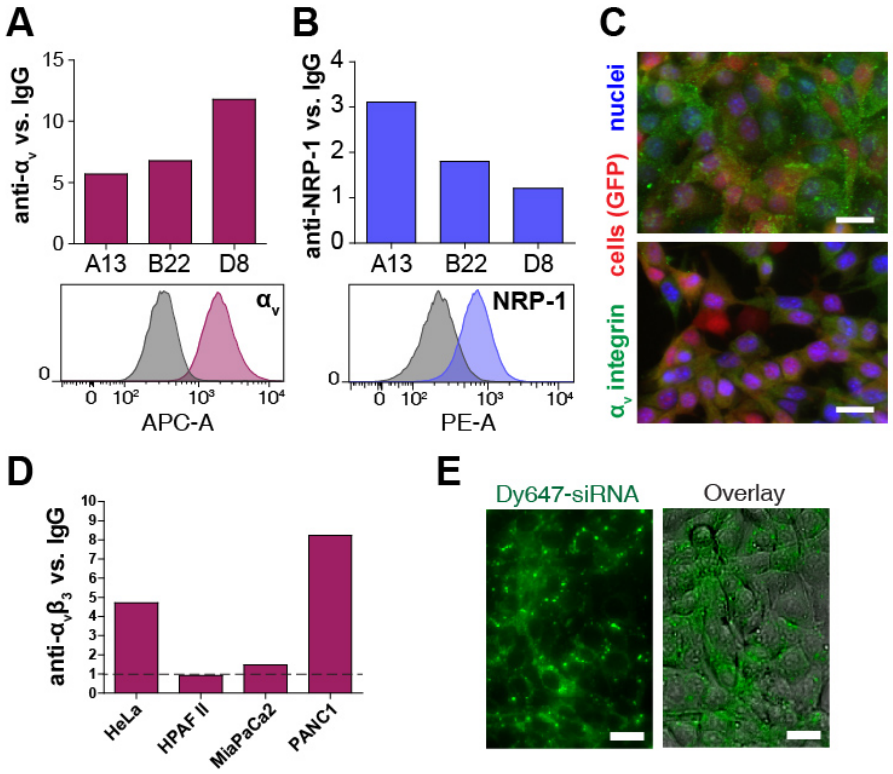

Figure 2-2: iRGD receptor expression on PDAC cell lines and delivery of siRNA into receptor-positive cells. (A) α_v integrin and **(B)** neuropilin-1 surface expression on murine Kras-p53 PDAC cell lines (A13, B22, and D8), quantified by live-cell flow cytometry and displayed relative to cells stained with IgG control + secondary antibody. **(C)** ICC stain showing localization of α_v integrin (green) on B22 cells (red, GFP). Nuclei counterstained with Hoechst (blue). Scale bars: 20 µm. **(D)** $\alpha_v\beta_3$ integrin surface expression on human PDAC cell lines (HPAF II, MIA PaCa-2, and PANC-1) with HeLa positive control, quantified by live-cell flow cytometry and displayed relative to cells stained with IgG control + secondary antibody. **(E)** DyLight647-tagged siRNA delivery by mTP-iRGD particles after 24 hours, showing cytosolic distribution. Scale bars: 20 µm.

found to aid with endosomal escape. When mixed in optimal molar ratios, these myr-TP-iRGD tandem peptides spontaneously complex with siRNA to form particles (**Fig. 2-1B**).

2.2.2 iRGD is suitable for targeting PDAC

While iRGD's complex mechanism initially focuses on targeting angiogenic blood vessels (**Fig. 2-1C**) and stromal cells, its feasibility as a targeting peptide in PDAC also requires expression of at least one of its receptors on tumor cells to facilitate final uptake of the particles. We note that because of the multivalency of iRGD units in each particle and the random nature of the proteolytic cleavage, it is likely that particles would display both integrin and NRP-1 affinity upon arrival at the tumor cells. To evaluate surface receptor expression in PDAC, we stained for surface expression of α_v integrins and neuropilin-1 in several murine cell lines (A13, B22, D8) derived from $Kras^{G12D/+}$;LSL-$Trp53^{fl/fl}$;Pdx-1-Cre GEM mice, using live-cell flow cytometry (**Fig. 2-2A-B**; representative histograms shown below). For B22 cells, we additionally confirmed the expected cellular distribution of α_v integrins using immunocytochemical stains (**Fig. 2-2C**, top image). In all cases, we measured surface expression of both α_v integrins and NRP-1. We also quantified $\alpha_v\beta_3$ integrin expression on three commonly used human PDAC cell lines compared to HeLa cells as a positive control, showing very high expression in PANC-1 cells, moderate expression in MIA PaCa-2 cells, and no expression on HPAF II cells. Additionally, both PANC-1 [157] and MIA PaCa-2 [120] cells have been shown in the literature to highly express neuropilin-1, and HPAF-II has shown moderate levels of NRP-1 [158]. Thus, expression of iRGD-recognized receptors is prevalent across PDAC cell lines of mouse and human origin.

Using the murine B22 cell line, we demonstrated intracellular delivery of siRNA via TPNs: fluorescence microscopy after myr-TP-iRGD TPN transfection of fluorescently-tagged siRNA showed diffuse cytoplasmic distribution of siRNA consistent with endosomal escape and necessary for functional siRNA processing and activity (**Fig. 2-2E**).

2.2.3 Optimization of iRGD TPN-mediated knockdown in vitro

To establish that siRNA delivered by iRGD TPNs is functional, we used firefly luciferase in B22 cells as a reporter gene for knockdown. In our initial experiments, we sought to optimize particle formulation by characterizing the ratio- and dose-dependency of gene knockdown (KD) by TPNs. To establish a reasonable range of peptide:siRNA ratios, we performed an electrophoretic mobility shift assay on particles formed at 5-30:1 ratios, in which siRNA

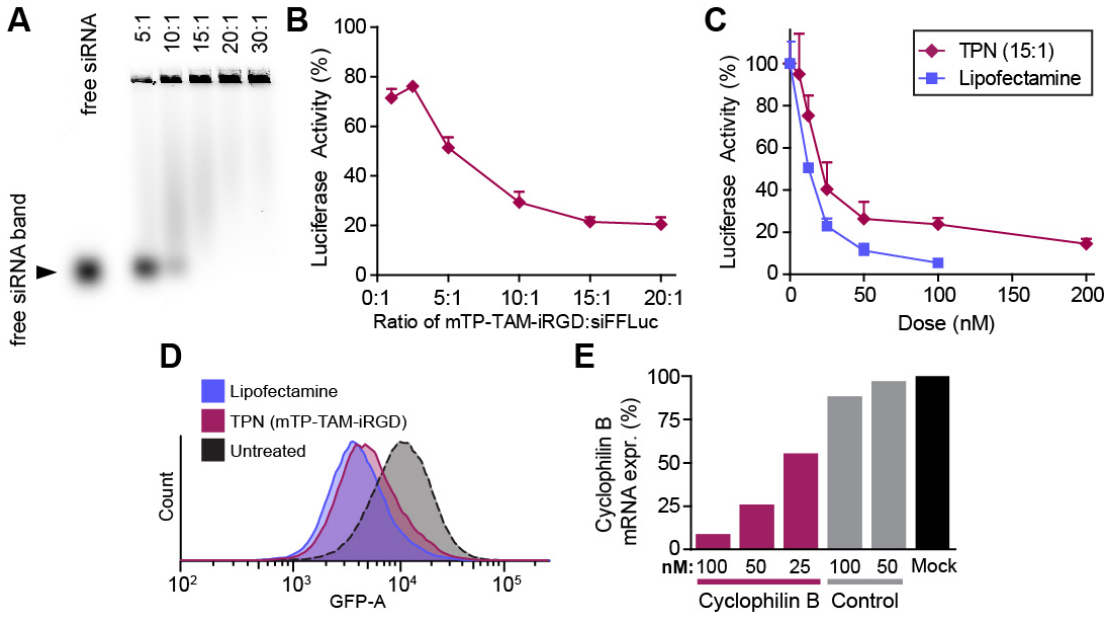

Figure 2-3: Optimization of iRGD TPNs in vitro. (A) Electrophoretic mobility shift assay showing encapsulation of siRNA at different ratios of peptide to siRNA. **(B)** 48-hour firefly luciferase knockdown in B22 cells as a function of peptide:siRNA ratio. **(C)** 48-hour luciferase knockdown dose curve for iRGD TPNs compared to lipofectamine RNAiMax positive control. **(D)** 48-hour GFP knockdown in B22 cells. **(E)** 48-hour knockdown of Cyclophilin B (Ppib) mRNA in B22 cells.

sequestered in particles is excluded from gel migration while unbound siRNA runs freely (**Fig. 2-3A**). The resulting gel showed partial complexation at a 5:1 ratio and essentially complete encapsulation at ≥10:1 ratios. Consistent with the encapsulation profiles, we observed improved reporter knockdown with increasing ratio, up to optimal function at ≥10:1 ratios corresponding to a ~1.7:1 N/P (nitrogen/phosphate) ratio (**Fig. 2-3B**) and siRNA concentrations ≥~50 nM (similar to lipofectamine RNAiMax, a standard reagent for *in vitro* transfection) **(Fig. 2-3C)**. Knockdown of GFP as assessed by flow cytometry assured us that the observed RNAi effects were not merely due to toxicity (**Fig. 2-3D**). Finally, to confirm that knockdown effects are in fact being mediated by mRNA knockdown, we quantified 48-hour knockdown of mouse cyclophilin B (*Ppib*) by specific siRNA and untargeted control siRNA, showing dose-dependent mRNA knockdown only with the cyclophilin B-targeted siRNA (**Fig. 2-3E**).

2.2.4 iRGD TPNs robustly knockdown Kras in several cell lines

Moving towards therapeutic applications, knockdown of *Kras* will be a vital component of potential therapeutic RNAi regimens in PDAC, with studies showing that PDAC cell lines stably expressing shRNA against *KRAS* grew much more slowly as implanted tumors *in vivo* [159], and local, prolonged intratumoral delivery of siRNA against mutant $Kras^{G12D}$ in established PDAC tumors inhibited tumor cell proliferation [160]. Thus, we wished to characterize the potency and effects of *Kras* knockdown in both mouse and human cell lines through iRGD TPN transfection. In B22 mouse cells, TPNs mediated ~90% knockdown of *Kras* mRNA at 48 hours, while a seed-matched siRNA control that accounted for miRNA-like seed sequence effects did not result in significant knockdown (**Fig. 2-4A**); furthermore, *Kras*

knockdown led to significant growth inhibition after 48 hours (**Fig. 2-4B**). In the PANC-1 human cell line, profound knockdown of >95% was observed, but the cells did not show an obvious growth phenotype in response to this knockdown, consistent with determination in the literature that PANC-1 cells are *KRAS*-mutated but *KRAS*-independent [161]. In contrast, in KRAS-dependent MIA PaCa-2 cells, we confirmed knockdown of *KRAS* mRNA (**Fig. 2-4D**) and K-Ras protein (**Fig. 2-4E**), and additionally observed inhibited cell proliferation when

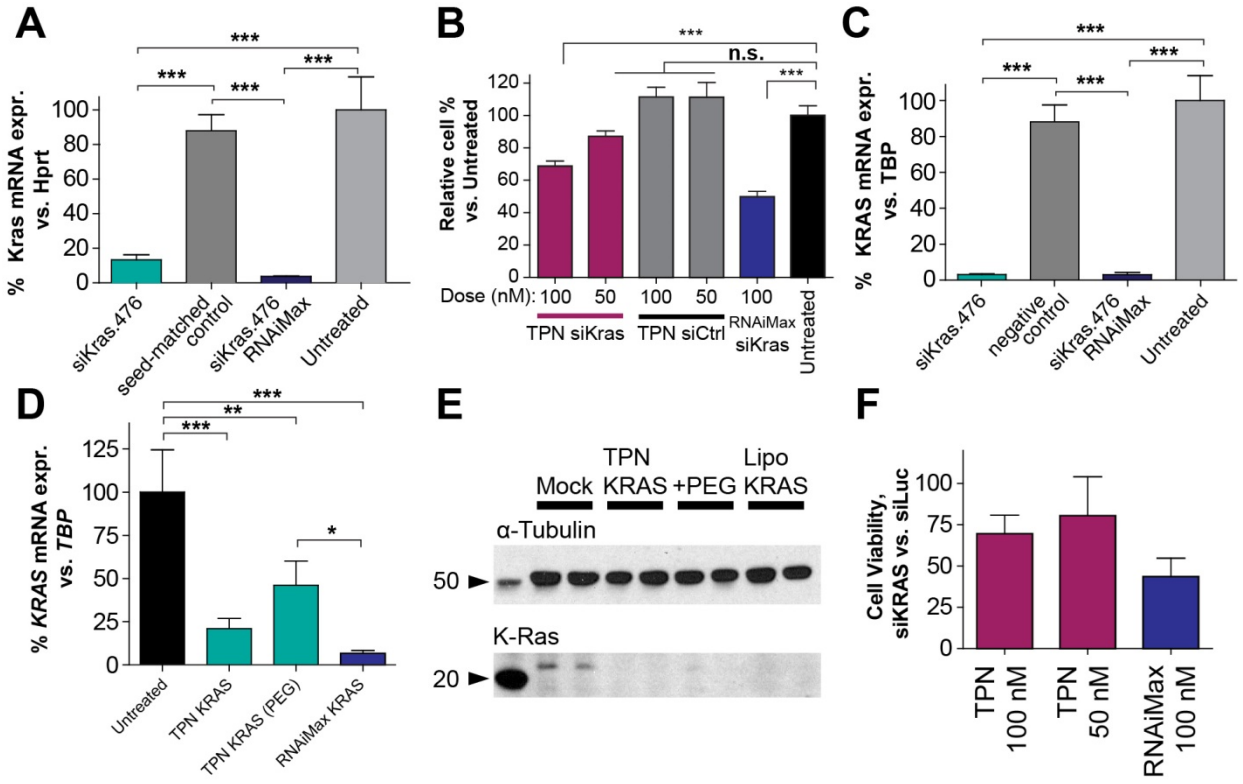

Figure 2-4: Knockdown of Kras using iRGD TPNs. (A) mRNA knockdown of Kras in murine KP B22 cells using siKras.476, versus a seed-matched control varying only positions 9-11 in the siRNA. mRNA levels normalized to Hprt housekeeping gene. **(B)** Growth inhibition of KP B22 cells 48 hours after TPN treatment with siKras, as measured by MTS assay. **(C)** mRNA knockdown of KRAS in the human PANC1 PDAC cell line, which is KRAS-independent. mRNA normalized to TBP housekeeping gene. **(D)** mRNA knockdown of KRAS in the human MIA PaCa-2 PDAC cell line, which is KRAS-dependent. **(E)** Protein knockdown of K-Ras in the human MIA PaCa-2 cell line, treated identically as the cells in panel D. **(F)** Growth inhibition of MIA PaCa-2 cells 48 hours after TPN treatment with siKRAS, as measured by MTS assay. Values displayed are the ratio of MTS signal in wells treated by TPN siKRAS vs. control TPN siLuciferase, in order to control for toxicity. A ratio of 100% would indicate no difference in growth.

comparing the cell viability signal between cells treated with siKras *versus* those treated with a negative control siRNA (**Fig. 2-4F**).

2.2.5 iRGD TPNs can knockdown multiple gene targets simultaneously

Because *KRAS* knockdown has the effect of slowing cell proliferation but not necessarily killing them, it will likely be important in the future to consider simultaneous knockdown of another gene target in addition to *KRAS*. Towards this goal, we have demonstrated prototypical knockdown of two genes simultaneously (*Kras* and *Ppib*) in B22 cells through both forward (**Fig. 2-5A**) and reverse (**Fig. 2-5B**) transfection. In both cases, splitting the siRNA dose between two different targets achieved similar levels of knockdown compared to devoting the entire dose to a single target, with the exception of *Ppib* in the reverse knockdown treatment.

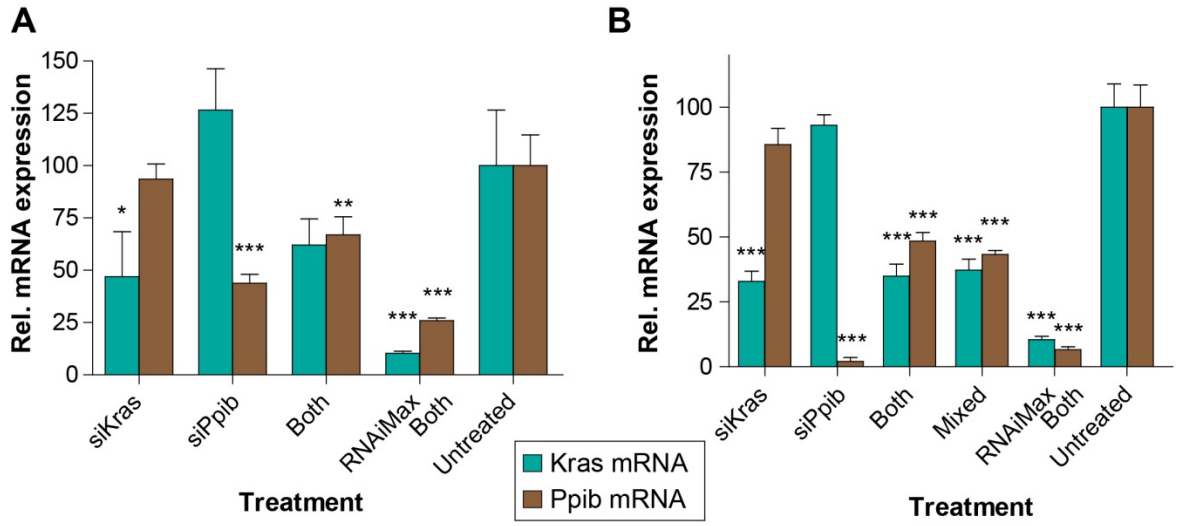

Figure 2-5: Dual knockdown using TPNs. (A) Knockdown of Kras and Ppib by iRGD TPNs containing siKras, siPpib, or both siRNAs simultaneously, dosed through forward transfection. **(B)** Knockdown of Kras and Ppib by iRGD TPNs containing siKras, siPpib, or both siRNAs simultaneously, dosed through reverse transfection (addition of suspended cells over particle solution). "Both" indicates particles encapsulating both types of siRNAs pooled together, while "Mixed" indicates a mixed solution of particles encapsulating one siRNA or the other. In all panels, statistical significance was computed by two-way ANOVA comparing to the untreated mRNA level, *: $p < 0.05$; **: $p < 0.01$; ***: $p < 0.005$.

Overall, the results in this section validate the capacity of iRGD tandem peptides to deliver siRNA to and effect knockdown in pancreatic cancer. The tandem peptide TPNs we have generated thus far can serve as the basis for a standardized *in vitro* assay to study candidate siRNA targets, particularly in combinations or alongside small molecule therapies.

2.3 Discussion

In this chapter, we have synthesized new iRGD-targeted tandem peptides for siRNA encapsulation and delivery, capitalizing on the modular construction of these peptides. While the relative expression levels of relevant $\alpha_v\beta_{3/5}$ integrins and neuropilin-1 vary between different cell lines, all cell lines tested showed expression of at least one of the two receptors for iRGD (**Fig. 2-2**), and moreover, the presence of iRGD-recognized integrins on angiogenic blood vessels and neuropilin-1 in cancer-associated stroma is well-documented. We have focused our early attention on knocking down *KRAS*, as it is by far the most prevalent oncogene in PDAC, and in contrast to other oncogenes like *EGFR* and *ERBB2*, it does not have a clinically-approved small molecule or antibody inhibitor. Although the presently studied *KRAS* siRNA sequences are not specific for mutated *KRAS* mRNA compared to wild-type, such specific siRNAs have been described in the literature and may add some degree of greater specificity for tumor cells, though a single mismatch in siRNA binding tends to be tolerated at the RISC level.

Delivery of siRNA against *KRAS* in various cell types all resulted in robust knockdown at the mRNA level, with confirmation that protein knockdown is similarly complete (**Fig. 2-4E**). The difference in knockdown levels in PANC-1 (>95%) and MIA PaCa-2 (~75%) (**Fig. 2-4C-D**) cells may reflect a number of factors, including the possibility that MIA PaCa-2 KRAS-

dependence selects against cells with the highest knockdown, alongside potential contributions of higher receptor expression on PANC-1 cells (**Fig. 2-2D**) as well as shorter doubling times in MIA PaCa-2 cells (40 hours vs. 52 hours [162]), which could reduce dilution of the fixed siRNA dose. The interpretation of growth inhibition assays beyond a determination of relative KRAS-dependence is difficult, as the cells have nearly unlimited resources at their disposal for continuing growth, in contrast to the vascularly-challenged tumor site, but on the other hand, the overall levels of siRNA exposure are comparatively high.

Nevertheless, the reality that *KRAS* knockdown is probably at best cytostatic necessitates the consideration of combination therapies, whether this be combination of *KRAS* knockdown with another siRNA or with a small molecule inhibitor. Thus, it is encouraging that TPNs are able to mediate knockdown of at least two genes simultaneously (**Fig. 2-5**). Strategies for curating siRNA combinations include trying to hit the same pathway at multiple points to cover for incomplete knockdown, inhibition of mutually redundant pathways, knockdown of synergistic targets (*i.e.* loss of one target sensitizes to knockdown of the other), and knockdown of multiple unrelated but potent targets. The identification of such targets is best performed through screening approaches, and we have been engaged in ongoing collaborations to test targets as they are discovered.

Because of the limitations of *in vitro* testing, we wished to study the behavior of iRGD TPNs in animal models of pancreatic cancer. We felt that, given the extensive diffusive barriers in PDAC as well as frequently advanced or metastatic presentation of disease, it would make the most sense to approach delivery in the animal from the standpoint of systemic delivery, in contrast to the intraperitoneal delivery that was previously explored for models of disseminated

ovarian cancer [149]. However, previous systemic biodistribution profiles of TPNs following intravenous delivery [149] as well as qualitative observations of particle aggregations in these *in vitro* experiments and in the CPP literature [163] strongly suggest that there is a need to develop strategies to stabilize the TPNs prior to characterizing the particles *in vivo*, which is the subject of the subsequent chapter.

2.4 Methods

Peptide synthesis: mTP-TAMRA-iRGD ($CH_3(CH)_{13}$-GWTLNSAGYLLGKINLKALAALAKKIL-GGGGK(TAMRA)CRGDKGPDC, Cys-Cys bridge) was synthesized by the Koch Institute Biopolymers Core. pTP-TAMRA-iRGD ($CH_3(CH)_{15}$-GWTLNSAGYLLGKINLKALAALAKKIL-GGK(TAMRA)GGCRGDKGPDC, Cys-Cys bridge) was synthesized by CPC Scientific.

siRNA: All siRNAs were synthesized by Dharmacon (GE Healthcare) with ON-TARGETplus specificity enhancement. The sequences used were as follows (given as the sense strand without overhangs): siLuc against firefly luciferase: 5′-CUUACGCUGAGUACUUCGA-3′, siGFP: 5′-GGCUACGUCCAGGAGCGCACC-3′, siKras.923 against murine *Kras*, sequence designed by Wen Xue: 5′-GGAAACCUUCUUUUUUCUAAG-3′, siKras.476 against murine and human *KRAS*, sequence designed by Mandar Muzumdar: 5′-ACCAUUAUAGAGAACAAAUUA-3′, siKras.923 seed-matched control: 5′-GGAAACCUAGAUUUUUCUAAG-3′, siKras.476 seed-matched control: 5′-ACCAUUAUUCUGAACAAAUUA-3′, siNC non-targeted control: 5′-UUCUCCGAACGUGUCACGUUU-3′.

Cell culture: All cell lines were cultured in DMEM supplemented with 10% fetal bovine serum (FBS), 100 U/mL penicillin, and 100 μg/mL streptomycin, with the exception of PANC-1 cells, which were grown in DMEM + 20% FBS + penicillin/streptomycin.

Antibody staining: For quantification of surface receptor expression, cells were trypsinized and brought to single-cell suspension in FACS buffer (1x PBS + 2% FBS). Primary antibody was added at 1 μg/million cells in 100 μL total solution (for mouse cells: rat anti-mouse α_v integrin (BD Pharmingen 551380) or rat IgG isotype control (Invitrogen); for human cells: mouse anti-$\alpha_v\beta_3$ integrin, direct PE conjugate (BioLegend 304406) or mouse IgG κ chain isotype control, direct PE conjugate (BioLegend 400112); for neuropilin-1 staining in all cells, rabbit anti-NRP-1 (Novus Biologicals NBP1-40666) or normal rabbit IgG isotype control (R&D)) and incubated for one hour on ice. For direct fluorophore-conjugated primary antibodies, cells were washed with PBS and resuspended in FACS buffer. Otherwise, after washing the cells 2x in PBS, cells were incubated with secondary fluorescently-tagged antibody (Invitrogen) for 45 minutes and

washed 1x in PBS. Cells were then analyzed on BD LSR-II or Fortessa HTS flow cytometers. Data were analyzed and compiled in FlowJo (TreeStar Software).

Electrophoretic mobility shift assay: TPNs were formed at 5-30:1 peptide (pTP-iRGD):siRNA ratios for a final concentration of 200 nM siRNA (DyLight 677-siLuc) in 1x PBS. 10 μL of each TPN sample or free siRNA was mixed with 2 uL of 30% glycerol and loaded into a 2% agarose gel. The gel was run at 100 V for 45 minutes in 1x TAE buffer and siRNA fluorescence was imaged on a LI-COR Odyssey infrared scanner (LI-COR Biosciences). Signal was quantified using ImageJ.

Transfection: For all *in vitro* transfection assays, TPNs were formed at the specified ratios by adding peptide diluted in Opti-MEM (Gibco, Life Technologies) to an equal volume of siRNA diluted in Opti-MEM, combining to form a final concentration of 100 nM siRNA. Cells were dosed in multi-well plates by removing growth media and adding TPN solution at 100 nM siRNA. The volumes used were as follows: 96-well plate (luciferase knockdown): 100 μL/well; 24-well plate: 500 μL; 12-well plate: 1 mL; 6-well plate (GFP knockdown): 2 mL. After 4-6 hours of incubation at 37 °C, media was replaced with normal growth media.

Fluorescence microscopy: Cells were transfected as described above. At the specified timepoints, cells were imaged live on a Nikon Eclipse T*i* inverted microscope using a 20x Plan Apo objective. Images were collected in NIS-Elements AR software (Nikon), with individual channels combined in Photoshop CS5 (Adobe) with linear level adjustments applied identically to all images within an experiment.

Luciferase and GFP knockdown: 48 hours after transfection of KP A13 or B22 cells with siLuc, luciferase function was quantified by lysing cells with Cell Culture Lysis Reagent (Promega); 10 μL of lysate was then mixed thoroughly with 40 μL of luciferin (Promega Luciferase Assay System) and loaded into a white 96-well plate (Corning 3600). Luciferase bioluminescence was quantified using a Centro LB 960 Microplate Luminometer (Berthold Technologies). Knockdown of destabilized GFP in HeLa dGFP cells was assessed at 24 hours post-transfection using flow cytometry, quantified using Flow-Jo software v. 7.6.5.

Quantitative PCR: mRNA was isolated by lysing cells with Buffer RLT (Qiagen), filtering out debris using the Qiashredder homogenizer (Qiagen), and then purifying mRNA using an RNeasy kit (Qiagen) according to manufacturer's instructions. mRNA concentration was quantified via NanoDrop 2000 Spectrophotometer (thermo). cDNA was reverse transcribed using the iScript cDNA synthesis kit (Bio-Rad). qPCR was performed on a C1000 Touch Thermal Cycler with CFX96 Touch Real-Time PCR Detection System (Bio-Rad) using the following primer pairs: mouse *Kras*: Forward 5′-ACAGTGCAATGAGGGACCAG-3′ and Reverse 5′-ATCGTCAACACCCTGTCTTGT-3′; mouse *Hprt* as loading control: Forward 5′-GTCAACGGGGGACATAAAAG-3′ and Reverse: 5′-CAACAATCAAGACATTCTTTCCA-3′; human *KRAS* (for MiaPaCa-2 experiments) Forward 5′-ACTGGGGAGGGCTTTCTTTG-3′ and

Reverse 5′-GCATCATCAACACCCTGTCT-3′; human *TBP* as loading control Forward 5′-GGAGAGTTCTGGGATTGTAC-3′ and Reverse 5′-CTTATCCTCATGATTACCGCAG-3′.

Western blotting: Protein was isolated by lysing cells in 1x RIPA buffer with protease inhibitors for 30 minutes. Protein was quantified using the bincinchoninic acid (BCA) assay (Pierce, Thermo) against bovine serum albumin standards and standardized to 2 mg/mL. Samples were then mixed 1:1 with Laemmli loading buffer and run on a Novex 4-12% Bis-Tris gel (Life Technologies) following manufacturer protocol, along with MagicMark XP and Kaleidoscope ladders. Bands were transferred to nitrocellulose membranes at 375 mA for 1 hour. The membrane was cut at the 30 kDa marker in order to stain for K-Ras (21 kDa) and α-tubulin (50 kDa) separately. The membranes were blocked with 5% skim milk in TBS-Tween (TBST) for 1 hour at 4 °C and then incubated with primary antibody diluted in 5% skim milk overnight at 4 °C: for K-Ras, F234 mouse monoclonal antibody (Santa Cruz) was used at a 1:100 dilution; for tubulin, mouse monoclonal anti-tubulin (Invitrogen 32-2500) was used at a 1:1000 dilution. Membranes were washed 2x in TBST for 5 min. shaking, then incubated with secondary antibody: goat anti-mouse (sc-2005, Santa Cruz) at a 1:2000 dilution in TBST. Following final 2x TBST washes, blots were imaged using the SuperSignal West Pico chemiluminescent substrate (Pierce, Thermo).

Growth inhibition studies: Cells were transfected as above in 96-well plates. After two days, cells were split into 24-well plates at 1:1 well correspondence, keeping all cells. After 4 days, cell counts were quantified using the CellTiter 96 AQueous One MTS assay (Promega) according to manufacturer instructions and read on an Infinite M200 Pro plate reader (Tecan) at 540 nm absorbance. To control for effects independent of Kras knockdown, Kras-treated wells were normalized against corresponding control siRNA-treated wells, with error propagated accordingly.

Combination knockdown studies: Transfection for combination knockdown studies proceeded identically as above, with the difference that combinations were prepared in two distinct ways: first, by pooling together the disparate siRNA sequences, each at half-concentration, then mixing with peptide to form TPNs (“both”), or second, by forming particles with each siRNA sequence separately, then pooling together the formed particles (“mixed”).

Chapter 3: Modular strategies for stabilizing self-assembled nanoparticles [^]

3.1 Introduction

Nucleic acid therapies hold great promise in modulating or correcting genetically-driven disease processes through modalities such as RNA interference (RNAi) [98], gene delivery [164], and gene editing through RNA-guided endonucleases [83]. However, nucleic acids are natively incapable of crossing cell and endosomal membranes due to their large size and dense negative charges. In addition, nucleic acids are susceptible to enzymatic degradation and can be immunostimulatory when unshielded [98]. Consequently, transportation of nucleic acids to the cell type of interest and subsequently to the correct intracellular compartment requires a delivery vehicle or direct chemical modification. Nanoscale delivery strategies have been broadly successful in preventing off-target delivery of small molecule drugs, making them an appealing solution to address the challenges of nucleic acid delivery. In particular, self-assembled nanomaterials represent an attractive approach to deliver nucleic acids because they can achieve high encapsulation efficiencies, possess a large mass percentage of cargo vs. carrier, enable facile formulation, and afford flexibility in the types and sequences of nucleic acid cargoes that can be incorporated. Like all nanoparticle systems, self-assembled systems can be susceptible to aggregation in biological fluids, which leads to mass accumulation in off-target organs with narrow capillary beds or active reticuloendothelial systems, such as the lungs, liver, and spleen. Self-assembled systems that involve electrostatic complexation of highly anionic nucleic acid cargoes also have an added inherent instability relative to other nanoparticle systems, manifesting as decomplexation in the presence of competing components in blood and tissues [165]. Improving the stability of nanocomplexes is therefore critical for maintaining their

integrity and longevity en route to target tissues and ultimately minimizing off-target delivery.

Particle stabilization strategies have frequently involved incorporation of hydrophilic molecules, most notably polyethylene glycol (PEG), to reduce particle-particle interactions as well as unwanted immune recognition [94]. Examples in the realm of self-assembled technologies include cyclodextrin-containing polymers (using PEG lipids: adamantane-PEG and targeted adamantane-PEG-transferrin) [132], lipidoids (admixed PEG lipids) [166, 167], polyethylenimine (direct PEGylation of the carrier) [168], and cell-penetrating peptides (partial PEGylation of the Pep-3 peptide carrier) [144]. To date, such strategies for overcoming instability have been largely vehicle-specific and empirically determined. Thus, while it is evident that PEG incorporation helps achieve particle stability, it is unclear how important parameters such as size and functional activity of the particles differ between strategies. To elucidate the decision-making process for selecting a method of PEG incorporation, a systematic comparison of modular, easily synthesized stabilizing components that could be deployed across varying platforms is needed.

In this chapter, we employed self-assembled tumor-penetrating nanocomplexes (TPNs), composed of tandem peptide carriers bound to siRNA cargo, to compare three modular particle stabilization strategies. In these studies, we used the original tandem peptide, comprised of a C-terminal targeting and penetrating "CendR" peptide, LyP-1 [169] and an amphipathic cell-penetrating peptide (transportan) [140] modified by an N-terminal saturated fatty acid tail. The targeting moiety, LyP-1, has been used to modify a variety of nanoparticle systems to increase tissue accumulation [170-173]. TPNs are formulated similarly to cationic polymer nanoparticles made from materials such as polyethylenimine and poly-L-lysine [174, 175]. In prior studies,

TPNs have mediated robust knockdown *in vitro* [148] and decreased tumor burden after intraperitoneal delivery of siRNA in a mouse model of advanced, disseminated ovarian cancer [149].

To further develop this technology for use in systemic delivery via the bloodstream - thereby permitting access to specific sites of disease - we hypothesized that modular PEGylated components non-covalently mixed with tandem peptides and siRNA during the complexation process could improve the physical and pharmacokinetic properties of TPNs. We thus sought to profile several chemical approaches to achieve this end. Specifically, we synthesized three classes of PEG-containing components that could self-assemble into our nanoparticle formulation: (1) PEG graft polymers, in which the PEG is pendant from a polymer backbone; (2) PEG lipids; and (3) PEGylated peptide carriers, where the PEGylated additive is a PEG-modified version of the tandem peptide itself. We compared these materials on the bases of particle formation (siRNA encapsulation and particle size), *in vitro* performance (cellular uptake of siRNA, cell-compartment distribution, and knockdown), and *in vivo* profile (blood circulation and organ distribution). In particular, we demonstrated that the addition of PEGylated peptide carrier led to stable nanoparticle formation, robust uptake and endosomal escape of siRNA cargo, preserved RNAi activity, and improved pharmacokinetics with enhanced initial blood circulation and reduced off-target organ accumulation. In the future, modular materials of this construction may be directly employed to stabilize not only newer iterations of tumor-penetrating tandem peptides (such as iRGD TPNs) in the setting of systemic administration, but also to instruct the stable formulation of other self-assembled nanoparticle systems using simple bioconjugation techniques.

3.2 Results

3.2.1 Modular PEG component candidates

As a framework for comparing modular strategies for nucleic acid nanocomplex stabilization, we designed three approaches with contrasting mechanisms of PEG incorporation: (1) Poly-L-Lysine-PEG, which incorporates via electrostatic interactions, (2) distearoylphosphatidylethanolamine (DSPE)-PEG, expected to incorporate into the particle via hydrophobic interactions, and (3) palmitoyl-transportan-PEG, expected to incorporate via a combination of hydrophobic and ionic interactions. For each of the three PEGylated compounds, we used a 5 kDa PEG chain, a length widely used in the literature [176] and successfully applied to several nanoparticle systems in our group [177, 178]. We were also interested in determining whether it is beneficial to display the targeting moiety on the distal end of the PEG chain, as such a modification could potentially improve cell-targeting functionality. For this purpose, we generated both untargeted and targeted (containing covalently-linked LyP-1, the same C-terminal "CendR" peptide on the mTP-LyP-1 tandem peptide) conjugates of each class of PEG (**Fig. 3-1A**). We explored several approaches to forming the PEGylated tumor-penetrating nanocomplexes (TPNs) and found only one order of operations that resulted in stabilized nanoparticles: We first mixed the PEG-containing component with the siRNA in water, then added an equivolume of the tandem peptide carrier (myr-transportan-LyP-1) in water, and finally diluted the particles in the appropriate buffer or media (**Fig. 3-1B**).

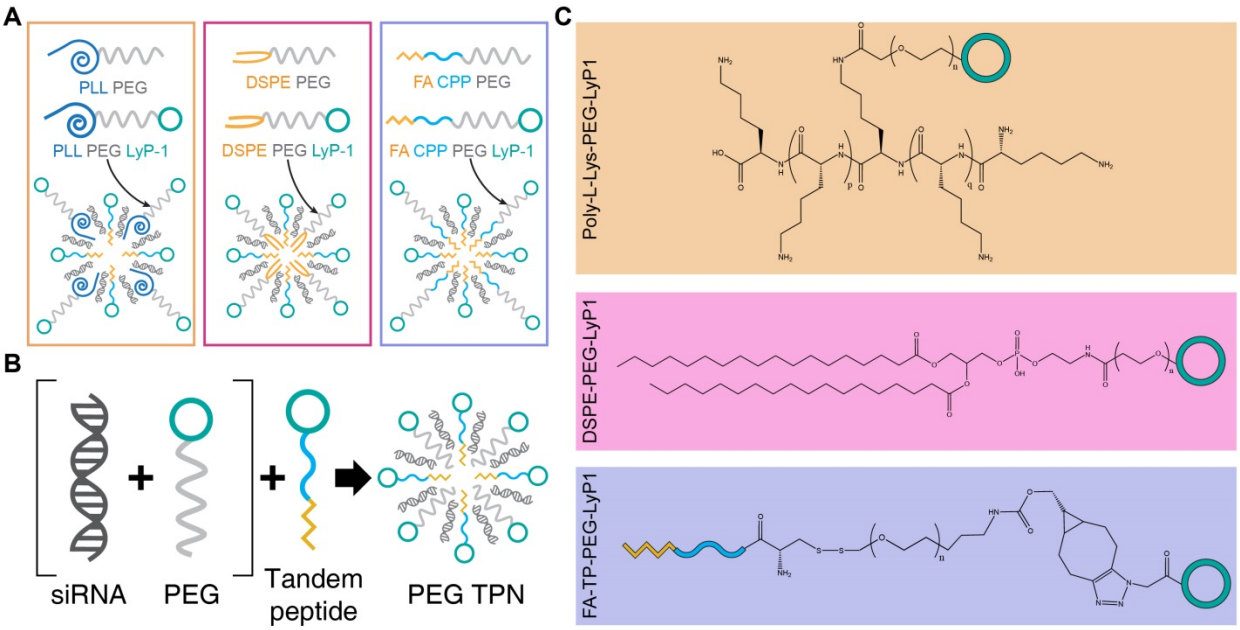

Figure 3-1. Schematic of approach to formulate PEGylated TPNs. (A) Schematic representations of PEG graft polymers, PEG lipids, and directly PEGylated carriers, either untargeted or targeted with the tumor-penetrating peptide LyP-1. **(B)** PEGylated TPNs are synthesized by first mixing siRNA cargo with one of the six PEGylated components at specified ratios, then subsequently adding the tandem peptide component. **(C)** Chemical structures of the three PEG-incorporating materials.

3.2.2 TPNs modified with modular PEG-containing components form stable nanoparticles

We began by comparing the physical properties of PEGylated TPNs to identify the formulation space in which TPNs can maintain nanoparticle stability in ionic solutions (PBS) while still fully encapsulating the siRNA cargo. In these experiments, we maintained a fixed 15:1 ratio of peptide:siRNA (N/P ratio of 2.5) and varied the PEGylated component from 0:1 to 15:1 PEG:siRNA to achieve final peptide:PEG:siRNA ratios ranging from 15:0:1 to 15:15:1. All three chemistries, targeted or not, showed complete encapsulation of free siRNA based on electrophoretic mobility shift assays (**Fig. 3-2A-F**). However, only the DSPE-PEG and pTP-PEG derivatives were able to prevent aggregation of the particles, defined as hydrodynamic diameters that remained below 400 nm after 30 minutes of incubation. Specifically, DSPE-PEG particles were observed to be stable at PEG content ratios of 15:2.5:1 and greater, and pTP-PEG

particles were stable at PEG content ratios of 15:5:1 and greater (**Fig. 3-2**). We were particularly interested in particles with diameters of ~100-200 nm or smaller, which fit within the estimated endothelial gap or fenestration sizes in the tumor vasculature [101] and take advantage of the improved effective diffusion coefficients that come with reduced particle diameter [103]. To satisfy this criterion, the minimum PEG content was 15:2.5:1 for DSPE-PEG, 15:5:1 for DSPE-PEG-LyP-1, and 15:7.5:1 for both pTP-PEG derivatives. To confirm that the hydrodynamic diameters reflected actual particle sizes, and to better understand the particle morphology, we also obtained cryo-TEM images of the 15:15:1 particle formulations of DSPE-PEG and pTP-PEG derivatives formed in PBS (**Fig. 3-3**). These images showed nanoscale particles comparable in size to the DLS measurements, with irregular morphology consistent with the appearance of other self-assembled nanocomplex systems. Recognizing that all these sizing studies focus

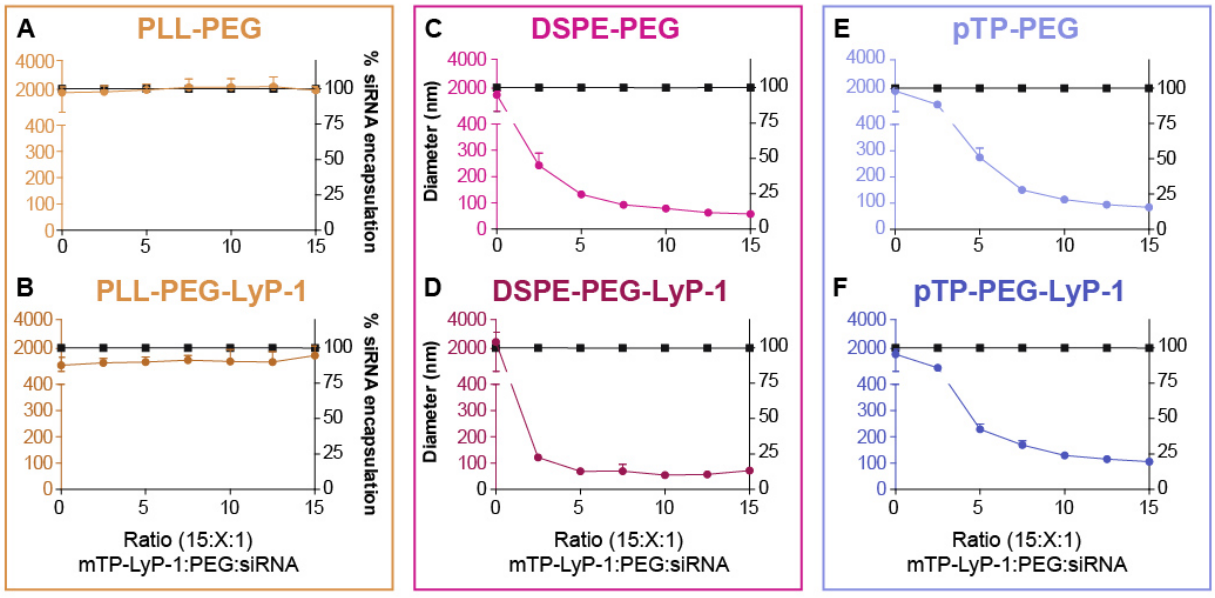

Figure 3-2. Physical properties of PEGylated TPNs. Hydrodynamic diameters and percent siRNA encapsulation for TPNs formed in 1× PBS and formulated with **(A)** PLL-PEG, **(B)** PLL-PEG-LyP-1, **(C)** DSPE-PEG, **(D)** DSPE-PEG-LyP-1, **(E)** pTP-PEG, or **(F)** pTP-PEG-LyP-1. Sizes determined by dynamic light scattering; particles; diameters >~400 nm are unstable. Percentage of siRNA encapsulated in particles determined by electrophoretic mobility shift assay.

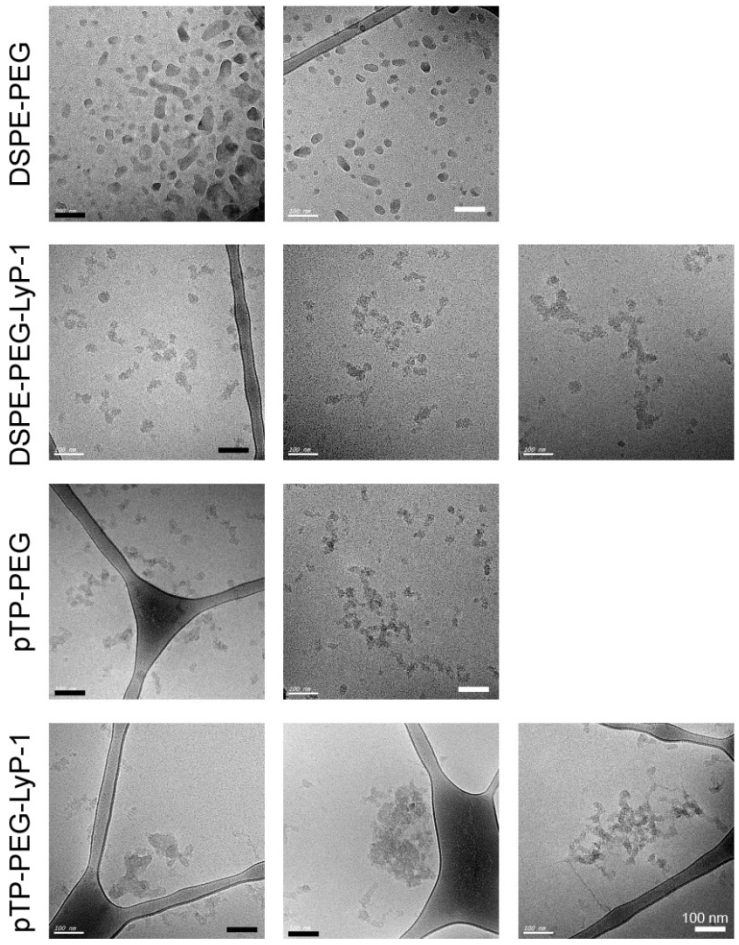

Figure 3-3. Cryo-TEM micrographs of PEGylated TPNs. Particles of each type were formed at a 15:15:1 ratio of peptide:PEG:siRNA. Scale bars: 100 nm.

on stability of the particles specifically in the face of ionic challenge, we next performed sizing studies in the context of 30% exosome-free fetal bovine serum. Here, we found that representative particles in the stable regime, the 15:15:1 pTP-PEG-LyP-1 TPNs, formed equivalent particles in serum and PBS; additionally, incubation at room temperature or at body temperature resulted in only slight changes in particle diameter (**Fig. 3-4**). In summary, modification of TPNs with DSPE-PEG and pTP-PEG derivatives resulted in ratio-dependent stabilization of the particles without compromising siRNA encapsulation.

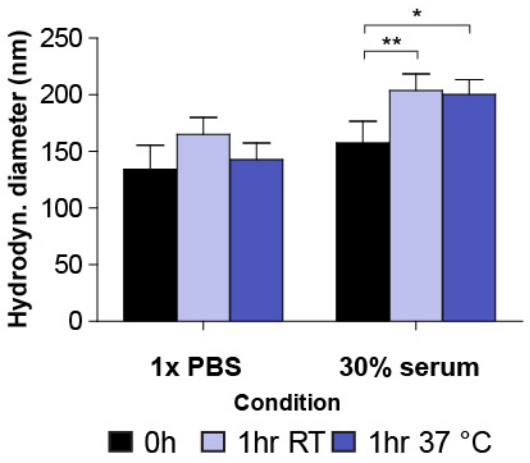

Figure 3-4. Serum stability of PEGylated TPNs. Diameters of 15:15:1 mTP-LyP-1:pTP-PEG-LyP-1:siRNA particles in isotonic buffer or 30% exosome-free FBS at room temperature or physiologic temperature.

3.2.3 Silencing function of PEG-containing TPNs is preserved in a subset of formulations

Excess PEG has been shown previously to have the capacity to interfere with delivery or function of siRNA cargo [179-181]; therefore, we next characterized the functional aspects of PEGylated TPNs *in vitro*. Since PLL-PEG derivatives were not able to stabilize nanoparticles, we focused on testing the DSPE-PEG and pTP-PEG derivatives, particularly at the 15:15:1 ratios that yielded the smallest particle sizes. The OVCAR-8 ovarian cancer cell line aberrantly expresses p32 on its surface, which acts as the receptor for the LyP-1 targeting peptide, thus making these cells suitable models for testing LyP-1-targeted PEG TPNs [149]. We first assessed the association of 15:15:1 PEGylated particles with the cells 24 hours after dosing with TPNs, quantifying both near infrared-labeled siRNA cargo and TAMRA-labeled peptide fluorescence by flow cytometry. This experiment showed that the association of siRNA with cells is increased in the case of TPNs with DSPE-PEG or pTP-PEG derivatives relative to non-PEGylated particles, whereas peptide association is not significantly altered (**Fig. 3-5A**). To determine the localization of siRNA at the cellular level, we visualized cells using fluorescent microscopy 24

hours following TPN dosing. Control non-PEGylated TPNs formed punctate aggregates in cells (**Fig. 3-5B**, bottom left) as well as extracellular formations observed prior to washing and imaging the cells (not shown). In contrast, all the PEG-containing TPN formulations were notable for the absence of punctate aggregates while still displaying diffuse cytoplasmic distributions of siRNA (**Fig. 3-5B**, center and right panels). Finally, to evaluate the function of this cytoplasmic siRNA, we compared the knockdown efficiency of siRNA against a firefly

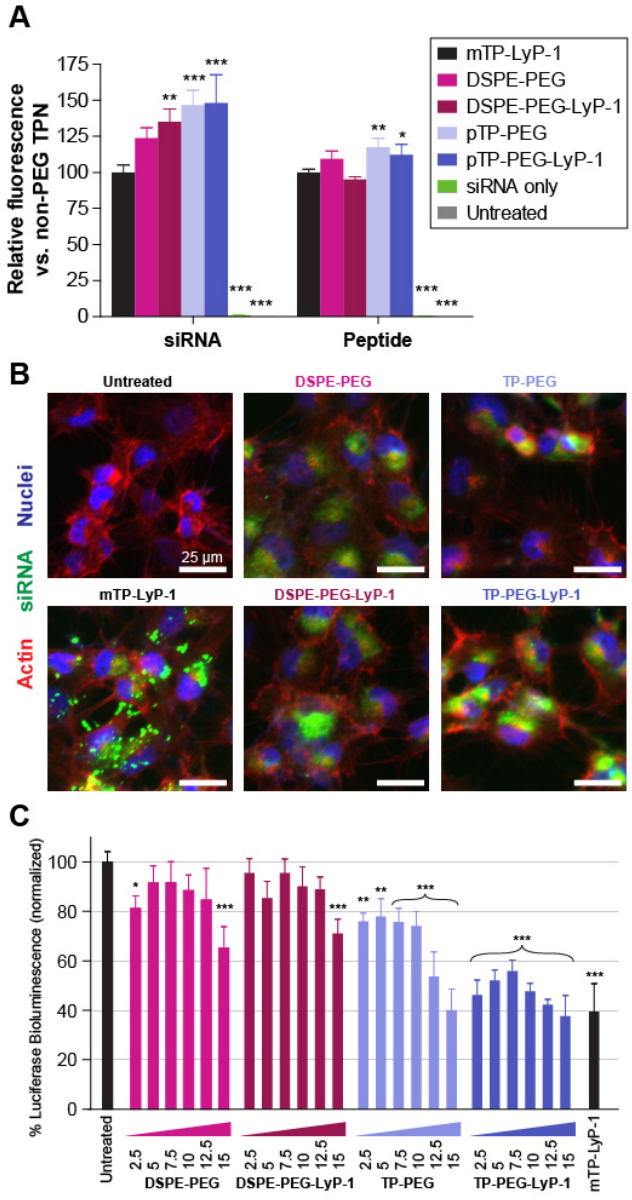

Figure 3-5. ***In vitro*** **functionality of PEGylated TPNs. (A)** 24-hour OVCAR-8 cell uptake of VivoTag750-labeled siRNA (left y-axis) and TAMRA-labeled peptide (right y-axis) incorporated into PEGylated TPNs, formed at a 15:15:1 peptide:PEG:siRNA molar ratio. Quantified using flow cytometry and normalized to mTP-LyP-1-only particles. Statistical significance by one-way ANOVA vs. mTP-LyP-1 particles. *: p<0.05; **: p <0.01; ***: p<0.005. **(B)** Representative fluorescent microscopy of OVCAR-8 cells, showing localization of DyLight-647-labeled siRNA (green). Actin filaments (red: Alexa Fluor 488-phalloidin) and nuclei (blue: Hoechst) stained to show cellular compartments. *Scale bar:* 25 µm. **(C)** 48-hour knockdown of firefly luciferase reporter protein in OVCAR-8 ovarian cancer cells by TPNs with varying ratios of PEG components admixed; measured by bioluminescence. Statistical significance of each condition vs. media-only untreated control determined by one-way ANOVA. *: p<0.05; **: p <0.01; ***: p<0.005.

luciferase reporter stably expressed in the OVCAR-8 cells when delivered by particles with various levels of PEG incorporation (**Fig. 3-5C**). To control for cell number in each well, luciferase activity was normalized relative to the total protein content per well. The knockdown in activity achieved by DSPE-PEG- and DSPE-PEG-LyP-1-containing TPNs was at best around 10-20%. In contrast, significant knockdown was observed in both the pTP-PEG and pTP-PEG-LyP-1 particles, with >20% knockdown in all pTP-PEG conditions and ~50-60% knockdown across all ratios of pTP-PEG-LyP-1-containing TPNs, the latter being equivalent to the level of knockdown mediated by unmodified TPNs in this reporter system.

3.2.4 PEG-containing TPNs show improved blood circulation and organ biodistribution

Based on the favorable physical properties and knockdown capacity of pTP-PEG and pTP-PEG-LyP-1 TPNs, we next sought to establish the *in vivo* profile of these particles. While the circulatory half-life of intravenously-administered nanocomplexes is typically quite brief and often comparable to that of free siRNA [96, 182], we hypothesized that these PEG modifications would modulate the circulatory kinetics by preventing premature clearance. Indeed, in mice injected with TPNs via tail vein (n=5 per condition) and monitored by serial blood draws over 160 minutes, both PEG-containing formulations showed increased blood concentrations in the initial phase through ~20-40 minutes after injection, relative to non-stabilized TPNs (**Fig. 3-6A**). In later phases (80 min. and after), no differences in blood concentration were noted. We hypothesized that these changes in the primary half-life could be linked with differential capture in various organs. To quantify the effect of PEG incorporation

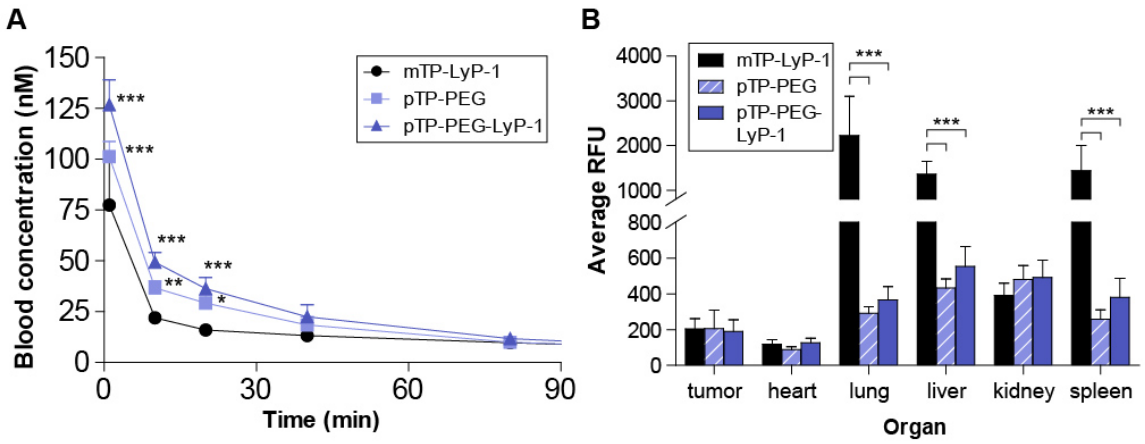

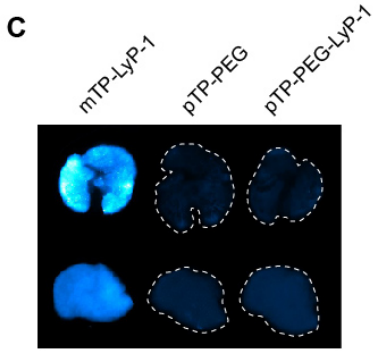

Figure 3-6. *In vivo* properties of PEGylated TPNs. (A) Circulation kinetics of unmodified TPNs and PEG TPNs incorporating pTP-PEG or pTP-PEG-LyP-1 at 15:15:1 peptide:PEG:siRNA ratios, read by near-infrared fluorescence of labeled siRNA. n=5 per condition. **(B)** Organ biodistribution of intravenously-administered unmodified TPNs vs. PEG TPNs with pTP-PEG or pTP-PEG-LyP-1 at 15:15:1 peptide:PEG:siRNA ratios, assessed 3 hours after injection. Statistical significance determined by two-way ANOVA with Bonferroni post-test. ***: $p<0.005$. n=7 per condition. **(C)** Representative near-infrared scans of lungs (top row) and liver lobes (bottom row) from the organ biodistribution experiment presented in panel (B).

on organ accumulation, we performed a biodistribution study in mice bearing subcutaneous flank xenografts of MDA-MB-435 human tumor cells. At three hours after intravenous administration of the PEGylated TPNs, we measured significant reductions in off-target pulmonary (8-fold in pTP-PEG, 6-fold in pTP-PEG-LyP-1), splenic (6-fold and 4-fold, respectively), and hepatic (3-fold and 2-fold) accumulation of siRNA cargo (**Fig. 3-6B**). Meanwhile, modified TPN accumulation remained unchanged in the tumors themselves. Therefore, the relative on-target accumulation was improved with the PEG-containing formulations. Overall, pTP-PEG and pTP-PEG-LyP-1-containing TPNs maintained higher blood concentrations during the first half-hour after administration and, moreover, resulted in greatly decreased distribution into off-target organs.

3.3 Discussion

The goal of this chapter was to compare modular PEG incorporation strategies in order to establish basic principles for electrostatically-complexed nanoparticles intended for systemic administration of siRNA cargo. In these studies, we contrasted three different classes of PEG incorporation strategies – PEG graft polymers, PEG lipids, and directly PEGylated peptide carriers – in their ability to form particles with desirable physicochemical properties while

	PLL-PEG		DSPE-PEG		pTP-PEG	
	- LyP-1	+ LyP-1	- LyP-1	+ LyP-1	- LyP-1	+ LyP-1
Encapsulates siRNA cargo	Yes	Yes	Yes	Yes	Yes	Yes
Forms < 200 nm stable nanoparticles	No	No	15:5:1 and higher	15:2.5:1 and higher	15:7.5:1 and higher	15:7.5:1 and higher
Mediates cell association of siRNA			Yes	Yes	Yes	Yes
Maximum silencing activity			~25%	~30%	~60%	~60%
Improves circulatory profile in systemic admin.					Yes	Yes
Reduces off-target organ accumulation					Yes	Yes

Table 3-1. Summary of results comparing three modular strategies for siRNA nanoparticle stabilization in non-targeted (- Lyp-1) and targeted (+ LyP-1) forms. Molar ratios are expressed as peptide carrier:PEG component:siRNA.

retaining silencing activity, as summarized in **Table 3-1**. To this end, our experiments found that PEG-peptide derivatives exhibited particle stability in physiologically relevant solutions and full packaging of siRNA cargo, while retaining full knockdown efficiency. These TPN

formulations were further examined for stability after intravenous administration in mice and displayed improved circulation and biodistribution profiles.

Comparison amongst the different PEG-incorporating strategies sheds light on possible principles at play in the formation of self-assembling nucleic acid carriers. In the case of the DSPE-PEG and PEG-peptide derivatives that yielded salt-stable particle formulations, adding increasing molar ratios of PEG reduced particle size without compromising incorporation of the siRNA, though the optimal ratio required for stable particle formation varied based on PEG carrier (**Fig. 3-2, Table 3-1**). As demonstrated by the curves depicting size vs. PEG ratio, these modular strategies enable tunability of mean particle size to within a fairly small, predictable range while using a fixed set of starting components, eliminating the need for synthesizing separate chemical entities during optimization. While peptide-PEG and PLL-PEG are both amino acid-based components with siRNA-binding capacity, only the peptide-PEG derivatives stabilized particles in the range tested. These empiric differences are likely due to the architecture of the two strategies: peptide-PEG was synthesized such that the peptide and PEG portions are oriented linearly, while PLL-PEG was synthesized by grafting PEG onto the side chains of PLL.

Another instructive dimension of these studies is the orthogonal view between physicochemical properties and functional activity of TPNs containing DSPE-PEG and peptide-PEG derivatives. Although stable particles can be achieved by a variety of methods, it has been documented that stabilization often comes at the expense of knockdown activity in siRNA carriers [179-181]. While both strategies generate stable particles and exhibit similar levels of cell association, the activity of peptide-PEG stabilized particles far outperformed their DSPE-PEG

counterparts at similar ratios (**Fig. 3-5C**), even after accounting for variables like particle size. In particular, the only formulation that performed on par with non-stabilized formulations was the targeted peptide-PEG-LyP-1. In the context of lipid-based carriers such as liposomes, DSPE-PEG is often an indispensable part of the formulation, but within the scope of self-assembled nanocomplexes examined here, we observed considerable decreases in knockdown activity compared to unmodified TPNs. The difference in activity between DSPE-PEG and peptide-PEG was not due to total material taken up by cells, as determined by quantification of cellular uptake using flow cytometry (**Fig. 3-5A**). It is possible that the PEG moiety affected nanoparticle release and accessibility of siRNA post-endosomal escape, and although the intracellular siRNA appears to show similar cytosolic distributions in each case (**Fig. 3-5B**), particles may be differentially trafficked. The functional activity of the various formulations depended not only on the type of derivative but also the relative ratio between the PEG concentration and the carrier peptide concentration. Improvements with additional PEG were seen in several PEG constructions, but we also noted – in line with studies in the literature – that particles formed purely of PEGylated material and siRNA show essentially no function (data not shown) [144, 179].

In our animal studies, we observed increased initial circulatory concentration of siRNA with PEGylated TPNs (**Fig. 3-6A**), consistent with the concomitant reduction in non-specific organ accumulation (**Fig. 3-6B**) and *in vitro* demonstration of size stability following serum incubation through at least one hour (**Fig. 3-4**). We did not note changes in tumor accumulation based on adding targeting to the PEG component, likely because the core carrier (mTP-LyP-1) was targeted in all formulations and was represented in the carrier at equal mole equivalents as

PEGylated material. Similar uptake between formulations was also reflected in the cellular association/uptake studies (**Fig. 3-5A**). Nevertheless, knockdown activity of peptide-PEG-LyP-1 nanoparticles was higher *in vitro* when compared to untargeted peptide-PEG nanoparticles (**Fig. 3-5C**), suggesting that there is an important role for targeting in the steps beyond organ-level localization. The PEG-targeting strategy represented here can be easily adopted for the introduction of alternative targeting moieties using the bio-orthogonal click chemistry handle, such as folate [183], transferrin [132, 184], and GalNAc [185].

Another key aspect of biodistribution studies is the issue of non-specific accumulation, known in the literature to be a major source of nanoparticle toxicity [94, 176]. We noted encouraging reductions in lung, liver, and spleen accumulation with PEG-containing formulations of TPNs. Entrapment in the lung capillaries – a first-pass effect that is often the consequence of large particle size or exposed cationic charges – was dramatically reduced by addition of either LyP-1 targeted or untargeted peptide-PEG components, showing up to an 8-fold decrease. This effect was confirmed by imaging, in which mice dosed with unmodified TPNs showed pronounced medium- and small-vessel fluorescence, absent from the lungs of mice dosed with PEGylated TPNs (**Fig. 3-6C**). Furthermore, it is likely that the altered surface characteristics following incorporation of hydrophilic PEG molecules as well as smaller particle size resulted in reduced recognition by the RES system in the liver and spleen [186], a well-known mechanism for rapid nanoparticle clearance.

As a whole, this study is a roadmap for future iterations of peptide-based nucleic acid carriers, even as targeting domains and cargoes are replaced and the applications of the technology are broadened. We have presented bioconjugate strategies that are easily adaptable

for any peptide sequence and accessible to non-chemists. We have also developed a battery of metrics that are generally available to many laboratories in order to discriminate between formulations for eventual systemic delivery. Particularly, our data suggest that PEG incorporation to preserve the architecture of the nanoparticle system may be a useful tactic for improving the stability, activity, and pharmacokinetics of the resulting nanocomplexes. Proximally, we are thus interested in applying this approach to stabilizing iRGD TPNs for use in PDAC, presented in Chapter 4 of this thesis. More broadly, we also believe this principle can also be extended to other electrostatically-assembled systems, as any nanoparticulate nucleic acid delivery platform designed for clinical applications will likely incorporate PEG or other stabilizing molecules as part of the formulation.

3.4 Methods

siRNA: siRNA was synthesized by Thermo Scientific/Dharmacon. Two sequences were used for these studies: negative control non-targeting siRNA (siNC, based on a control sequence published by Qiagen), sense strand 5′-UUCUCCGAACGUGUCACGUUU-3′; and firefly luciferase siRNA (siLuc), sense strand 5′-CUUACGCUGAGUACUUCGA-3′. All siRNAs were synthesized with dTdT overhangs. For the gel mobility shift assay and microscopy imaging, siLuc was synthesized with a 5′ DyLight 677 fluorophore or 5′ DyLight 647 fluorophore, respectively.

Near-infrared siRNA labeling: For biodistribution studies, siNC with 5′ and 3′ amine termini was labeled with VivoTag-S750 amine-reactive dye (Perkin Elmer) by reacting the siRNA with a 10:1 molar ratio of dye to siRNA for 1 hour shaking at room temperature. siRNA was purified twice by precipitation. siRNA yield and labeling efficiency were quantified on a NanoDrop spectrophotometer (Thermo Scientific). Final labeling was ~2.4 dyes per siRNA duplex.

Peptides: Myristoyl-transportan-LyP-1 tandem peptide was synthesized by CPC Scientific (sequence: myr-GGWTLNSAGYLLGKINLKALAALAKKIL-GGGG-CGNKRTRGC, Cys-Cys bridge). Fluorescently-labeled peptide was synthesized by Selleckchem, with a tetramethylrhodamine (TAMRA)-tagged lysine inserted into the glycine spacer. FAM-labeled LyP-1 bearing an azide (Azidoacetyl-GGG-cyclo-(EGNKRTRGK)), FAM-labeled LyP-1 bearing a

cysteine (C-K(5FAM)-C6-cyclo(CGNKRTRGC)) and transportan bearing a C-terminal cysteine (myristic acid-GGWTLNSAGYLLGKINLKALAALAKKILC) were synthesized by CPC Scientific, Inc.

DSPE-PEG and DSPE-PEG-LyP-1 synthesis: DSPE-PEG-MAL 5K (Nanocs) was reacted with 1.1 equivalents of cysteine-bearing LyP-1 in 50 mM triethylamine, N,N-dimethylformamide and stirred overnight. The final conjugate was purified into water using a PD-10 desalting column (GE Healthcare Life Sciences). DSPE-PEG 5K was purchased from Avanti Polar Lipids.

pTP-PEG and pTP-PEG-LyP-1 synthesis: OPSS-PEG-SVA 5K (Laysan Bio) was reacted with 5 equivalents of N-[(1R,8S,9s)-Bicyclo[6.1.0]non-4-yn-9-ylmethyloxycarbonyl]-1,8-diamino-3,6-dioxaoctane (Sigma) for 3 hours at room temperature. The resulting conjugate was dialyzed using a 3,500 MWCO membrane and lyophilized. This product was dissolved in DMF and reacted with 1.2 equivalents of transportan bearing a C-terminal cysteine for 3 hours at room temperature. 1.2 equivalents of LyP-1-azide were added and reacted further overnight. The final product was dialyzed using a 3,500 MWCO membrane into water. pTP-PEG was synthesized by omitting the LyP-1 peptide.

PLL-PEG and PLL-PEG-LyP-1 synthesis: OPSS-PEG-SVA was added to 1-5 kDa Poly-L-Lysine (Sigma-Aldrich) to modify 5% of lysines. The mixture was reacted for 1 hour at room temperature in PBS. 1.2 equivalents of cysteine-bearing LyP-1 were added and reacted overnight. Unreacted LyP-1 was removed using a PD-10 desalting column. PLL-PEG was synthesized by omitting the LyP-1 peptide.

Nanoparticle formulation: All siRNA, PEG-containing components, and peptides were resuspended as concentrated stocks in nuclease-free water (Life Technologies). Particles were formulated by mixing the siRNA, PEG-containing component, and peptide in 1:1:2 volumetric ratios, first thoroughly mixing the siRNA with the PEG and subsequently mixing in the peptide to create a concentrated solution of TPNs. Finally, this solution was adjusted to the desired dilution and buffer composition with appropriate diluent.

Dynamic light scattering: TPNs were formulated at 15:1 peptide:siRNA molar ratios and 0-15:1 PEG:siRNA. 10x RNAse-free PBS pH 7.4 (Life Technologies) was added after particle formation to achieve 1x PBS and a final siRNA concentration of 200 nM. Hydrodynamic diameters were obtained using a DynaPro Plate Reader (Wyatt Technology) to analyze 50 μL of each sample, n=3 per condition.

Gel mobility shift assay: TPNs were formed at the specified ratios for a final concentration of 200 nM siRNA (DyLight 677-siLuc) in 1x PBS. 10 uL of each TPN sample or free siRNA was mixed with 2 uL of 30% glycerol and loaded into a 2% agarose gel. The gel was run at 100 V for 45 minutes in 1x TAE buffer and siRNA fluorescence was imaged on a LI-COR Odyssey infrared scanner. Signal was quantified using ImageJ.

Cell culture: OVCAR-8 cells stably expressing firefly luciferase (OVCAR-8 Luc+) were a generous gift from the lab of Joyce Liu (Dana Farber Cancer Center). They were cultured in RPMI 1640 media with 10% FBS and 100 U/mL penicillin/100 μg/mL streptomycin. Unless stated otherwise, OVCAR-8 Luc+ cells were plated in 96-well plates with 8,000 cells per well 24 hours prior to the start of each experiment. MDA-MB-435 cells (ATCC) were grown in DMEM with 10% FBS and 100 U/mL penicillin and 100 μg/mL streptomycin.

Transfection: For all *in vitro* transfection assays, TPNs were formed at the specified ratios for a final concentration of 100 nM siRNA in Opti-MEM serum-free media (Life Technologies, Gibco). TAMRA-labeled tandem peptide was used to allow tracking and quantification on microscopy and flow cytometry. Cells were dosed in 96-well plates by removing growth media and adding 100 nM TPN solution, n=4 per condition. After 4-6 hours of incubation at 37 °C, media was replaced with RPMI 1640 supplemented with 10% fetal bovine serum for a further 20 hours.

Luciferase knockdown: OVCAR-8 Luc+ cells were transfected with 100 nM siLuc using the standard protocol above. Forty-eight hours after transfection, luciferase activity was assessed using the firefly Luciferase Assay System (Promega) and protein content of each well was determined using the bicinchoninic acid assay (Pierce). Bioluminescent signal was quantified on an Infinite M200 Pro plate reader (Tecan) and normalized by total protein content of each well.

Microscopy: OVCAR-8 cells were plated at 8,000 cells/well on black glass-bottom 96-well plates pre-coated for 30 minutes with 100 μg/mL rat tail collagen (Becton Dickinson Biosciences). Cells were transfected with TPNs at the stated ratios with a final concentration of 100 nM DyLight 647-siRNA. After 24-hours, cells were rinsed with CellScrub Buffer (Genlantis) to remove nonspecifically adsorbed materials and fixed with 4% paraformaldehyde. Cells were stained with Alexa Fluor 488 conjugated phalloidin (Invitrogen) according to manufacturer's instructions.

Uptake flow cytometry: OVCAR-8 cells were transfected in a 96-well plate as described above, n=4 per condition. Twenty-four hours after the start of transfection, cells were trypsinized and brought to single-cell suspension in 100 μL PBS + 2% FBS. TAMRA-peptide fluorescence (561/582) and VivoTag-S750-siLuc fluorescence (640/780) in live single cells was measured on a BD LSR II flow cytometer and analyzed using FlowJo software.

Circulation time: Swiss Webster mice were intravenously (tail vein) injected under isoflurane anesthesia with non-PEGylated TPNs, 15:15:1 pTP-PEG TPNs, or 15:15:1 pTP-PEG-LyP-1 TPNs at 0.5 nmol siRNA dose per mouse, n=5 per condition. VivoTag-S750 siRNA was used to minimize interference from autofluorescent background. Retro-orbital blood draws (10 μL each) were taken at 1, 10, 20, 40, 80, and 160 minute timepoints following injection using heparinized glass capillaries (VWR) and scanned using a LI-COR Odyssey near-infrared scanner. Fluorescence was quantified using ImageJ and converted to blood concentrations using a standard curve of ex vivo blood samples spiked with known concentrations of VivoTag-labeled siRNA.

Organ biodistribution: NCR/nude mice were implanted with MDA-MB-435 xenografts subcutaneously (5x106 cells per flank, bilaterally) and tumors were allowed to grow for approximately 1 month when the primary axis diameter reached ~5 mm. The mice were then injected intravenously in the same manner and dose as for the circulation time study using VivoTag-S750 labeled siRNA, n=7 per condition. After 3 hours, mice were euthanized and necropsy was performed to remove the lungs, heart, left kidney, one liver lobe, spleen, and both tumors. Organs were scanned using a LI-COR Odyssey near-infrared scanner (LI-COR Biosciences) and analysis of average fluorescence intensity was performed in ImageJ.

Statistical Analysis: Knockdown data were analyzed by one-way ANOVA with Tukey post-test. siRNA uptake, circulation time, and organ biodistribution were analyzed by two-way ANOVA with Bonferroni post-test. All statistical analyses were performed using GraphPad Prism software.

Chapter 4: PEGylated iRGD TPNs for siRNA delivery to pancreatic cancer [^]

4.1 Introduction

We have now shown that iRGD-targeted TPNs mediate robust knockdown of single and multiple targets in PDAC cells *in vitro* (Chapter 2) and that TPNs formed with the original LyP-1 tandem peptides can be stabilized using various modular techniques for incorporating PEG (Chapter 3). The head-to-head comparison of these different techniques (summarized in **Table 3-1**) clearly demonstrated the superiority of stabilizing TPNs with PEGylated peptide derivatives constructed as fatty acid-CPP-PEG-targeting peptide conjugates, so we wished to apply this principle to iRGD-targeted PEG components to generate "second-generation TPNs." In this chapter, we characterize PEGylated iRGD TPNs on the basis of particle formation and stability, pharmacokinetics, distribution into various models of PDAC, and capacity to deliver therapeutically active siRNA to a xenograft model of PDAC. We show that the addition of transportan-PEG-iRGD to the formulation of iRGD TPNs confers the same nanoparticle stability and beneficial pharmacokinetic properties seen with LyP-1 TPN reformulation, thus enabling uniform delivery of siRNA cargo to advanced pancreatic tumors *in vivo* through intravenous administration. A first study in the use of PEGylated iRGD TPNs as a therapeutic agent showed statistically significant inhibition of tumor growth in a trial comparing gemcitabine standard-of-care, siKras TPNs, and placebo, though this result will require future follow-up to complete characterization of the delivery system *in vivo*.

4.2 Results

4.2.1 Addition of peptide-PEG conjugates stabilizes iRGD TPNs

We adapted the biochemical synthesis described in Chapter 3 to insert PEG linearly between fatty acid-transportan and iRGD, separating the CendR domain from the CPP-siRNA particle core so as to leave it accessible for target binding (**Fig. 4-1A**). Particles containing various ratios of mTP-iRGD:mTP-PEG-iRGD:siRNA all fully encapsulated siRNA cargo based on a gel electrophoretic mobility shift assay, with the exception of particles composed entirely of mTP-PEG-iRGD and siRNA (**Fig. 4-1B**). As with the LyP-1 TPNs, increasing the proportion of PEG-peptide in the TPNs yielded smaller and more stable particles based on dynamic light scattering (DLS) (**Fig. 4-1C**), confirmed on TEM (**Fig. 4-1D**). To further characterize the degree

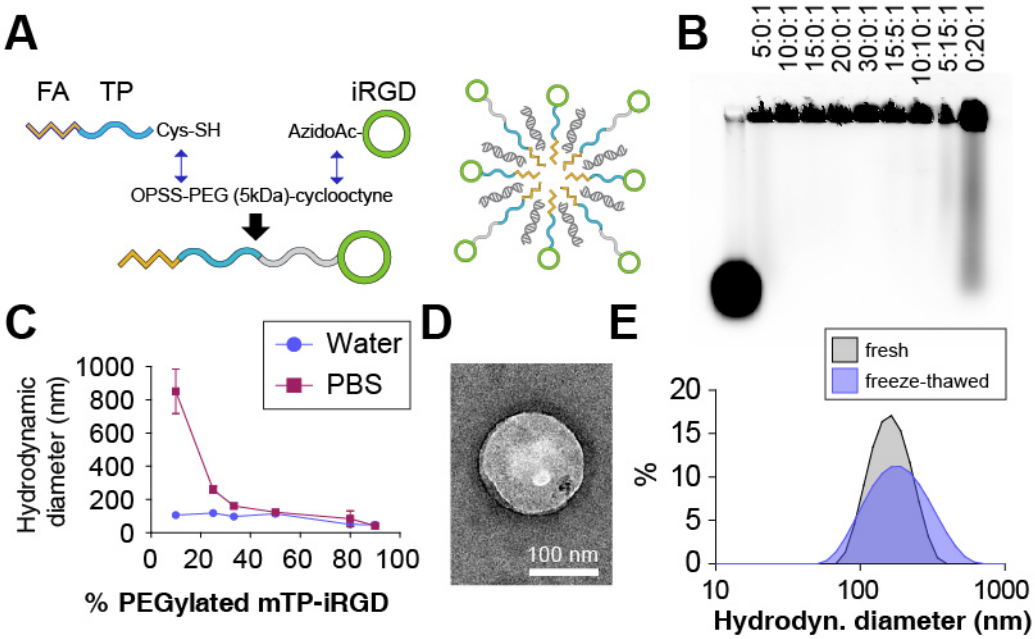

Figure 4-1. Physical properties of PEGylated iRGD TPNs. (A) Summary of chemical synthesis of transportan-PEG-iRGD and schematic of PEGylated iRGD TPN. **(B)** Electrophoretic mobility shift assay showing encapsulation of siRNA cargo at various peptide:PEG:siRNA ratios as indicated above each lane. **(C)** iRGD TPN hydrodynamic diameter as a function of PEG content, determined by dynamic light scattering. **(D)** Representative TEM of an iRGD TPN composed at a 10:10:1 peptide:PEG:siRNA ratio in 1x PBS. **(E)** DLS sizing histogram comparing fresh TPNs and reconstituted particles following a freeze-thaw cycle.

of particle stability, we subjected 10:10:1 PEGylated iRGD TPNs to a prolonged freeze-thaw cycle, showing that the particle distribution among thawed particles closely mirrored that of the original, freshly-made particles (**Fig. 4-1E**). This suggests that either the particles remain intact through freezing, or that self-assembly occurs reproducibly upon restoration of the original temperature conditions.

We next wished to determine whether PEGylation might impact the endosomal escape process, a key function of tandem peptides and CPPs in general, so we compared the free PEGylated peptide and regular mTP-iRGD species in their capacity to lyse red blood cells (RBCs). At concentrations representative of those achieved in the endosome (rather than the lower concentrations in the bloodstream), we found that the RBC lysis curves were virtually indistinguishable (**Fig. 4-2A**). Similarly, TPNs composed of different ratios of PEGylated and non-PEGylated tandem peptides showed comparable RBC lysis curves (**Fig. 4-2B**). These findings are corroborated by microscopy images showing that PEGylated iRGD TPNs rapidly associated with cells and endosomes (**Fig. 4-2C**, fluorescently-tagged peptide localization at 5 hours) and led to diffuse cytoplasmic release of siRNA cargo (**Fig. 4-2D**, fluorescently-tagged siRNA localization at 24 hours). Meanwhile, comparisons between images of cells treated with PEGylated vs. plain TPNs reveal extracellular peptide (**Fig. 4-2C**, right, white arrowheads) and siRNA (**Fig. 4-2D**, right) aggregates in the non-PEGylated conditions that were entirely absent with PEG-stabilized particles. Thus, addition of TP-PEG-iRGD to iRGD TPNs stabilizes the complexes as nanostructures, preventing aggregation while still allowing endosomal escape and cytoplasmic delivery of siRNA cargo.

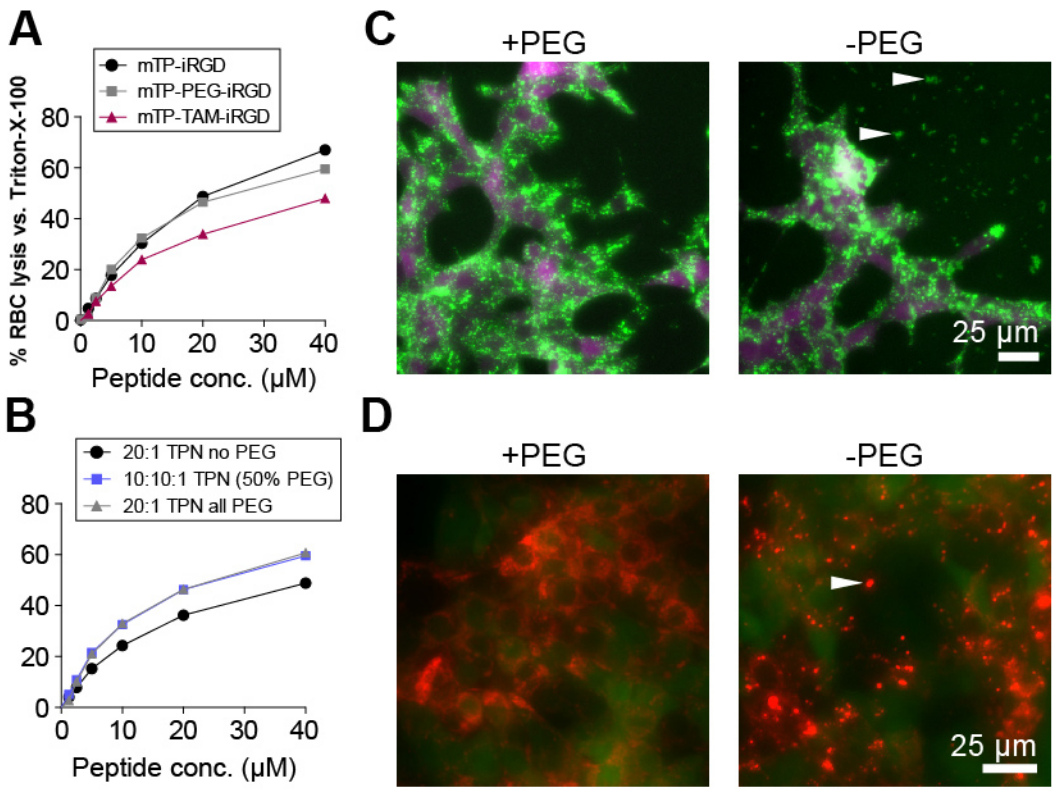

Figure 4-2. Capacity of PEGylated iRGD tandem peptides and TPNs to mediate endosomal escape. **(A)** Red blood cell lysis assay to determine endosomal escape capacity as a function of peptide or peptide-PEG concentration. **(B)** RBC lysis assay for formed iRGD TPNs as a function of peptide concentration in the TPNs. **(C)** Localization of fluorescently-tagged mTP-iRGD 5 hours after transfection with 10:10:1 (left) or 10:0:1 (right) iRGD TPNs. White arrowheads indicate aggregates that are not localized to any cells. Green: TAMRA-labeled peptide; Magenta: GFP (cells) **(D)** Localization of fluorescently-tagged siRNA 24 hours after transfection with 10:10:1 (left) or 10:0:1 (right) iRGD TPNs. Red: DyLight-647-labeled siRNA; Green: GFP (cells).

4.2.2 Impact of PEG incorporation and fatty acid selection on particle function

It is known that over-PEGylation can inhibit delivery of siRNA [11], so we also compared the knockdown of various PEG ratios. In B22 cells, superimposed plots of particle size and luciferase knockdown at various PEG doping levels show that there is a clear window (in the range of ~15:2.5-5:1) where knockdown still occurs and the particles are stabilized (**Fig. 4-3A**). More reassuringly, *KRAS* knockdown in PANC-1 cells was only moderately impacted by the higher ratios of PEGylated peptides (**Fig. 4-3B**). Therefore, PEGylated iRGD TPNs maintain function *in vitro* while improving nanoparticle properties.

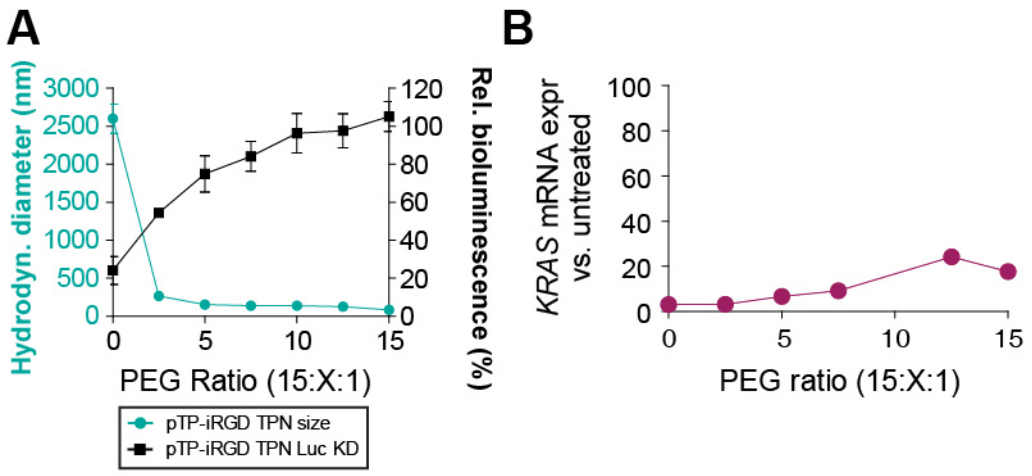

Figure 4-3. Impact of PEGylation on iRGD TPN-mediated knockdown. (A) Comparison between particle size and 48-hour luciferase knockdown in B22 cells at various ratios of PEG incorporation. **(B)** *KRAS* knockdown in PANC-1 cells at various ratios of PEG incorporation.

Another dimension of iRGD TPN formulation not yet explored is the impact of the N-terminal fatty acid's chain length on TPN function and toxicity. To investigate this variable, we synthesized three peptide variants of transportan-iRGD bearing myristic acid (C_{14}), palmitic acid (C_{16}), or stearic acid (C_{18}) N-terminal tails. In B22 cells, we saw that shorter fatty acid chains led to greater apparent knockdown of luciferase, but control cells treated with a negative control siRNA also showed the same trend of reduced luciferase activity, likely reflective of general toxicity (**Fig. 4-4A**). Furthermore, in PANC-1 cells, we quantified *KRAS* mRNA knockdown to be equivalently potent for mTP-iRGD and pTP-iRGD, but less so for sTP-iRGD (**Fig. 4-4B**). From these studies, we concluded that palmitoyl-modified peptides represented strong knockdown while showing reduced toxicity associated with myristoyl-modified peptides, though these effects were fairly subtle. Thus, going forward, we focused on using pTP-iRGD and pTP-PEG-iRGD as the core reagents for forming iRGD TPNs.

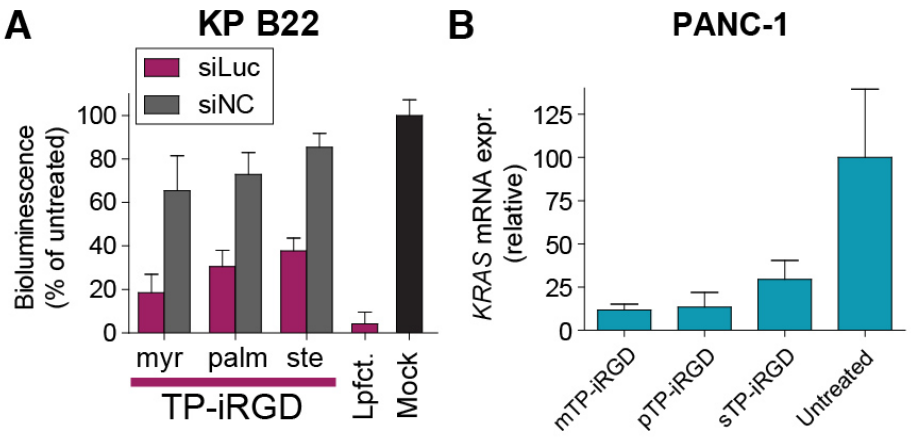

Figure 4-4. Comparison between iRGD tandem peptides bearing different N-terminal lipid tails. **(A)** 48-hour luciferase activity following transfection of siLuciferase or control siRNA (siNC) by tandem peptides with fatty acid tails of different length. **(B)** 48-hour *KRAS* mRNA knockdown by TPNs composed of tandem peptides with variable fatty acid tail length.

4.2.3 PEGylation of iRGD TPNs improves their pharmacokinetic profile

To study the ramifications of PEG stabilization on iRGD TPN pharmacokinetics, we first injected PEG TPNs (10:10:1) particles into mice to contrast the organ biodistribution against non-PEGylated TPNs (**Fig. 4-5A**), noting marked reductions in lung, spleen, and liver accumulation consistent with the changes seen following PEGylation of LyP-1 TPNs. PEGylation also had a modest effect on extending the blood circulation time of iRGD TPNs (**Fig. 4-5B**), resulting in a ~30% increase in primary half-life when using a biexponential decay to fit the circulatory concentration data. These results demonstrate the generalizability of the PEG-induced pharmacokinetic changes first documented in **Figure 3-6**.

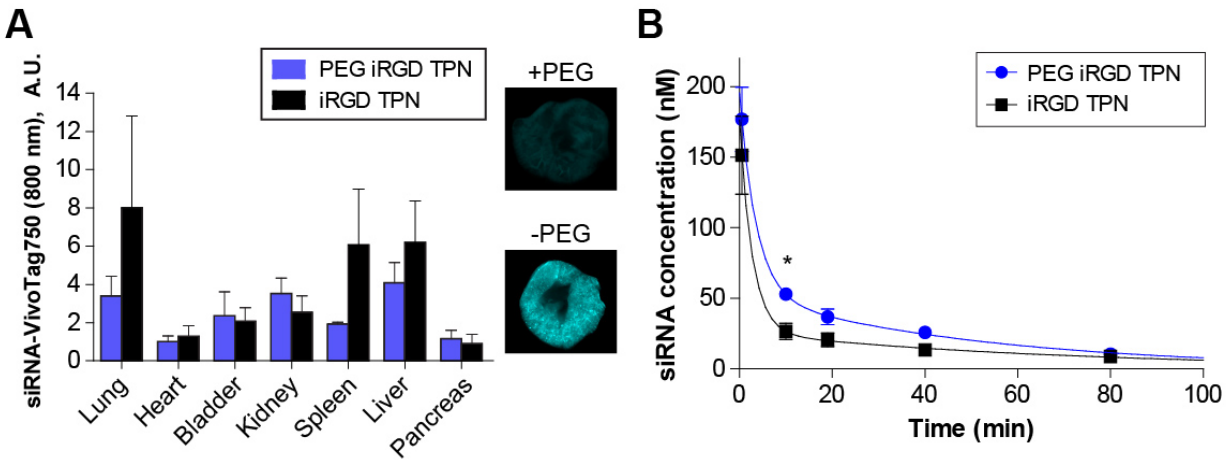

Figure 4-5. Pharmacokinetic properties of PEGylated iRGD TPNs. (A) Organ biodistribution of siRNA delivered by systemically-injected PEGylated vs. plain iRGD TPNs. Inset: comparison between lungs of animals dosed with PEGylated TPNs (above) and plain TPNs (bottom). **(B)** Comparison of circulation kinetics of PEGylated vs. plain iRGD TPNs. Curve fit is a biexponential decay.

4.2.4 Delivery of siRNA to animal models of PDAC

The use of CendR-based cyclic peptides for delivery of RNAi to PDAC *in vivo* is justified by prior evidence pointing to the applicability of iRGD to pancreatic cancer. Indeed, iRGD has been previously shown to home to and penetrates deep into both orthotopic models of PDAC [7]. To show that this effect still applies when iRGD is tethered to TPNs, we first injected PEGylated iRGD TPNs into mice bearing orthotopically-implanted PDAC allografts (B22 cells), either intravenously (representative image: **Fig. 4-6A, left**) or intraperitoneally (representative image: **Fig. 4-6A, right**). We noted that accumulation of siRNA was present throughout the tumor receiving the dose intravenously, whereas the tumor receiving the dose intraperitoneally only showed accumulation around the outer rim of the tumor. We next injected PEGylated iRGD TPNs into mice bearing advanced (~1 cm or larger) GEM PDAC (tumor genotype: $Kras^{G12D/+};p53^{-/-}$), showing uniform delivery throughout the tumors (representative cross-section and linear intensity traces shown in **Fig. 4-6B**).

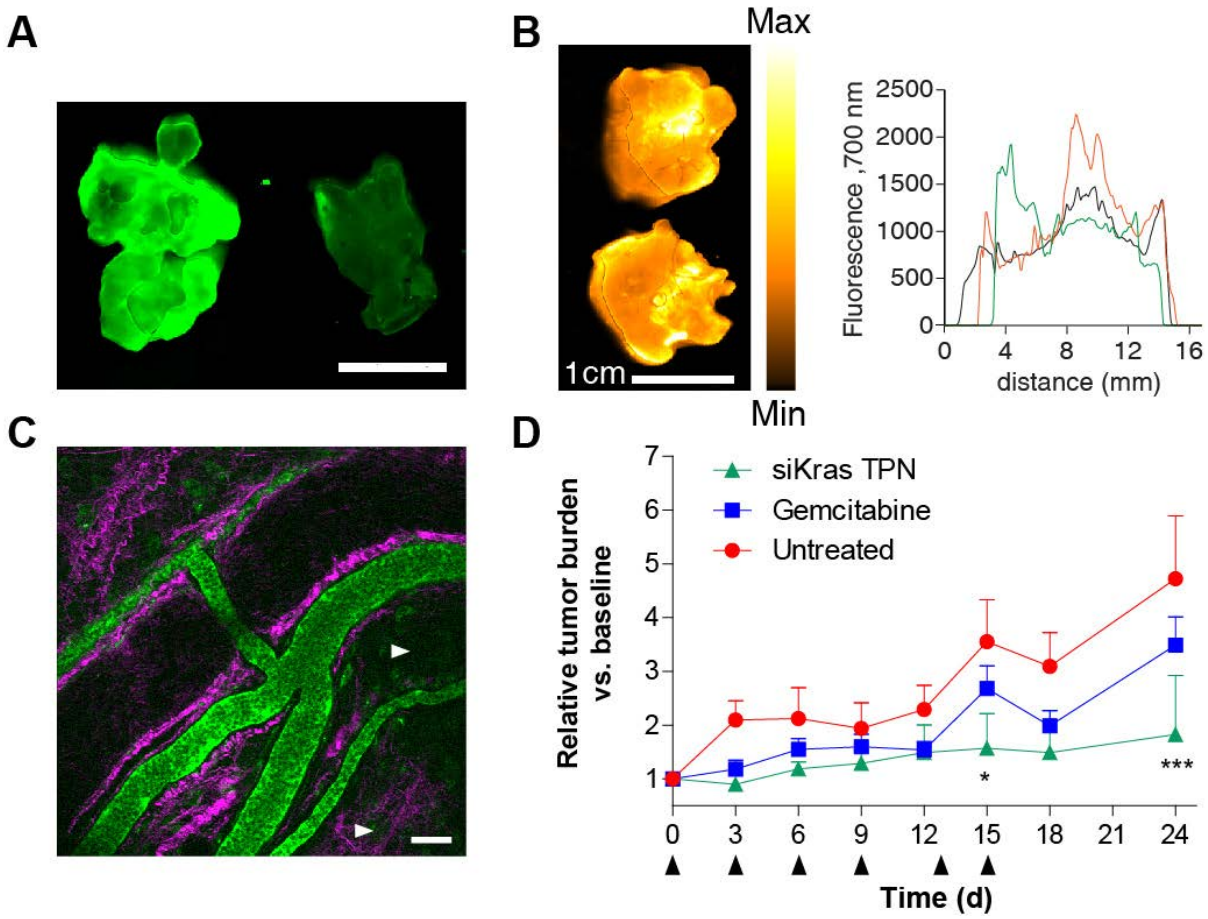

Figure 4-6. iRGD TPN-mediated delivery of siRNA in models of pancreatic cancer. (A) PEGylated iRGD TPN delivery of fluorescently-tagged siRNA (green) to orthotopic pancreatic cancer allografts, either intravenously (left) or intraperitoneally (right). Scale bar = 1 cm. **(B)** PEGylated iRGD TPN delivery of fluorescently-tagged siRNA to a Kras-p53 GEM model of PDAC, with representative tumor cross-sections shown at left and linear intensity traces shown at right. **(C)** Intravital imaging of a subcutaneous pancreatic cancer xenograft showing PEGylated iRGD TPNs (green) in the bloodstream and accumulation in the particles in tumor cell compartments (white arrowheads). Still image taken 8 minutes following injection at a depth of 80 µm from the surface. Scale bar = 50 µm. **(D)** Normalized growth curves of mice bearing MIA PaCa-2 flank tumors treated with gemcitabine, PEGylated iRGD TPNs carrying siRNA against *KRAS*, or left untreated. Error bars indicate SEM. Statistical significance determined by two-way ANOVA with Bonferroni post-test, *: $p < 0.05$; ***: $p < 0.001$.

To understand the dynamics of TPN distribution in the tumor leading to the observed tumor accumulation in the preceding biodistribution experiments, we performed timelapse intravital imaging on MIA PaCa-2 flank xenografts in animals dosed with PEGylated iRGD TPNs. In these intravital timelapse sequences, we noted that TPN accumulation had already begun by the first image 5 minutes after injection, with a plateau reached at ~10 minutes (**Fig. 4-**

6C). This is consistent with the circulation kinetics measured previously as well as unpublished observations by collaborators that free iRGD-mediated accumulation is greatest at ~15-30 minutes post-injection. Moreover, fluorescent pixels consistent with optically resolvable collections of complexes were visualized in all regions of the tumor, including the otherwise "dark" regions outside the stroma and vessels that are likely occupied by tumor cells. Interestingly, in tumor vessels with irregular circulation patterns, the TPN fluorescent intensity was maintained throughout the imaging period, in contrast to the circulation profile obtained from retro-orbital blood draws, suggesting that particles may persist in the tumor circulatory environment with a longer half-life than in general circulation.

With evidence of tumor-penetrating delivery of siRNA to pancreatic tumors, we have begun therapeutic trials in a MIA PaCa-2 xenograft model of pancreatic cancer, a model cell line selected based on our earlier results in Chapter 2 showing receptor expression for iRGD and growth inhibition *in vitro* in response to *KRAS* knockdown. In the initial trial, we compared systemic treatment with siRNA against *KRAS* ("siKras") delivered by PEGylated iRGD TPNs with standard intraperitoneally-delivered chemotherapy (gemcitabine) or no treatment (placebo injections only), dosed six times over 18 days. siKras treatment resulted in statistically-significant slowing of tumor growth, with tumor burden increasing to 1.8 times the original volume over 24 days after the start of treatment, compared to 4.7 times in the untreated group and 3.5 times in the gemcitabine-treated group (**Fig. 4-6D**).

Thus, PEGylated iRGD TPNs deliver siRNA rapidly to tumors in a highly distributed fashion throughout the tumor tissue, and treatment with iRGD TPNs delivering siRNA against *KRAS* preliminarily results in slowed tumor growth.

4.3 Discussion and future work

In this chapter, we have shown that the preferred PEG formulation identified in Chapter 3 involving the non-covalent addition of targeted transportan-PEG conjugates is extensible to use in iRGD-targeted TPNs. The properties of iRGD TPNs stabilized with transportan-PEG-iRGD mirrors those of LyP-1 TPNs stabilized with transportan-PEG-LyP-1, particularly nanoparticle stability in physiologically isotonic solutions resulting in favorable size distributions of approximately ~100-200 nm (**Fig. 4-1C-D**), maintained encapsulation of siRNA cargo (**Fig. 4-1B**), cytoplasmic delivery of siRNA without extracellular or intracellular aggregation (**Fig. 4-2C**), improved circulation kinetics (**Fig. 4-5A**), and reduced off-target organ accumulation (**Fig. 4-5B**). The additional finding that PEGylated iRGD TPNs retain size characteristics following a freeze-thaw cycle in 1x PBS without cryoprotectants (**Fig. 4-1E**) is encouraging evidence that the self-assembled complexation is robust against conditions that can irreversibly damage or aggregate other types of nanoparticles, such as gold [187] or iron oxide. Given its practical implications for translatability, this result warrants follow-up work investigating the functionality of particles stored frozen or freeze-dried for extended periods of time and subsequently reconstituted, and the question remains whether the particles are disassembled and reassembled or if they remain intact through phase changes.

We have further established that PEGylated peptides and PEGylated TPNs still mediate membrane disruption (**Fig. 4-2A-B**) based on a red blood cell lysis assay, thus quantifying the effect observed qualitatively in fluorescent microscopy images showing diffuse cytoplasmic delivery of tagged siRNA in cells treated with iRGD TPNs (**Fig. 4-2C-D**). However, in pancreatic cancer models *in vitro*, we observed a more pronounced trade-off between particle

size and knockdown function for iRGD TPNs (**Fig. 4-3**), compared with the LyP-1 particles in Chapter 3; fortunately, an optimal window still exists in which the nanocomplexes retain nanoscale size while also mediating functional knockdown. The apparent impact of high PEG concentrations on TPN function in spite of unchanged endosomal escape properties is consistent with a similar phenomenon seen in Chapter 3, wherein DSPE-PEG-stabilized particles still led to cytoplasmic delivery, though the siRNA function was reduced.

We also considered design variables in the TPN formulation beyond PEGylation, particularly the impact of different fatty acid chain lengths on particle function and toxicity, since this parameter can greatly impact membrane interactions. While the effects of the fatty acid length on particle formation and function were fairly subtle, we found that palmitoyl (C_{16})-modified tandem peptides represented the best knockdown while not contributing excess toxicity.

To establish that PEGylated iRGD TPNs are suitable for distributing siRNA into pancreatic tumors and to obtain evidence of their tumor-penetrating properties, we sought to understand the pharmacokinetics of PEGylated iRGD TPNs *in vivo*, approaching their characterization from several angles. Circulation time studies have shown moderate increases in primary half-life with addition of PEG, while all the particles show a longer secondary half-life, though the significance and configuration of this long-circulating population remains unclear (**Fig. 4-5A**). The rapid clearance of TPNs from the general circulation is in agreement with our finding that peak tumor accumulation on a local level is achieved within ~10 minutes of initial dosing, based on intravital imaging of pancreatic cancer xenografts. The appearance of fluorescent TPN collections relatively far from vessels indirectly suggests that the particles can

penetrate through tumor or stromal tissue and can explain the fairly uniform cross-sectional distribution of TPNs when delivered intravenously to models of pancreatic cancer, including orthotopic grafts of tumor cells growing in the pancreas as well as transgenic Kras-p53 autochthonous tumors (**Fig. 4-6A-B**). Importantly, such distribution could only be achieved with intravenous delivery, as these large and dense tumors, similar in appearance to human PDAC, cannot easily be accessed "outside-in" through intraperitoneal delivery (**Fig. 4-6A**). Because of the improved organ biodistribution profile with the PEGylated iRGD TPNs (**Fig. 4-5B**) showing reduced accumulation in the lungs, liver, and spleen, intravenous delivery of TPNs is a feasible route of administration.

Preliminary therapeutic trial results in a xenograft PDAC model have shown a promising response to *KRAS* interference, with significantly lower tumor burden in mice after a ~3-week treatment course versus untreated controls. Compared with a common standard-of-care chemotherapeutic regimen still used in the clinic, gemcitabine monotherapy, TPNs carrying siRNA against Kras appeared to be more effective in slowing tumor growth. The partial response of the MIA PaCa-2 tumors to gemcitabine therapy was consistent with the level of response seen in the literature [120]. Immediate further studies with control siRNAs will be necessary to fully rule out general toxicity or off-target effects as the causes of tumor response, but reassuringly, monitoring of animal body weights as well as careful observation of animals after dosing suggested that the particles were well-tolerated at the doses administered.

Moving forward, it will be important to conduct similar trials in larger cohorts, employing models of pancreatic cancer that better represent the full picture of pancreatic cancer, namely orthotopic models and autochthonous genetically-engineered mouse models.

Moreover, given that *KRAS* inhibition alone appears to be insufficient to cause tumor regression, as has been seen with the clinical experience of small molecule inhibitors of *KRAS* signaling pathways, we will work with collaborators to credential new genetic targets that may be targeted by siRNA in combination with *KRAS* inhibition.

To summarize, in this chapter, we have formulated and tested PEGylated iRGD TPNs for siRNA delivery to models of pancreatic cancer. These results confirm the modular flexibility of the tandem peptide platform to accommodate new targeting domains and non-covalent additives, as well as the extensibility of the stable formulation strategies identified in Chapter 3 from one tandem peptide to another. These "second-generation" TPNs have shown robust delivery to advanced pancreatic tumors and promising preliminary therapeutic responses, though future follow-up will be needed to complete our understanding of the nanocomplexes' active mechanisms and to assemble viable RNAi-based therapeutic strategies for treating pancreatic cancer.

4.4 Methods:

Synthesis of mTP-PEG-iRGD and pTP-PEG-iRGD: OPSS-5 kDa PEG-SVA (Laysan Bio) was reacted with 5 equivalents of N-[(1R,8S,9s)-Bicyclo[6.1.0]non-4-yn-9-ylmethyloxycarbonyl]-1,8-diamino-3,6-dioxaoctane (Sigma) for 3 hours at room temperature. The resulting conjugate ("OPSS-PEG-alkyne") was dialyzed using a 3,500 MWCO membrane and lyophilized. Subsequently, OPSS-PEG-alkyne was dissolved in DMF and reacted with 1.2 equivalents of myristoyl- or palmitoyl-transportan-Cys with free thiol for 3 hours at room temperature. 1.2 equivalents of azidoacetyl-CRGDKGPDC (iRGD), Cys-Cys linkage, were added and the reaction was allowed to proceed overnight at room temperature. The final product was dialyzed using a 3,500 MWCO membrane into water and lyophilized.

Dynamic light scattering (DLS): PEGylated TPNs were formed as previously described (see Chapter 3.4) at a final siRNA concentration of 200 nM in 1x PBS or water. 50 μL of each particle solution was analyzed on a Zetasizer Nano ZS90 Particle Analyzer System (Malvern). For

freeze-thaw experiments, particles were frozen at -20 °C for a day and subsequently thawed prior to DLS analysis.

Transmission electron microscopy: 10:10:1 mTP-TAM-iRGD:mTP-PEG-iRGD:siLuc TPNs were formed as previously described (see Section 3.4) at a final siRNA concentration of 900 nM. 5 μL of the particle solution was pipetted onto a formvar/carbon TEM grid (Ted Pella) and allowed to dry overnight. Before imaging, the grids were rinsed with RNase free water to remove excess salt and re-dried. Images were obtained using the JEOL 2100F transmission electron microscope in the Koch Institute Nanotechnology Materials Core.

Red blood cell lysis assays: Fresh murine red blood cells (RBCs) were obtained by collecting whole blood via cardiac puncture, mixing 1:1 with 5 mM EDTA/1x PBS to prevent coagulation, and then centrifuging at 500xg. Serum and buffy coat were removed and RBC pellet was washed with 150 mM NaCl, re-pelleted, then resuspended in 10x volume of PBS. For each condition, 90 μL of diluted red blood cells was mixed with 10 μL of the peptide of interest at 10x the desired concentration. 0.1% Triton X-100 was used as a positive control (treated as 100% hemolysis). Samples were incubated for 1 hour at 37 °C. Intact RBCs were pelleted by tabletop centrifugation and supernatant was transferred to a clear 96-well plate, with free hemoglobin quantified on a SpectraMax Plus spectrophotometer at 541 nm absorbance.

Fluorescence microscopy: Cells were transfected as described above. At the specified timepoints, cells were imaged live on a Nikon Eclipse T*i* microscope using a 20x Plan Apo objective. Images were collected in NIS-Elements AR software (Nikon), with individual channels combined in Photoshop CS5 (Adobe) with linear level adjustments applied identically to all images within an experiment.

***In vitro* knockdown:** For luciferase knockdown experiments, KP B22 GFP-Luciferase murine PDAC cells (created by Mandar Muzumdar in the Jacks lab) were plated at 2500 cells/well in a 96-well plate 24 hours prior to transfection. TPNs for transfection were prepared and administered as previously described to a final concentration of 100 nM siLuc (sense strand 5′-CUUACGCUGAGUACUUCGA-3′) in Opti-MEM. Luciferase function was quantified by lysing cells with Cell Culture Lysis Reagent (Promega); 10 μL of lysate was then mixed thoroughly with 40 μL of luciferin (Promega Luciferase Assay System) and loaded into a white 96-well plate (Corning 3600). Luciferase bioluminescence was quantified using a Centro LB 960 Microplate Luminometer (Berthold Technologies). For *KRAS* knockdown experiments, PANC-1 cells (generous gift from the Hahn lab) were plated in a 12-well plate 24 hours prior to transfection. Cells were transfected with TPNs containing 100 nM siKras.476 (sense strand 5′-ACCAUUAUAGAGAACAAAUUA-3′) for 24 hours in 1 mL Opti-MEM per well, followed by media exchange to DMEM + 10% FBS for 24 hours. *KRAS* mRNA expression was quantified by real-time quantitative PCR.

Quantitative PCR: mRNA was isolated by lysing cells with Buffer RLT (Qiagen), filtering out debris using the Qiashredder homogenizer (Qiagen), and then purifying mRNA using an

RNeasy kit (Qiagen) according to manufacturer's instructions. mRNA concentration was quantified via NanoDrop 2000 Spectrophotometer (thermo). cDNA was reverse transcribed using the iScript cDNA synthesis kit (Bio-Rad). qPCR was performed on a C1000 Touch Thermal Cycler with CFX96 Touch Real-Time PCR Detection System (Bio-Rad) using the following primer pairs: human *KRAS* (for PANC-1 experiments) Forward 5′-ACAGTGCAATGAGGGACCAG-3′ and Reverse 5′-ATCATCAACACCCTGTCTTGT-3′, human *TBP* Forward 5′-GGAGAGTTCTGGGATTGTAC-3′ and Reverse 5′-CTTATCCTCATGATTACCGCAG-3′.

Electrophoretic mobility shift assay: TPNs were formed at the specified ratios for a final concentration of 200 nM siRNA (DyLight 677-siLuc) in 1x PBS. 10 μL of each TPN sample or free siRNA was mixed with 2 uL of 30% glycerol and loaded into a 2% agarose gel. The gel was run at 60 V for 45 minutes in 1x TAE buffer and siRNA fluorescence was imaged on a LI-COR Odyssey infrared scanner. Signal was quantified using ImageJ.

Circulation time: Swiss Webster mice were intravenously (tail vein) injected under isoflurane anesthesia with non-PEGylated iRGD TPNs or 15:10:1 iRGD TPNs at 0.5 nmol siRNA dose per mouse, n=3 per condition. VivoTag-S750 siRNA was used to minimize interference from autofluorescent background. Retro-orbital blood draws (10 μL each) were taken at 1, 10, 20, 40, 80, and 160 minute timepoints following injection using heparinized glass capillaries (VWR) and scanned using a LI-COR Odyssey near-infrared scanner. Fluorescence was quantified using ImageJ and converted to blood concentrations using a standard curve of *ex vivo* blood samples spiked with known concentrations of VivoTag-labeled siRNA.

Organ biodistribution: Swiss Webster mice were then injected intravenously in the same manner and dose as for the circulation time study using VivoTag-S750 labeled siRNA, n=3 per condition. After 3 hours, mice were euthanized and necropsy was performed to remove the lungs, heart, kidneys, liver, and spleen. Organs were scanned using a LI-COR Odyssey near-infrared scanner (LI-COR Biosciences) and analysis of average fluorescence intensity was performed in ImageJ.

Orthotopic pancreatic cancer transplant model: Intrapancreatic tumor xenografts were generated as described in [44]. Briefly, NCR/nude mice were anesthetized and the surgical site was sterilized. A ~5 mm incision was made in the left mid-abdomen and the spleen and pancreas were exteriorized with forceps. 50 μL of cell solution in Opti-MEM + 10% growth factor-reduced, phenol red-free Matrigel (BD) was injected using sterile syringe and needle. After 1 minute to allow solidification of Matrigel, spleen and pancreas were returned to the abdominal cavity; the peritoneum was then sutured together and the skin approximated by wound clips.

Intravital imaging: NCR/nude mice were implanted with bilateral flank grafts of MIA PaCa-2 xenografts at $2x10^6$ cells per flank. Tumors were imaged when they reached a major-axis diameter of ~1 cm. Mice were injected intravenously with 10:10:1 pTP-TAMRA-iRGD:mTP-

PEG-iRGD:siRNA negative control at a 0.3 nmol siRNA dose, alongside fluorescently-tagged dextran (70 kDa FITC dextran, Life Technologies) in order to identify patent vessels. Surgical exteriorization of the flank tumor was performed by Jeffrey Wyckoff, with the mice adequately anesthetized with inhaled isoflurane, and the tumor was mounted against a glass slide over the microscope objective for imaging. Second-harmonic generation microscopy was used to visualize collagen fibrils (pseudocolored magenta in the image), while TAMRA fluorescence (TRITC channel) was used to track TPNs (pseudocolored green in the image). Images were collected every 3 minutes over the course of 15 minutes, beginning 5 minutes post-injection due to the time elapsed to perform the surgery and locate suitable imaging regions. Sequences were captured as z-stacks with 21 layers, separated from adjacent slides by a depth of 10 μm.

Therapeutic trial: NCR/nude mice were implanted with bilateral flank grafts, each seeded with $2x10^6$ cells in 100 μL Opti-MEM plus 10% growth factor-reduced phenol red-free matrigel. Mice were divided into 5 groups of nearly equal average tumor burden (~170 mm^3 total tumor burden per mouse at the start of treatment) and standard deviation of tumor burden. The three treatment groups, n=4 each were as follows: (1) D5W i.v. injection and 1x PBS i.p. injection, (2) D5W i.v. injection and 100 mg/kg gemcitabine i.p., (3) 15:2.5:1 pTP-TAM-iRGD:pTP-PEG(5kDa)-iRGD:siKras.476 (see Section 2.4 for sequences) 0.5 mg/kg i.v. injection and 1x PBS i.p. injection. The dose schedule was every three days with the exception of one dose displaced by one day, for a total of 6 doses. Doses based on body weight were administered on the basis of a 25 g mouse receiving 100 μL i.p. and i.v.; volumes were then scaled according to actual mass. Tumor sizes were measured every three days by calipers by a researcher blinded to treatment regimens, with tumor burden per mouse computed as the sum of the volumes of the two flank tumors, approximated as half of the product of the major axis and minor axis squared.

Chapter 5: CRISPR/Cas9 delivery using tandem peptides [^]

5.1 Introduction

Accurate animal models of cancer are the cornerstone of preclinical testing for new cancer therapies, particularly those that are designed to interact with and overcome the complex, three-dimensional milieu of the tumor. This cannot be more true than in pancreatic cancer, where it is apparent that the unique barriers to effective therapy are not well-represented by *in vitro* cell culture or conventional animal models. Indeed, the majority of cells in the typical pancreatic cancer are non-tumor cells: stromal cells, immune cells, and blood vessel-associated cells.

The present state-of-the-art models of pancreatic cancer are transgenic mice that activate oncogenes and lose tumor suppressors in response to Cre recombinase under the control of the Pdx1 promoter, discussed at length in Section 1.2.4. The sets of mutations represented in these models have included several of the core mutations seen in pancreatic cancer: *Kras* activation [31], *Tp53* knockout [188] or dominant negative variants (Li-Fraumeni syndrome) [31], and *p16-Ink4a/p19*^{Arf} inactivation [32]. However, in contrast to spatially-refined models such as those for lung cancer, in which inhaled viral Cre recombinase leads to sporadic mutations in the lung epithelium [46], these pancreatic cancer models introduce the mutations into all exocrine and endocrine cells, resulting in explosive tumor growth and rapid deterioration of the host, with animal death occurring in some models within 8 weeks. Actual pancreatic cancers tend to be clonal and arise as a single cancer, with insidious onset that is notable not so much for rapid progression but rather for its prolonged asymptomatic advance. Mutation of the organ *en masse* limits the capacity of these models to be used in trials studying therapeutic response – both

because the tumors are unnaturally aggressive and because it is difficult to match cohorts as the promoter event is outside of human timing control – and also limits the ability to study advanced disease with local and metastatic spread, since primary disease burden causes death before these events occur. Furthermore, a new transgenic mouse must be made to study any new gene or combinations thereof, a time-consuming process on the order of years.

Gene editing techniques have the potential to ameliorate all these shortcomings of current models of pancreatic cancer. In particular, RNA-guided endonuclease technologies such as the Type II CRISPR/Cas9 system have shown great promise in empowering researchers to instigate custom mutations in cells in a modular manner. CRISPR/Cas9 functions by using a universal Cas9 nuclease directed to cut at a specific site in the genome by a short guide RNA (sgRNA). The sgRNA contains an addressing sequence ~20 bp long fused to a longer constant region that associates with the Cas9 protein in a 1:1 fashion. Thus, it suffices to design the addressing sequence, for which robust tools are publicly available [189], in order to induce double-strand breaks at desired sites. Cutting alone introduces insertions or deletions (indels) through error-prone non-homologous end joining (NHEJ) repair, while concomitant administration or synthesis of a DNA template can encourage repair by homologous recombination. The combination of these techniques allows creation of the same types of mutations needed to induce tumorigenesis. Moreover, implementation of CRISPR/Cas9-based tumor models by delivery of the necessary components would (1) allow sporadic mutations by only invoking the nuclease in a subset of cells, (2) temporally define cohorts based on the time of dosing, and (3) permit the rapid generation of tumor models containing any combination of

target genes, with turnaround on the order of days to weeks to design and synthesize new sgRNAs and DNA templates.

Exciting progress has been made in specific organs of interest: *Pten* and *Tp53* tumor suppressor mutations as well as beta-catenin HDR-mediated activating mutations have been created in the mouse liver using hydrodynamic injection [92], and AAVs have been administered intratracheally to generate p53 and HDR-mediated $Kras^{G12D}$ mutations at a success rate of ~0.1% each, increasing to ~1.3 and 1.8%, respectively, after 9 weeks due to positive selection [190]. Additionally, 7C1 nanoparticles originally developed for siRNA delivery to endothelial cells [128] and adjacent cancers [67] have been used as the first demonstration of a targeted vehicle for CRISPR/Cas9 delivery [190]. However, at present, there are no delivery methods that target CRISPR/Cas9 components to the pancreas (or indeed most other organs of interest), which would require systemic administration as well as a targeted delivery vehicle.

Thus, we considered whether tandem peptides might be adapted to encapsulate and deliver CRISPR/Cas9 components, based on the biochemical similarity of guide RNAs and DNA repair templates to siRNA. In this chapter, we demonstrate that tandem peptides can not only deliver functional guide RNA and DNA templates to cells expressing Cas9 *in vitro*, but they can also deliver pre-complexed guide RNA and Cas9 protein into cells without pre-existing Cas9 expression. Combined with the development of a new tandem peptide targeted to normal pancreatic tissue, these findings represent important progress towards creating a platform that can generate customized, sporadic models of pancreatic cancer.

5.2 Results

5.2.1 Formation of tandem peptide-CRISPR component particles

CRISPR/Cas9 is an extremely versatile tool that has been engineered to perform gene editing through both non-templated (NHEJ) and templated (homologous recombination) modes. Because the core components are RNA and DNA oligonucleotides, we hypothesized that tandem peptides would be able to encapsulate and deliver these components analogously to siRNA, albeit with modified ratios to reflect differences in conformation and net charge per molecule. We specifically envisioned three different particle compositions intended for distinct uses: (1) tandem peptide-sgRNA particles, which can introduce indels in cell lines and mice expressing Cas9; (2) tandem peptide-sgRNA-single stranded DNA (ssDNA) particles, which introduce double-stranded breaks (DSBs) to promote incorporation of the DNA template by homology-directed repair (HDR); and (3) tandem peptide-sgRNA-Cas9 particles, which deliver sgRNA alongside Cas9 in either protein or mRNA form for gene editing in cells that do not express Cas9 (**Fig. 5-1A**). In the third particle type, if the Cas9 is to be incorporated in protein form, we expect that the Cas9 and sgRNA must be pre-complexed before peptide encapsulation, since while Cas9 and the tandem peptide are both cationic materials that bind the sgRNA, Cas9 requires prioritized access to specific regions of the guide RNA while the tandem peptide does not (**Fig. 5-1B**).

Central to our approach has been consideration of the various genetic architectures that can give rise to key mutations. In order to introduce activating oncogenic mutations, which typically arise in a single allele as missense mutations in crucial binding pocket or conformationally active residues, two primary strategies are possible, differentiated by the

construct containing the mutation and method used to turn on the mutant gene. First, in analogy to or superimposed upon existing Lox-Stop-Lox or FRT-Stop-FRT constructs, Cas9 can mediate excision of a transcriptional stop cassette upstream from a copy of the mutated gene by inducing a pair of double-stranded breaks that are then repaired by homologous recombination or NHEJ. This approach is characterized in Sections 5.2.2 and 5.2.4. Second, to create an oncogenic mutation on a wild-type background, the mutation may be introduced on a DNA

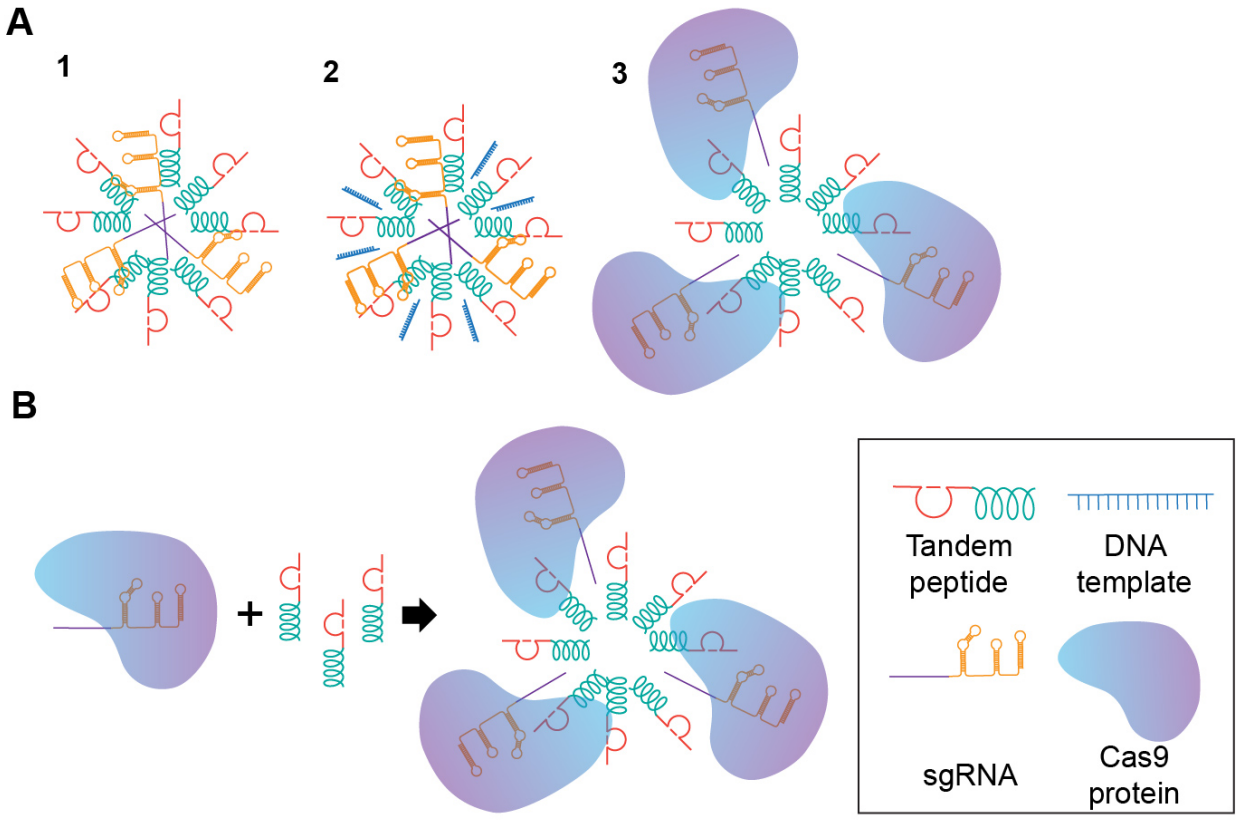

Figure 5-1. Overview of CRISPR/Cas9 tandem peptide particles. (A) Three distinct cargo formulations of CRISPR/Cas9 tandem peptide nanocomplexes. **1:** tandem peptides carrying sgRNA only, to be delivered to cells containing Cas9-NLS and introduce indels or NHEJ/HDR-mediated excision; **2:** tandem peptides carrying sgRNA and a DNA template, to be delivered to cells containing Cas9-NLS and introduce specific mutations via homologous recombination of the host genome with the DNA template; **3:** tandem peptides carrying sgRNA pre-complexed with Cas9 to mediate gene editing in ordinary cells. **(B)** Formation of particle type 3 requires a specific formulation order, as informed by [154]. Guide RNA is first incubated with Cas9 in a concentrated solution, then tandem peptide is added. If non-covalent PEG stabilizers are being used, the PEG is added after sgRNA-Cas9 complexation but before the tandem peptide.

template for HDR, with success depending on careful design of the template and adequate concentrations of the template to out compete non-productive NHEJ. This approach is explored in Section 5.2.3. Finally, for tumor suppressor mutations, which are typically missense or nonsense mutations that result in non-functional protein, the simplest approach is to introduce small insertions or deletions (indels) by allowing low-fidelity NHEJ repair at the DSB site, since probabilistically, this will result in highly detrimental frameshift mutations. This is presented in Section 5.2.4.

5.2.2 Tandem peptides can encapsulate and deliver guide RNA

To begin, we used DLS to confirm particle formation by mixing our prototypical tandem peptide, pTP-iRGD, with sgRNA. As a starting point, we formed particles at approximately a 10:1 weight ratio (N/P ratio of ~3), comparing particle sizes in water and PBS with varying pTP-PEG-iRGD molar ratios (**Fig. 5-2A**). These formulations led to particle formation with similar properties to tandem peptide-siRNA particles, including recapitulation of the particle-stabilizing effect of adding the PEGylated component.

To test whether these particles can deliver functional sgRNA into cells, we used a reporter system in cells bearing both a FRT-Stop-FRT-GFP cassette as well as constitutive Cas9. One sgRNA directed against FRT (which, unlike LoxP sites, contains a PAM) would theoretically suffice to guide Cas9 to cut at both adjacent FRT sites, and subsequent repair that omits the intervening sequence would lead to GFP reporter expression. After screening several sgRNAs against FRT ("sgFRT"), we selected the most efficient candidate, sgFRT 64, and used this to compare different formulations of tandem peptide-sgFRT complexes on the basis of

sgRNA dose (given for a 12-well format: 0.5 μg is ~16 nM) and different peptides (**Fig. 5-2B**; schematic of the approach shown in **Fig. 5-2C**). Both fluorophore-labeled and unlabeled tandem peptides led to GFP expression in a dose-dependent manner, with unlabeled pTP-iRGD performing slightly better with a maximum of ~16% GFP-positive cells. In contrast, treatment with another CPP previously characterized for siRNA transfection, CADY [163], did not result in GFP-positive cells.

Acknowledging that optimized *in vitro* conditions may not completely represent the environmental conditions under which these particles would need to perform *in vivo*, we next tested two variables: replacing Opti-MEM with regular serum-containing media, and determining the effect of PEGylation on particle function (using the same PEGylated peptide extensively characterized in Chapter 4) (**Fig. 5-2D**). The pTP-iRGD complexes maintained functional sgRNA-mediated excision in the presence of normal-serum media, though the efficiency was reduced by roughly half. The addition of a PEG component, likely necessary for systemic delivery, reduced efficiency when doped in as more than 10% of the peptide concentration. Finally, we were interested in obtaining a complete dose curve to examine the tunability of the system, as the ability to control the number of mutated cells depends on the reliability and predictability of the relationship between dose and effect. Accordingly, we noted that the relationship indeed fit closely with a linear trend (**Fig. 5-2E**), with $r^2 = 95.5\%$. Therefore, tandem peptides can deliver sgRNA in a tunable manner, and these particles are functional in serum as well as when stabilized using modular PEG components as described previously.

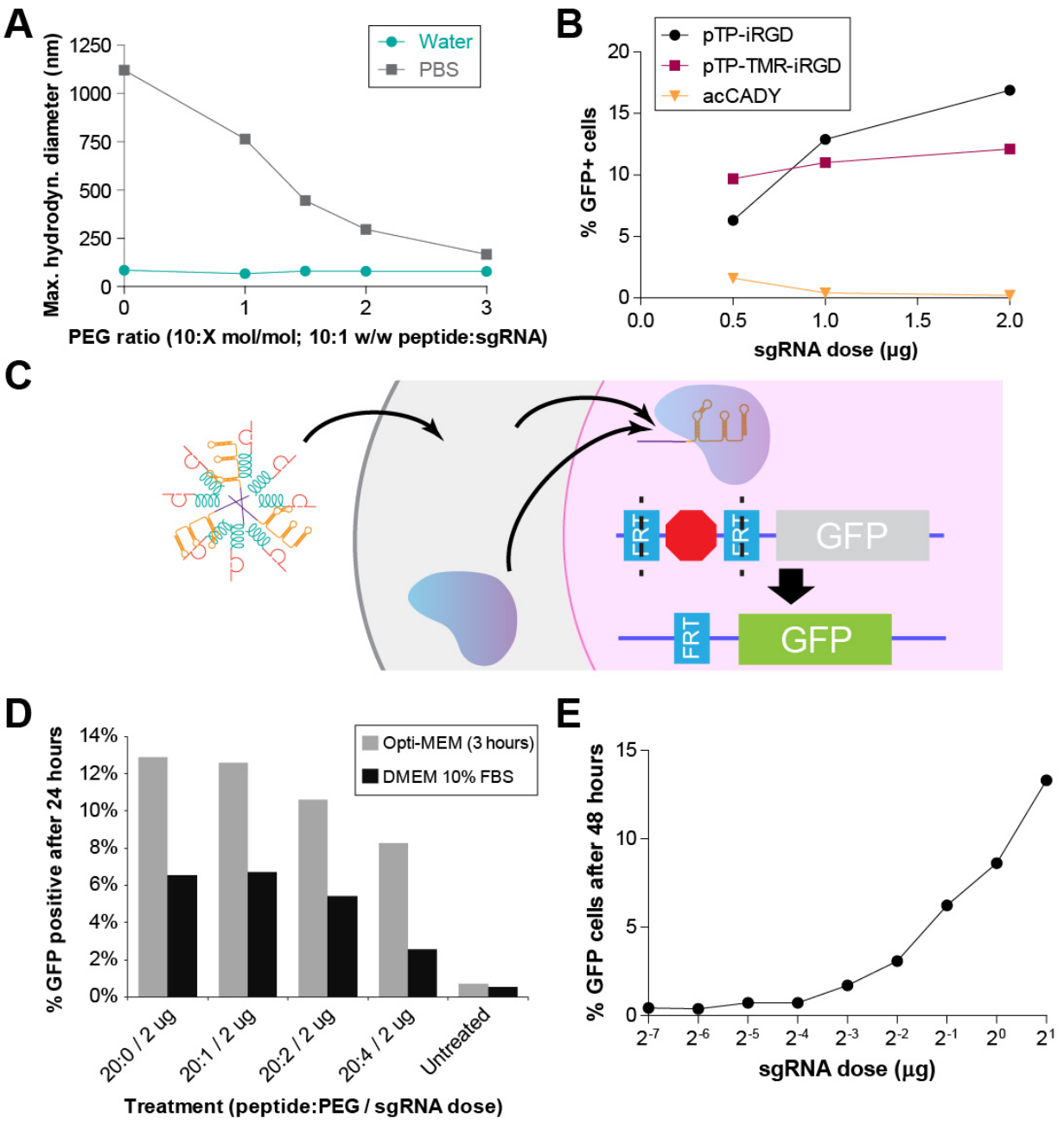

Figure 5-2: Encapsulation and delivery of sgRNA by tandem peptides *in vitro*. (A) Prototypical particle formation with tandem peptide and sgRNA at a fixed 10:1 weight ratio of peptide to sgRNA. As seen in Chapters 3 and 4, the addition to PEGylated peptide, specified by molar ratio, prevents aggregation of the particles in ionic solution. **(B)** Gene editing following sgRNA delivery by tandem peptides, compared to a non-tandem peptide CPP, acetyl-CADY. In this system, sgRNA against FRT is delivered to cells containing a FRT-Stop-FRT-GFP cassette and Cas9; thus, two cuts can mediate excision of the transcriptional stop cassette and lead to GFP activation, as depicted in the schematic in panel **(C)**. **(D)** Activity of sgRNA-tandem peptide nanocomplexes in Opti-MEM vs. full serum media and as a function of added PEG. **(E)** Dose titration in a 24-well format showing tunability of gene editing rates.

5.2.3 Tandem peptides deliver sgRNA and ssDNA for HR-mediated gene editing

In a second configuration, we created particles encapsulating a single-stranded DNA template in addition to the sgRNA in order to encourage incorporation of a defined mutation through homology-directed repair (HDR). Notably, viral vectors cannot easily deliver multiple copies of DNA templates. As a first test system, we sought to introduce a uniquely identifiable mutation into the gene encoding the tdTomato fluorescent protein, such that we could query not only whether the insertion actually took place by quantitative real-time genomic PCR, but also the relative frequency of insertion compared to all indel formation events, manifesting as tdTomato-negative cells. In this experiment, the ssDNA contained ~100 bp homology arms on either side of the sgRNA-targeted site and additionally a 10-bp insertion serving not only as a unique primer substrate but also to ablate the PAM sequence on the template, preventing Cas9-mediated cleavage of the template. Homologous recombination events that successfully incorporate the 10-bp insertion can be approximately quantified through qPCR. This is accomplished by comparing the cycle times for a primer pair amplifying all copies of the gene and a closely matched primer pair of presumed comparable efficiency, in which one primer sits atop the inserted sequence and the other within the gene but outside the template, to avoid amplification of the template itself (**Fig. 5-1A**). In cells receiving sgRNA and the DNA template, the ratio of native sequences to mutated sequences was 100-200:1. Because the cells were homozygous for tdTomato, and additionally, tdTomato is a homodimer of dsRed at the protein and DNA level, this could represent a range of efficiencies at the *cellular* level, ranging from recombination at all four recognized sites in 0.5-0.75% of cells to recombination at a single site in 2-3% of cells. An intermediate interpretation assuming that one allele is completely modified

per cell is presented in **Fig. 5-3B** for comparative purposes. When this figure is compared to the percentage of cells losing Tomato fluorescence, an approximate HDR rate can be obtained, with the highest rates of correct insertion occurring when the relative ratio of DNA template to sgRNA dose is highest (**Fig. 5-3C**).

Following up on this result, we next performed a similar experiment, introducing a set of synonymous mutations into cells with homozygous wild-type *Kras*, towards the incorporation of specific activating oncogenic mutations (**Fig. 5-3D**). sgKras and a *Kras* DNA template were delivered by iRGD tandem peptides at a 2.5:1 weight ratio of peptide to total nucleic acid. Assuming that HDR is a rare event occurring randomly on an allelic basis, we quantified the percentage of cells incorporating the mutations in *Kras* if all affected cells ended up heterozygous (**Fig. 5-3E**). The efficiency of ~2.5% was comparable to our prior results using the tdTomato reporter gene; particles containing PEG (5:1 pTP-iRGD:pTP-PEG-iRGD molar ratio) showed somewhat diminished efficiency. Delivery of the DNA template alone led to a very small (~1 log lower) rate of HDR, and untreated cells had undetectable amplicon at the end of the 40-cycle run with the mutated primer set. Thus, tandem peptides are able to deliver sgRNA and DNA templates simultaneously and thus promote mutation through homology-directed repair.

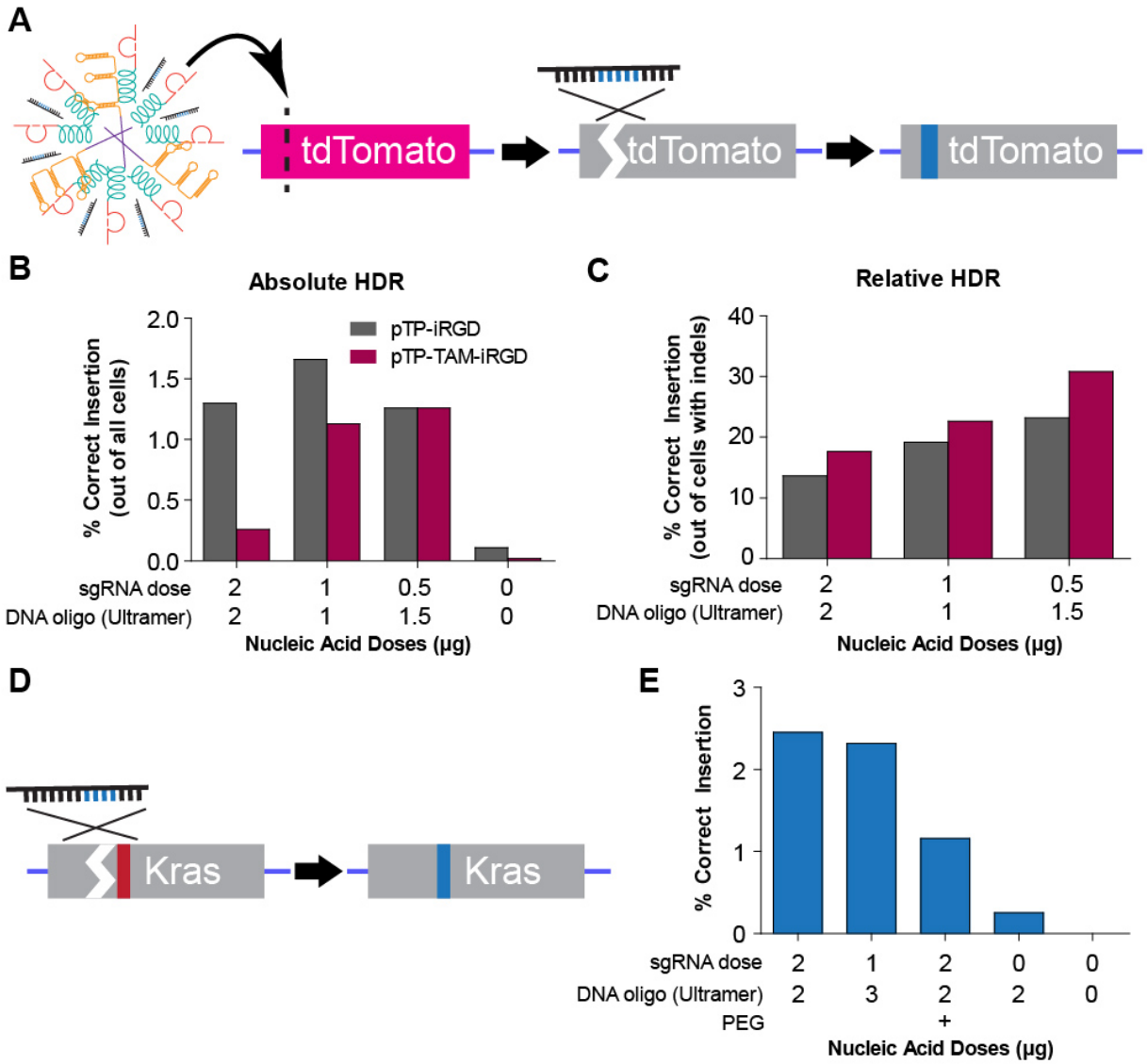

Figure 5-3. Delivery of sgRNA and DNA templates *in vitro*. (A) Schematic showing a particle consisting of tandem peptides binding both sgRNA against tdTomato and a DNA template with homology to the region surrounding the target cleavage site. Recombination of the genomic DNA with the template leads to incorporation of a foreign sequence that can be detected by qPCR. **(B)** Overall efficiency of insert incorporation into tdTomato, measured as the percentage of cells containing the correct inserted sequence, computed by qPCR. Doses are given for 24-well plate format. **(C)** Incorporation rate as a percentage of cells that were cleaved by sgTomato-Cas9, determined by flow cytometry to detect tdTomato-negative cells. **(D)** Schematic showing HDR incorporating a DNA template with homology to the region surrounding the *Kras* target cleavage site. Recombination of the genomic DNA with the template leads to incorporation of synonymous mutations that can be detected by qPCR. **(E)** Overall efficiency of *Kras* mutation incorporation, measured as the percentage of cells containing the correct inserted sequence if at most one allele was recombined per cell.

5.2.4 Tandem peptides deliver functional Cas9-sgRNA complexes

As a final particle configuration, we sought to develop a strategy for delivering Cas9 alongside sgRNA for use in systems where cells do not natively express Cas9. Having previously demonstrated that tandem peptides can deliver functional mRNA encoding GFP (**Fig. 8-1** in the Appendix), we first considered whether we could deliver Cas9 mRNA. However, we found this approach to be highly inefficient, perhaps as a consequence of the bulk of Cas9 in the mRNA format (~4500 bp). We therefore attempted an alternative approach: delivery of Cas9 protein. Zuris et al. noted that cationic lipids could deliver loaded Cas9-sgRNA complexes, likely through association with negative charges on portions of the sgRNA not involved in Cas9 binding.

First, we returned to an excision-based construct, a pancreatic cancer cell line bearing a FRT-Stop-FRT-GFP cassette without any endogenous expression of Cas9 (**Fig. 5-4A**). As Cas9 can bind a single sgRNA at a time, we premixed the two components in equal molar quantities. In cells treated with tandem peptide, Cas9 protein, and sgFRT, ~5% across a range of doses from 25 nM to 100 nM (**Fig. 5-4A, bottom**), whereas cells dosed with only peptide-sgFRT particles were indistinguishable from untreated baseline cells, ensuring that Cas9 delivery was indeed occurring. Because we did not know *a priori* what magnitudes of efficiencies to expect, we benchmarked the tandem peptides against a positive control, Lipofectamine RNAiMax, one of the better-tolerated lipid transfection reagents characterized in the literature. We observed that in this particular model system, tandem peptides consistently outperformed RNAiMax.

We tested the same strategy in a single-cut indel assay using HeLa cells expressing destabilized GFP, a stand-in reporter to mimic a tumor suppressor gene to be knocked out,

hypothesizing that such a system would be much more efficient than the comparatively complex excision constructs. As expected, we saw higher rates of successful events (i.e. GFP knockout), peaking at ~20% in cells treated with 50 nM each of sgRNA and Cas9. As in the GFP knock-in system, we found that omission of Cas9 from the particles left the cell populations at baseline, and performance of the tandem peptides was comparable to RNAiMax. Additionally,

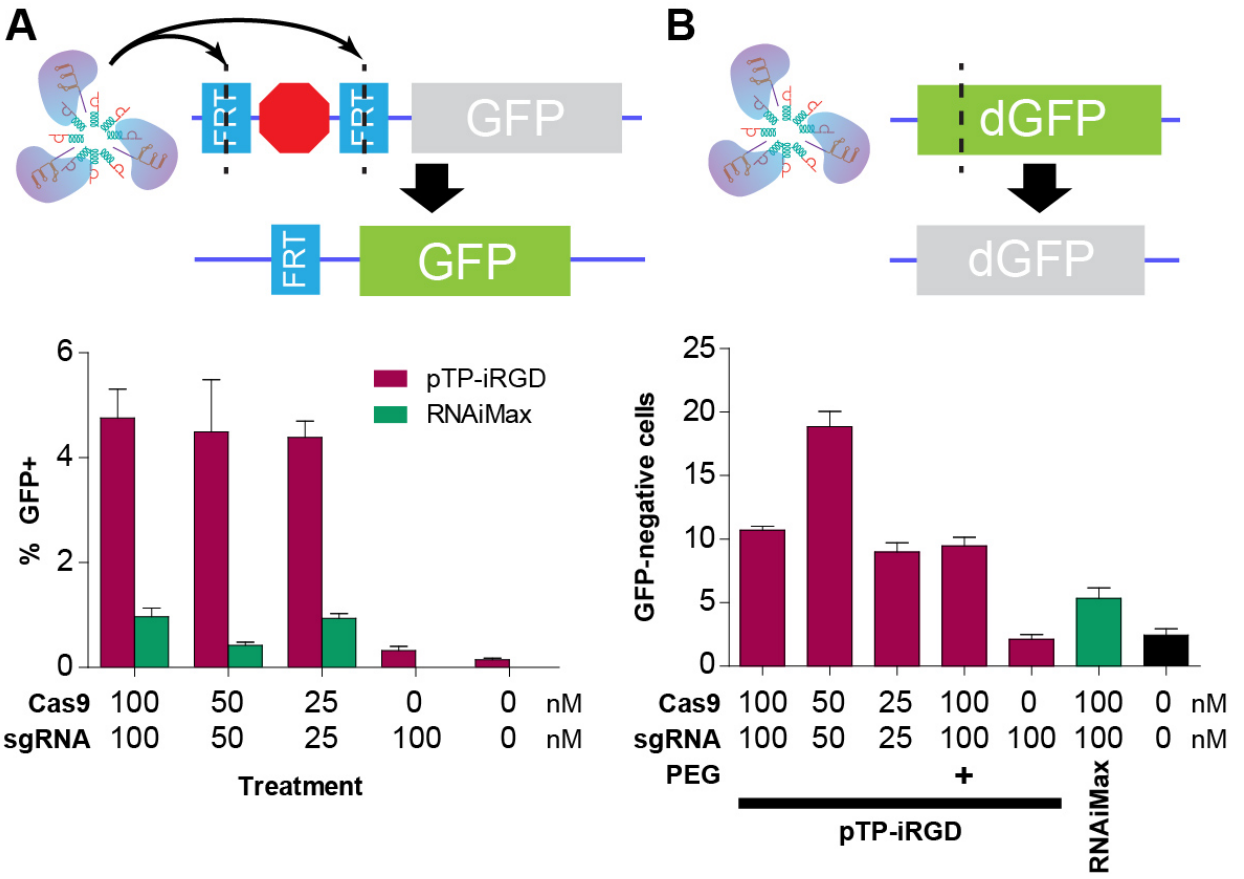

Figure 5-4. Delivery of sgRNA-Cas9 complexes *in vitro*. (A) *Top:* Schematic showing nanocomplex delivering sgRNA-Cas9 complexes that must cut at two identical FRT sites to turn on a GFP reporter. *Bottom:* pTP-iRGD-mediated delivery of functional sgFRT leads to reconstitution of GFP reporter across a large dose range, as quantified by flow cytometry. RNAiMax delivery is shown as a positive control; particles with sgFRT and no Cas9 serve as the negative control. **(B)** *Top:* Schematic showing nanocomplex delivering sgRNA-Cas9 complexes that must introduce a single indel in a destabilized GFP reporter in order to eliminate dGFP fluorescence. Bottom: pTP-iRGD-mediated delivery of functional sgGFP eliminates dGFP expression. PEGylated particles show equivalent efficacy, while particles lacking Cas9 perform identically to untreated controls.

PEGylated tandem peptide particles (10:1 peptide:PEG ratio) maintained functional delivery of sgRNA-Cas9 complexes on par with unPEGylated particles at the same dose. Overall, we established that tandem peptides can deliver functional pre-complexed sgRNA-Cas9.

5.2.5 Tandem peptides that target the healthy pancreas

For the characterization work above, we employed iRGD tandem peptides because the *in vitro* cell lines were all of cancer origin or transformed. However, to generate pancreatic cancer models in mice, it is necessary to target the healthy pancreas rather than pancreatic cancer itself. To this end, we have synthesized a new tandem peptide, replacing the CendR domain with the linear SWCEPGWCR targeting domain that was found to recognize normal pancreatic tissue by the Ruoslahti lab [191, 192]. This peptide can deliver functional sgRNA in the model systems presented previously, though at reduced efficiency in the cell types tested, likely because these cell-line based models are not actively targeted by the pancreas-homing peptide (data not shown). Importantly, in biodistribution studies, we observed considerably enhanced accumulation of fluorescently labeled siRNA in the pancreata of mice dosed with pTP-SWCEPGWCR or pTP-SWCEPGWCR + pTP-PEG-SWCEPGWCR particles (abbreviated as "pTP-PANC + pTP-PEG-PANC"), a finding that we believe will extend to sgRNA cargoes as well (**Fig. 8-2** in the Appendix).

5.3 Discussion

We have shown that tandem peptides, originally developed for siRNA and miRNA delivery, are capable of encapsulating and delivering cargoes consisting of CRISPR/Cas9

components. To date, we are not aware of any attempts to deliver CRISPR/Cas9 components using specific organ- or tumor-targeted carriers, which have the advantage of potentially opening up new organ-specific applications of gene editing *in vivo*. Furthermore, the tandem peptide system is designed to work with the "mature" active forms of CRISPR/Cas9 elements – guide RNA, DNA templates, Cas9 protein – a property shared with transfection agents like cationic lipids but in contrast to viral and naked plasmid delivery. This is of relevance to the on-target specificity of gene editing: it has been established that high levels of constitutive Cas9 nuclease activity promotes non-specific cutting of the genome, and several strategies to reduce off-target cutting have employed methods to decrease overall formation of Cas9-sgRNA complexes [87, 88]. Considering the time- and concentration-integrated Cas9 activity over time as the overarching determinant of off-target cutting, it is likely that delivery of mature CRISPR/Cas9 components, which are by nature transient and non-replicating (though still catalytic), could potentially reduce nonspecific cutting in the longer timeframe – an important consideration for ensuring that cancer models are arising due to the intended edits rather than unexpected ones.

The three distinct particle formations demonstrated in our work exemplify the versatility of the system and suitability for introducing multiple types of mutations – including frameshift mutations (**Fig. 4-4B**), nucleotide substitutions (**Fig. 4-3D-E**), and more extensive insertions (**Fig. 4-3A-C**) – that are needed to model common cancer genotypes. Among model systems representing oncogenic activation, excisional configurations involving two cuts by a single guide (i.e. the FRT-Stop-FRT system) showed the greatest efficiency, with ~15% reporter expression with sgRNA delivery (**Fig. 4-2B**) and ~5% with sgRNA-Cas9 delivery (**Fig. 4-4A**). In

contrast, HDR had a maximum success rate of ~2.5% in Cas9-expressing cells, assuming modification of one allele per cell. We also had attempted two-cut excisional systems involving two different sgRNAs in order interface with Lox-Stop-Lox systems and observed that this worked as well, but at rates far below the preceding systems (~0.5-1% success, data not shown). For inducing tumor suppressor-type mutations, strategically-placed indel formation sufficed, showing ~20% knockout with sgRNA-Cas9 delivery.

The ability to deliver Cas9 protein alongside sgRNA cargo presents the opportunity to work with *in vivo* models that lack constitutive or inducible Cas9 expression, particularly interfacing with existing mouse models. For example, the particles could be used in place of nonspecific virally-delivered flippase in the FRT-Stop-FRT-Kras^{G12D}/p53$^{FRT/FRT}$ mouse to create sporadic Kras-p53 tumors, provided adequate specificity of the sgRNA-Cas9-containing particles. We note that *non-covalent* CPP-mediated delivery of proteins has been rarely described, with the Pep-1 peptide being the primary exemplar, forming complexes with proteins via hydrophobic interactions [193]. Indeed, a prior system for CPP-mediated CRISPR/Cas9 component delivery directly fused Cas9 with polyarginine and saw comparatively low efficiency *in vitro*, which may have partially been a consequence of the protein fusion and lack of pre-complexation of Cas9 with the guide RNA. Proponents of lipid transfection strategies have suggested that CPPs are inherently less suited to the delivery of Cas9 [154], but based on our results showing comparable if not improved efficacy with tandem peptide-mediated delivery of sgRNA-Cas9 complexes compared to Lipofectamine RNAiMax in certain model systems, it is likely that the mode of Cas9 incorporation is of greater relevance than the particular delivery technology.

Given that past systems with high gene editing efficiency *in vitro* can still end up showing low frequencies of editing *in vivo*, it will be necessary to continue developing and optimizing tandem peptides to achieve higher efficiencies, though only a few Cas9-mediated cutting events are necessary in the case of positively-selected phenotypes such as tumorigenesis. We are presently working with various *in vivo* models such as Cas9-expressing mice to demonstrate proof-of-concept gene editing by tandem peptides. We are simultaneously validating sgRNAs targeted against relevant proto-oncogene and tumor suppressor genes in order to move beyond reporter systems and assess for the induction of PDAC and its precursor lesions, pancreatic intraepithelial neoplasias (PanINs). Overall, the modular adaptation of the tandem peptide platform for CRISPR/Cas9-mediated gene editing has been an exciting step towards unlocking new potential applications, such as the generation of previously uncharacterized genetic models of pancreatic cancer.

5.4 Methods

sgRNA synthesis: sgRNAs were synthesized by David Canner using a MEGAscript SP6 transcription kit (Life Technologies). The guide sequences used were as follows: GFP: GGGCACGGGCAGCTTGCCGG [194]; FRT: TCCTATTCTCTAGAAAGTAT; tdTomato: GGCCACGAGTTCGAGATCGA.

Peptide and peptide-PEG synthesis: pTP-iRGD, pTP-TAM-iRGD, and mTP-TAM-iRGD were synthesized as described in Section 2.4. Acetyl-CADY (GLWRALWRLLRSLWRLLWRA) was synthesized by the Koch Institute Biopolymers Core.

Tandem peptide-CRISPR nanocomplex synthesis: For particles containing only sgRNA cargo, non-stabilized particles were formed by adding peptide to sgRNA, both diluted in equal volumes of Opti-MEM, to reach the desired concentration. Weight ratios of 2.5-10:1 were employed in initial experiments. PEG-stabilized particles were formed as described in Chapter 3.4, with full particle formation in water prior to 20x dilution in Opti-MEM. For particles containing sgRNA and DNA template, the two cargoes were pre-mixed at the weight ratios

indicated prior to particle formation using the aforementioned techniques. For particles containing Cas9 and sgRNA, Cas9 and sgRNA were pre-complexed in water for 5 minutes (volume ~10 μL). Subsequently, PEG (if being used) and peptide were added to the Cas9-sgRNA solution in that order, to a total volume of ~1/20th the final volume. Particles were then diluted in Opti-MEM to the final concentration.

sgRNA transfection: 3TZ fibroblasts containing FRT-Stop-FRT-GFP Cas9-blasticidin constructs were generously provided by the Jacks lab. Cells were plated in 24-well plates at . For conventional complex formation, pTP-iRGD, pTP-TAM-iRGD, or acetyl-CADY were mixed in equal volume with sgRNA in Opti-MEM for a final peptide concentration of 2.09 μM and sgRNA quantity as listed (0.5, 1, or 2 μg per well). For PEGylated formulations, pTP-PEG-iRGD was mixed with the sgRNA in water (1/20th of the final volume), then peptide was added, and finally the solution was diluted in Opti-MEM to the same final peptide and sgRNA concentrations as before. 500 μL of tandem peptide complexes were administered per well in a 24-well plate (scaled to 1 mL for a 12-well plate or 100 μL for a 96-well plate).

sgRNA and DNA template transfection: Particles were formed as described above. Cells expressing tdTomato were transfected with both sgRNA targeting tdTomato as well as a single-stranded DNA template with the sequence: 5′-ATGGTGAGCAAGGGCGAGGAGGTCATCAA-AGAGTTCATGCGCTTCAAGGTGCGCATGGAGGGCTCCATGAACGGCCACGAGTTCGAG ATC*AGTGCGAGTC*GAGGGCGAGGGCGAGGGCCGCCCCTACGAGGGCACCCAGACCGCC AAGCTGAAGGTGACCAAGGGCGGCCCCCTGCCCTTCGCCTGGGACATCCTGTCC containing a unique 10-bp insertion indicated by the italics. 72 hours following dosing, cells were harvested; the percentage of tdTomato-negative cells was determined by flow cytometry, while the rest of the cells were processed to isolate genomic DNA using standard techniques. Primers were designed to distinguish tdTomato loci that incorporated the unique insertion from the native sequence: Forward (normal) 5′-CGGCCACGAGTTCGAGAT-3′; Forward (insertion-specific) 5′-GAGTTCGAGATCAGTGCGAGT-3′; Reverse: CCTTGGAGCCGTACATGA.

Kras experiments were performed in 12-well plates at 2 μg each of sgRNA and template or 1 μg sgRNA and 3 μg template per well, otherwise in the same fashion as above. The single-stranded DNA template used was 5′-TTATTGTAAGGCCTGCTGAAAATGACTGAG-TATAAACTTGTGGTGGTTGGAGCTGATGGCGTAGGCAAGAGCGCCTTGACGATACAGCT AATTCAGAATCACTTTGTG*GACGAATACGATCCCACAATC*GAGGTAACGCTGCTCTACAG TCTGCGTGCGCTTGTAAAGGACGGCAGCCAGCCGCTTTGAAAAAGATATCA-3′. Synonymous mutations are located in the region indicated by italics. To quantify homologous recombination frequency, we used the primer pair Forward 5′-GTGTGAGACATGTTCTAATTTAGTTGT-3′, present only on the gene, and Reverse 5′-CGATTGTGGGATCGTATTCGT-3′, specific to the mutated sequence on the DNA template.

Cas9-sgRNA transfection: In all experiments, Cas9 with a C-terminal NLS (PNA Bio) was used. For GFP-on experiments, 3TZ fibroblasts containing FRT-Stop-FRT-GFP (but no Cas9) were plated in 96-well plates at 2,500 cells/well, 24 hours prior to dosing. Cas9-sgFRT particles were

formed as previously described, at the concentrations specified (1.5 μM pTP-iRGD, variable sgRNA/Cas9 concentrations of 25, 50, or 100 nM each). Lipofectamine RNAiMax controls were prepared according to manufacturer instructions, mixing the RNAiMax reagent with equivolume pre-complexed sgRNA and Cas9 in Opti-MEM. Transfection was conducted for 3-4 hours in 100 μL per well; media was then exchanged to DMEM with 10% FBS. Cells were assayed after 24 hours on an LSR-II flow cytometer (Becton Dickinson) and analyzed using Flow-Jo (TreeStar). For GFP-off experiments, HeLa dGFP cells were plated in 96-well plates at 1,250 cells/well, 48 hours prior to dosing. Cells were assayed after 48 hours on an LSR Fortessa flow cytometer (BD) and analyzed using Flow-Jo.

Chapter 6: Discussion and Perspectives [^]

6.1 Summary and future work

We have engineered peptide-based nanocomplexes specifically designed to address the constraints and challenges of pancreatic cancer. In particular, these particles can deliver siRNA addressing key genetic mutations in PDAC, with embedded mechanisms for penetrating through the tumor environment using the CendR peptide, iRGD. Nearly all pancreatic cancer lines tested, mouse and human, expressed both receptors for iRGD, and iRGD TPNs mediated robust knockdown of *Kras* as well as a combination of *Kras* and another siRNA target simultaneously.

We next developed methods for generally and optimally stabilizing tandem peptide-siRNA complexes for systemic intravenous delivery, since the depth and encasement of the tumor makes it difficult to access from the intraperitoneal space, borne out in our head-to-head comparison. In particular, the addition of peptide-PEG conjugates as non-covalent dopants led to stable nanoscale assemblies resistant to aggregation and displaying much more favorable intravenous biodistribution. We applied this strategy to stabilize iRGD TPNs, showing similar benefits in particle formation and, further, uniform siRNA delivery into heterotopic, orthotopic and autochthonous models of pancreatic cancer. Preliminarily, PEGylated iRGD TPNs delivering siRNA against *KRAS* slowed growth of subcutaneous PDAC xenografts, though of course these experiments must be thoroughly repeated, and further studies in genetically-engineered animal models of PDAC will be necessary to validate the tumor-penetrating strategy.

Finally, we have demonstrated proof-of-concept delivery of CRISPR/Cas9 delivery using tandem peptides, which is one of the first instances of using active receptor-targeted nanoparticles with the CRISPR/Cas9 system. The tandem peptide platform can be formulated to deliver sgRNA, sgRNA with a DNA template for homology-directed repair, and sgRNA with Cas9 protein. Such modes of delivery can mediate gene edits of the types necessary to generate activating oncogenic and loss of tumor suppressor mutations, towards generation of new, sporadic models of pancreatic cancer. Future work will include further development and characterization of pancreas-targeted tandem peptides, validation of sgRNAs targeted to relevant genes not yet modeled by GEM mouse lines, and studies to demonstrate that tandem peptides can facilitate CRISPR/Cas9-mediated gene editing *in vivo*.

6.2 The modularity of tandem peptide systems

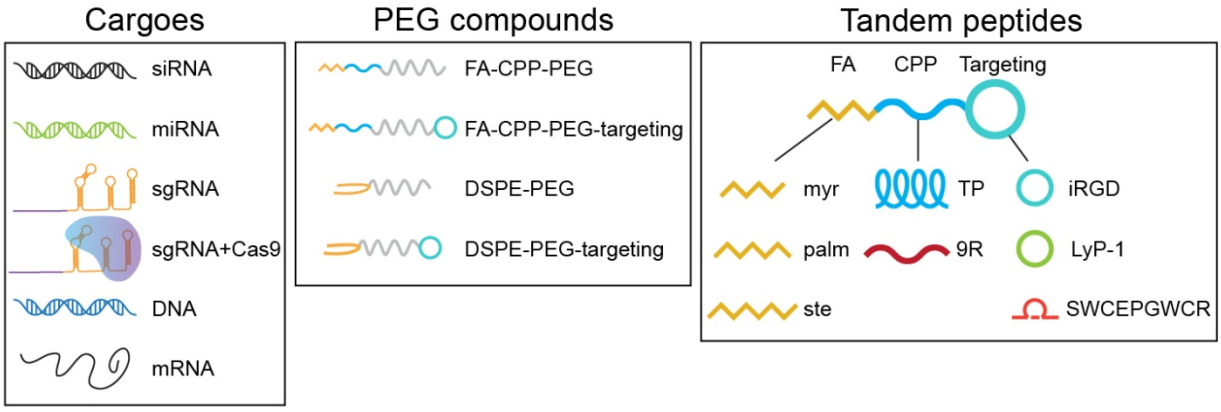

Figure 6-1. The modular formation of tandem peptide-based nanocomplexes.

One important dimension of this work has been unlocking the full modular vision for tandem peptide-mediated delivery: interchangeability of the targeting domain, flexibility in the formulation with and without PEG, and adaptability to new cargoes beyond siRNA (**Fig. 6-1**).

Indeed, through this thesis and associated work, we have demonstrated the inherent versatility of the tandem peptide platform, to the point where some variants of the particles are more properly rechristened tandem peptide nanocomplexes rather than tumor-penetrating nanocomplexes. So far, we have delivered cargoes including siRNA, miRNA (**Fig. 8-3** in the Appendix), sgRNA, sgRNA complexed to Cas9, DNA oligonucleotides, and mRNA. The different nucleic acid cargoes are notable because of their comprehensive spectrum of actions from a bioengineering perspective: siRNAs and miRNAs function as transient inhibitors or modulators of gene function, mRNA is a transient "activator" (in the broadest sense) of gene function, sgRNA is a permanent route to gene inactivation, and sgRNA combined with a DNA template may be used as a permanent route to gene activation. Thus, tandem peptide nanocomplexes can be leveraged to mediate inactivation or activation of genes on tunable time-scales.

To alter the tropism and functions of the carrier, we have swapped out the targeting domain, demonstrating tandem peptides containing iRGD or SWCEPGWCR domains in addition to the original LyP-1. The multifunctional properties of CendR peptides, as well as the fact that the receptors for LyP-1 and iRGD and commonly seen in multiple tumor types each, establishes the ground generalizability to the system. The further exchangeability of such targeting motifs grants even greater coverage of tumor types. This flexibility helps to mitigate against the risk of "over-specifying" a targeted strategy – tumor markers that are organ-dependent, for instance, may be downregulated as a tumor becomes more malignant and eventually metastatic. On the other hand, stress-related phenomena such as p32 upregulation (for LyP-1) and angiogenesis of leaky blood vessels (for iRGD) are broadly observed across

many tumors. Indeed, alpha$_v$ integrins are not only upregulated in many pancreatic cancers, as shown in Chapter 2, but also in ovarian cancers as well, as demonstrated by colleagues in our group. A further extension, not yet explored in depth, is that given the thousands of peptide copies comprising each tandem peptide nanocomplex, it is possible to represent multiple targeting ligands. Depending on the valencies used, such an approach could help address the heterogeneity of targeted cells of interest, or alternatively enhance specificity by only mediating strong binding when co-ligands simultaneously bind.

The implications of this modularity are far-reaching in terms of future applications of the technology. With the continual discovery of newer and more specific cancer targets, the flexibility and adaptability of delivery platforms to incorporating new targeting moieties will be important in permitting delivery to different types of tumors and tumor cells. At present, a major time-limiting step is the synthesis of tandem peptides, whose length and complexity (e.g. cyclization) reduce yields with current technology. However, as demonstrated in the chemical synthesis of PEGylated derivatives such as transportan-PEG-LyP-1, -iRGD, and -SWCEPGWCR, it is possible to create larger libraries of tandem peptides from smaller pieces. Another bottleneck is that currently, targeting materials – including peptides, aptamers, small molecules, and their natural analogue, antibodies – typically rely upon rounds of empiric screens and selection. It is possible that the conformational complexity of cell-surface targets such as proteins or oligosaccharides may never yield to rational design strategies in the way that, for instance, genome targeting has yielded to rationally-designed RNA-guided endonuclease systems and mRNA targeting has yielded to RNAi. Nevertheless, the repertoire of unique ligand-target pairs continues to grow, and the TPN platform is well-poised to adapt to novel

targeting ligands, including non-peptide domains that may be linked through straightforward bioconjugate techniques.

Cargo flexibility is potentially even more powerful. shRNA and CRISPR/Cas9-powered screens are generating unprecedented lists of genetic targets that have the potential to become new RNAi therapies, and TPNs are well-poised to test these new targets alone and in combination. Indeed, given that many pancreatic cancers are or can become resistant to loss of *KRAS* signaling, it will be necessary to redouble efforts to identify and credential new targets that will enhance or synergize with *KRAS* pathway blockade.

Beyond RNAi, there are doubtless many undiscovered natural paradigms for the facile manipulation of genetic and extragenetic material, not to mention new frontiers in manmade uses of nucleic acids, already populated by DNA origami [195] and shape assembly [196, 197], DNA data encoding [198], and RNA aptamers [107]. It is beneficial to design delivery vehicles that not only complement existing cargoes, but also conceive of their parameters in such a general manner as to prepare for future innovations – in much the same way that pill capsules can accommodate new drugs and endoscopes can accommodate new imaging technology. Indeed, it may turn out that a combination of cargoes encompassing multiple modes of action may surpass any one alone, such as a combination of transient and permanent cellular manipulations as alluded to earlier in this discussion.

6.3 The future of tandem peptides as self-assembled nanosystems

In this vein, I would also like to reflect on the implications of our findings in the larger context of self-assembled nanosystems, which need not be restricted to nucleic acids or

peptides. As touched upon in Chapter 3.1, self-assembly is an attractive paradigm as it allows the facile generation of new formulations with different or improved functional capacities in the preclinical setting. Further down the drug pipeline, spontaneous self-assembly means that in clinical use, the components that make up TPNs could very well be delivered as mixtures of stable, lyophilized or frozen components that re-form the expected nanoparticles when reconstituted, as evidenced by the facts that we generate the particles within minutes by resuspending lyophilized individual components in aqueous diluent and simply mixing, and that the particles remain intact after freeze-thaw. While most synthetic self-assembled systems form on the basis of either electrostatic interactions or hydrophobic partitioning, with TPNs perhaps incorporating both mechanisms, nature provides alluring examples of more complex self-assembled structures, such as clathrin baskets and viral capsids. The assembly of such natural structures is enticing for the reproducibility and fixed final product – properties that we have begun to emulate through the efforts to incorporate PEG into the TPN structure in Chapters 3 and 4 – but these materials are also equally if not more fascinating in that such assembly is invariably reversible under the desired conditions. Indeed, a viral capsid that could not uncoat the viral genome would be selected against immediately. While the kinetics and triggers of cargo release from synthetic materials is typically a focal topic in the formation of drug depots, wafers, or highly structured or layered particles, the tuning of such parameters in self-assembled nanosystems is also very important.

The advent of "smart materials" that interact with the host rather than simply acting unilaterally upon the host has opened up great possibilities for self-assembled systems. To some degree, the CendR peptides we have incorporated begin to tap into that host-responsive

potential by combining traditional receptor targeting with active penetration mechanisms. The next step in this direction is to enable interaction with the host in ways that help tailor the therapeutic to the scenario at hand.

In our lab, I have been fortunate to work with Kevin Lin on the conception and study of self-assembled nanocomplexes designed to dynamically release anticoagulants only when needed, termed nanoparticle self-titrating anticoagulants (nanoSTATs) [177]. This negative-feedback design links up with the complex feedback loops of the coagulation process to help restore coagulatory homeostasis in the hypercoagulable setting. In the final nanoSTAT design, the peptide carrier consisted of short cationic segments separated by thrombin-cleavable sequences and partially substituted with 5 kDa PEG. The interaction between the peptide carrier, inspired by protamine and with similarities to the CPPs polyarginine and polylysine, and its highly anionic heparin cargo draws many parallels to TPN formation, including the eventual particle size just shy of 100 nm. Ultimately, these nanoSTATs were able to release heparin in response to a model of pulmonary thromboembolism and prevent fibrin deposition and morbidity, while not extending the bleeding time in a tail nick model of physiologic clotting. Of perhaps greater relevance to the studies in this thesis, kinetic experiments using a thrombin generation assay (TGA) confirmed the host-responsive mechanism of these self-assembled electrostatic nanocomplexes, wherein early low-level thrombin activity met little resistance, but increasing thrombin levels resulting from positive feedback cycles in the coagulation cascade triggered release of heparin on the timescale of minutes that ultimately curtailed further thrombin activity.

This of course raises the question of whether TPNs and tandem peptide nanocomplexes more generally may be engineered to be rapidly responsive to their environment – and when it would be beneficial to do so. The simplest such mechanism would involve enhancing functional cellular interactions in a tumor-dependent manner, *e.g.* by inserting an matrix metalloproteinase-specific cleavage sequence into the transportan-PEG stabilizing constructs such that PEG may be cleaved off to expose and mobilize additional cell-penetrating domains to enhance localization. Additionally, such an approach may counteract the PEG-dependent loss of functional efficiency observed in TPNs by effectively converting PEGylated TPNs at the site of disease (that therefore no longer require PEG) to non-PEGylated TPNs. Alternatively, responsiveness to cues present in the endosome (e.g. pH) may cleave PEG just preceding the endosomal escape step. Precedent is set by a clever approach previously developed by our group to increase iron oxide nanoparticle tumor uptake by unveiling polyarginine domains [199].

Beyond therapeutic enhancement, TPNs can also be engineered to provide diagnostic information. In the current design, the only cleavage site is in iRGD, which converts the cyclic peptide into a linear one. However, sequence placement that instead leads to fragmentation of the tandem peptide could yield a small cleavage product that could be detected, for example, in the urine – a concept that has been explored for diagnostic applications in our group's synthetic biomarker platform [200, 201]. The central synthetic biomarker construct consists of a nanoparticle core too large to be excreted, bearing multivalent cleavable peptide-fluorophore substrates that can be detected in the urine by ELISA or mass spectrometry if they are cleaved off of the core. While certain design constraints differ when considering a diagnostic component

of TPNs – for instance, cleavage in the bloodstream by released circulating proteases could impede TPN delivery of the therapeutic component, and nanocomplex components are known to escape into the urine despite their particle size – the design tools are available to realize such a hybrid diagnostic-therapeutic ("theragnostic") nanocomplex. Thus, there are many opportunities to take advantage of the straightforward creation of self-assembled nanosystems to build in more complex responsive behaviors that enable new or improved functionality.

6.4 Nanoparticle systems

Ultimately, regulatory considerations aside for the moment, the treatment of cancer is agnostic to the chemical and technological basis of its components. At one level, this means that future iterations of delivery vehicles may remain strategically similar but replace core materials (*e.g.* tumor-penetrating nanocomplexes that replace the CPP with alternative non-peptide transfecting agents, or replace the CendR component with a hypothetical small molecule recapitulating its function). On another level, it means that we should not be fearful of cross-pollinating or assembling technologies and paradigms that may complement each other.

During my earliest project in the Bhatia lab, I worked with Geoffrey von Maltzahn to devise a strategy for tissue targeting predicated on a two-step stigmergic (environmentally-mediated) communication system [202]. Here, gold nanorods mediate mild hyperthermia (43-45 °C) via near infrared laser-induced surface plasmon resonance and locally unwind collagen fibrils to reveal cryptic epitopes, which are then targeted by a second particle species displaying gelatin-binding fibronectin fragments. This strategy *in vitro* led to a 7-fold increase in secondary particle binding compared to controls lacking gold nanorods or heated in environments lacking

collagen. When exploring this strategy *in vivo*, we noted that there was considerable benefit from the heating effects alone, consistent with the literature documenting both vascular and stromal changes in response to mild hyperthermia [203-205].

Alexander Bagley, a colleague in the group, has generalized and expanded the principles by which tumor hyperthermia might enhance treatment with nanoparticles as well as its limitations [206], and preliminary experiments have shown that the uptake of TPNs into tumors is indeed enhanced by mild hyperthermia. With the plethora of ECM components and scarcity of vessels in the PDAC environment, this hyperthermia could very well provide the ECM modulation and vessel permeability needed to further improve TPN accumulation and penetration. Trials of combining hyperthermia with gemcitabine chemotherapy have shown benefit, and this modulating effect may be more pronounced with TPNs as a consequence of the larger size of nanoparticles [207]. This is but one example of how interfacing the tandem peptide platform with complementary approaches may yield beneficial therapeutic interactions.

6.5 Conclusion

In summary, we have designed a nanoparticle-based approach for nucleic acid delivery to pancreatic cancers. iRGD TPNs, particularly with non-covalent PEG stabilization, show promise in conveying gene-specific therapies to models of PDAC *in vitro* and *in vivo*. Of course, further work will be needed to fully characterize and apply this technology effectively, including preclinical testing in more advanced animal models – perhaps one day even in genetically-driven models of PDAC created through tandem peptide-mediated delivery of CRISPR/Cas9 components. Given the frequency of *KRAS*-mutated yet knockdown-insensitive

pancreatic cancers, it will be important to identify additional genetic targets that would enhance the therapeutic response. TPNs are well-poised to serve as a target validation platform for both single and multiple siRNA knockdown targets. Although there are many follow-up studies that need to be performed, we are already very encouraged by the modularity and adaptability of the tandem peptide platform that will facilitate future work in these avenues of investigation and beyond. The versatility of tandem peptides is important in the face of the rapidly progressing field of nanotechnology, whose potential to positively shift and impact our approach to treating cancer and particularly pancreatic cancer is only beginning to be realized.

Chapter 7: References [^]

[1] Fast stats: An interactive tool for access to SEER cancer statistics. Surveillance Research Program, National Cancer Institute (2015).

[2] PP Provenzano, C Cuevas, AE Chang, VK Goel, DD Von Hoff, and SR Hingorani. Enzymatic targeting of the stroma ablates physical barriers to treatment of pancreatic ductal adenocarcinoma. *Cancer Cell*, 21 (2012) 418-429.

[3] M Hidalgo. Pancreatic cancer. *N Engl J Med*, 362 (2010) 1605-1617.

[4] DP Ryan, TS Hong, and N Bardeesy. Pancreatic adenocarcinoma. *N Engl J Med*, 371 (2014) 1039-1049.

[5] N Howlader, A Noone, M Krapcho, J Garshell, D Miller, S Altekruse, C Kosary, M Yu, et al. SEER cancer statistics review, 1975-2011, 2014.

[6] JP Neoptolemos, DD Stocken, H Friess, C Bassi, JA Dunn, H Hickey, H Beger, L Fernandez-Cruz, et al. A randomized trial of chemoradiotherapy and chemotherapy after resection of pancreatic cancer. *N Engl J Med*, 350 (2004) 1200-1210.

[7] GY Locker, S Hamilton, J Harris, JM Jessup, N Kemeny, JS Macdonald, MR Somerfield, DF Hayes, et al. ASCO 2006 update of recommendations for the use of tumor markers in gastrointestinal cancer. *J Clin Oncol*, 24 (2006) 5313-5327.

[8] T Frebourg, E Bercoff, N Manchon, J Senant, JP Basuyau, P Breton, A Janvresse, P Brunelle, et al. The evaluation of CA 19-9 antigen level in the early detection of pancreatic cancer. A prospective study of 866 patients. *Cancer*, 62 (1988) 2287-2290.

[9] CL Wolfgang, JM Herman, DA Laheru, AP Klein, MA Erdek, EK Fishman, and RH Hruban. Recent progress in pancreatic cancer. *CA Cancer J Clin*, 63 (2013) 318-348.

[10] M Distler, F Rückert, M Hunger, S Kersting, C Pilarsky, HD Saeger, and R Grützmann. Evaluation of survival in patients after pancreatic head resection for ductal adenocarcinoma. *BMC Surg*, 13 (2013) 12.

[11] PA Philip. Targeted therapies for pancreatic cancer. *Gastrointest Cancer Res*, 2 (2008) S16-S19.

[12] DD Von Hoff, T Ervin, FP Arena, EG Chiorean, J Infante, M Moore, T Seay, SA Tjulandin, et al. Increased survival in pancreatic cancer with nab-paclitaxel plus gemcitabine. *New England Journal of Medicine*, 369 (2013) 1691-1703.

[13] T Conroy, F Desseigne, M Ychou, O Bouché, R Guimbaud, Y Bécouarn, A Adenis, J-L Raoul, et al. FOLFIRINOX versus gemcitabine for metastatic pancreatic cancer. *New England Journal of Medicine*, 364 (2011) 1817-1825.

[14] MM Oken, RH Creech, DC Tormey, J Horton, TE Davis, ET McFadden, and PP Carbone. Toxicity and response criteria of the eastern cooperative oncology group. *Am J Clin Oncol*, 5 (1982) 649-655.

[15] DP Ryan, H Mamon. Initial chemotherapy and radiation for nonmetastatic locally advanced unresectable, borderline resectable, and potentially resectable exocrine pancreatic cancer. Post TW (Ed.) UpToDate. UpToDate, Walthalm, MA, 2015.

[16] HL Kindler, D Niedzwiecki, D Hollis, S Sutherland, D Schrag, H Hurwitz, F Innocenti, MF Mulcahy, et al. Gemcitabine plus bevacizumab compared with gemcitabine plus placebo in patients with advanced pancreatic cancer: Phase III trial of the cancer and leukemia group B (calgb 80303). *J Clin Oncol*, 28 (2010) 3617-3622.

[17] P Rougier, H Riess, R Manges, P Karasek, Y Humblet, C Barone, A Santoro, S Assadourian, et al. Randomised, placebo-controlled, double-blind, parallel-group phase III study evaluating aflibercept in patients receiving first-line treatment with gemcitabine for metastatic pancreatic cancer. *Eur J Cancer*, 49 (2013) 2633-2642.

[18] T Ioka, T Okusaka, S Ohkawa, N Boku, A Sawaki, Y Fujii, Y Kamei, S Takahashi, et al. Efficacy and safety of axitinib in combination with gemcitabine in advanced pancreatic cancer: Subgroup analyses by region, including japan, from the global randomized phase III trial. *Jpn J Clin Oncol*, (2015).

[19] PA Philip, J Benedetti, CL Corless, R Wong, EM O'Reilly, PJ Flynn, KM Rowland, JN Atkins, et al. Phase III study comparing gemcitabine plus cetuximab versus gemcitabine in patients with advanced pancreatic adenocarcinoma: Southwest oncology group-directed intergroup trial s0205. *J Clin Oncol*, 28 (2010) 3605-3610.

[20] MJ Moore, D Goldstein, J Hamm, A Figer, JR Hecht, S Gallinger, HJ Au, P Murawa, et al. Erlotinib plus gemcitabine compared with gemcitabine alone in patients with advanced pancreatic cancer: A phase III trial of the national cancer institute of canada clinical trials group. *Journal of Clinical Oncology*, 25 (2007) 1960-1966.

[21] PA Philip. Development of targeted therapies for pancreatic cancer. *Lancet Oncol*, 12 (2011) 206-207.

[22] KP Olive, MA Jacobetz, CJ Davidson, A Gopinathan, D McIntyre, D Honess, B Madhu, MA Goldgraben, et al. Inhibition of hedgehog signaling enhances delivery of chemotherapy in a mouse model of pancreatic cancer. *Science*, 324 (2009) 1457-1461.

[23] MA Jacobetz, DS Chan, A Neesse, TE Bapiro, N Cook, KK Frese, C Feig, T Nakagawa, et al. Hyaluronan impairs vascular function and drug delivery in a mouse model of pancreatic cancer. *Gut*, 62 (2013) 112-120.

[24] K-J Lou. Stromal uncertainties in pancreatic cancer. *Science-Business eXchange*, 7 (2014).

[25] Andrew D Rhim, Paul E Oberstein, Dafydd H Thomas, Emily T Mirek, Carmine F Palermo, Stephen A Sastra, Erin N Dekleva, T Saunders, et al. Stromal elements act to restrain, rather than support, pancreatic ductal adenocarcinoma. *Cancer Cell*, 25 (2014) 735-747.

[26] Berna C Özdemir, T Pentcheva-Hoang, Julienne L Carstens, X Zheng, C-C Wu, Tyler R Simpson, H Laklai, H Sugimoto, et al. Depletion of carcinoma-associated fibroblasts and fibrosis induces immunosuppression and accelerates pancreas cancer with reduced survival. *Cancer Cell*, 25 (2014) 719-734.

[27] ES Calhoun and SE Kern. Molecular genetics of pancreatic cancer. A Lowy, S Leach, P Philip (Eds.) Pancreatic cancer, Springer US, 2008, pp. 27-39.

[28] NT Ihle, LA Byers, ES Kim, P Saintigny, JJ Lee, GR Blumenschein, A Tsao, S Liu, et al. Effect of KRAS oncogene substitutions on protein behavior: Implications for signaling and clinical outcome. *Journal of the National Cancer Institute*, 104 (2012) 228-239.

[29] A Maitra and RH Hruban. Pancreatic cancer. *Annu Rev Pathol*, 3 (2008) 157-188.

[30] PS Moore, B Sipos, S Orlandini, C Sorio, FX Real, NR Lemoine, T Gress, C Bassi, et al. Genetic profile of 22 pancreatic carcinoma cell lines. Analysis of K-ras, p53, p16 and DPC4/Smad4. *Virchows Arch*, 439 (2001) 798-802.

[31] SR Hingorani, L Wang, AS Multani, C Combs, TB Deramaudt, RH Hruban, AK Rustgi, S Chang, et al. Trp53R172H and KrasG12D cooperate to promote chromosomal instability and widely metastatic pancreatic ductal adenocarcinoma in mice. *Cancer Cell*, 7 (2005) 469-483.

[32] AJ Aguirre, N Bardeesy, M Sinha, L Lopez, DA Tuveson, J Horner, MS Redston, and RA DePinho. Activated Kras and Ink4a/Arf deficiency cooperate to produce metastatic pancreatic ductal adenocarcinoma. *Genes Dev*, 17 (2003) 3112-3126.

[33] CJ Whatcott, H Han, RG Posner, and DD Von Hoff. Tumor-stromal interactions in pancreatic cancer. *Crit Rev Oncog*, 18 (2013) 135-151.

[34] RS Herbst and SM Lippman. Molecular signatures of lung cancer – toward personalized therapy. *N Engl J Med*, 356 (2007) 76-78.

[35] J Downward. Targeting RAS signalling pathways in cancer therapy. *Nat Rev Cancer*, 3 (2003) 11-22.

[36] GJ Riely, ML Johnson, C Medina, NA Rizvi, VA Miller, MG Kris, MC Pietanza, CG Azzoli, et al. A phase II trial of salirasib in patients with lung adenocarcinomas with KRAS mutations. *J Thorac Oncol*, 6 (2011) 1435-1437.

[37] B Alagesan, G Contino, AR Guimaraes, RB Corcoran, V Deshpande, GR Wojtkiewicz, AF Hezel, KK Wong, et al. Combined MEK and PI3K inhibition in a mouse model of pancreatic cancer. *Clin Cancer Res*, 21 (2015) 396-404.

[38] C Chang-Yew Leow, S Gerondakis, and A Spencer. MEK inhibitors as a chemotherapeutic intervention in multiple myeloma. *Blood Cancer Journal*, 3 (2013) e105.

[39] MR Junttila, V Devasthali, JH Cheng, J Castillo, C Metcalfe, AC Clermont, DD Otter, E Chan, et al. Modeling targeted inhibition of MEK and PI3 kinase in human pancreatic cancer. *Mol Cancer Ther*, 14 (2015) 40-47.

[40] A Gopinathan and DA Tuveson. The use of GEM models for experimental cancer therapeutics. *Dis Model Mech*, 1 (2008) 83-86.

[41] M DuPage, AF Cheung, C Mazumdar, MM Winslow, R Bronson, LM Schmidt, D Crowley, J Chen, et al. Endogenous T cell responses to antigens expressed in lung adenocarcinomas delay malignant tumor progression. *Cancer Cell*, 19 (2011) 72-85.

[42] P Sarraf, E Mueller, D Jones, FJ King, DJ DeAngelo, JB Partridge, SA Holden, LB Chen, et al. Differentiation and reversal of malignant changes in colon cancer through PPARgamma. *Nat Med*, 4 (1998) 1046-1052.

[43] MH Kulke, GD Demetri, NE Sharpless, DP Ryan, R Shivdasani, JS Clark, BM Spiegelman, H Kim, et al. A phase II study of troglitazone, an activator of the PPARgamma receptor, in patients with chemotherapy-resistant metastatic colorectal cancer. *Cancer J*, 8 (2002) 395-399.

[44] MP Kim, DB Evans, H Wang, JL Abbruzzese, JB Fleming, and GE Gallick. Generation of orthotopic and heterotopic human pancreatic cancer xenografts in immunodeficient mice. *Nat Protoc*, 4 (2009) 1670-1680.

[45] VP Muniz, JM Barnes, S Paliwal, X Zhang, X Tang, S Chen, KD Zamba, JJ Cullen, et al. The arf tumor suppressor inhibits tumor cell colonization independent of p53 in a novel mouse model of pancreatic ductal adenocarcinoma metastasis. *Mol Cancer Res*, 9 (2011) 867-877.

[46] M DuPage, AL Dooley, and T Jacks. Conditional mouse lung cancer models using adenoviral or lentiviral delivery of Cre recombinase. *Nat Protoc*, 4 (2009) 1064-1072.

[47] SR Hingorani, EF Petricoin, A Maitra, V Rajapakse, C King, MA Jacobetz, S Ross, TP Conrads, et al. Preinvasive and invasive ductal pancreatic cancer and its early detection in the mouse. *Cancer Cell*, 4 (2003) 437-450.

[48] KP Olive, DA Tuveson, ZC Ruhe, B Yin, NA Willis, RT Bronson, D Crowley, and T Jacks. Mutant p53 gain of function in two mouse models of Li-Fraumeni syndrome. *Cell*, 119 (2004) 847-860.

[49] S Weissmueller, E Manchado, M Saborowski, JP Morris, E Wagenblast, CA Davis, S-H Moon, NT Pfister, et al. Mutant p53 drives pancreatic cancer metastasis through cell-autonomous PDGF receptor β signaling. *Cell*, 157 (2014) 382-394.

[50] KR Hess, GR Varadhachary, SH Taylor, W Wei, MN Raber, R Lenzi, and JL Abbruzzese. Metastatic patterns in adenocarcinoma. *Cancer*, 106 (2006) 1624-1633.

[51] K Kojima, SM Vickers, NV Adsay, NC Jhala, HG Kim, TR Schoeb, WE Grizzle, and CA Klug. Inactivation of Smad4 accelerates Kras(G12D)-mediated pancreatic neoplasia. *Cancer Res*, 67 (2007) 8121-8130.

[52] A Fire, S Xu, MK Montgomery, SA Kostas, SE Driver, and CC Mello. Potent and specific genetic interference by double-stranded RNA in *Caenorhabditis elegans*. *Nature*, 391 (1998) 806-811.

[53] J Winter, S Jung, S Keller, RI Gregory, and S Diederichs. Many roads to maturity: microRNA biogenesis pathways and their regulation. *Nat Cell Biol*, 11 (2009) 228-234.

[54] RC Lee, RL Feinbaum, and V Ambros. The *C. elegans* heterochronic gene lin-4 encodes small RNAs with antisense complementarity to lin-14. *Cell*, 75 (1993) 843-854.

[55] LP Lim, ME Glasner, S Yekta, CB Burge, and DP Bartel. Vertebrate microRNA genes. *Science*, 299 (2003) 1540.

[56] C-Z Chen. MicroRNAs as oncogenes and tumor suppressors. *N Engl J Med*, 353 (2005) 1768-1771.

[57] GA Calin and CM Croce. MicroRNA signatures in human cancers. *Nat Rev Cancer*, 6 (2006) 857-866.

[58] YS Lee, K Nakahara, JW Pham, K Kim, Z He, EJ Sontheimer, and RW Carthew. Distinct roles for *Drosophila* Dicer-1 and Dicer-2 in the siRNA/miRNA silencing pathways. *Cell*, 117 (2004) 69-81.

[59] SM Elbashir, J Harborth, W Lendeckel, A Yalcin, K Weber, and T Tuschl. Duplexes of 21-nucleotide RNAs mediate RNA interference in cultured mammalian cells. *Nature*, 411 (2001) 494-498.

[60] PC Zamecnik and ML Stephenson. Inhibition of rous sarcoma virus replication and cell transformation by a specific oligodeoxynucleotide. *Proc Natl Acad Sci U S A*, 75 (1978) 280-284.

[61] JR Ecker and RW Davis. Inhibition of gene expression in plant cells by expression of antisense RNA. *Proc Natl Acad Sci U S A*, 83 (1986) 5372-5376.

[62] R Juliano, X Ming, and O Nakagawa. Cellular uptake and intracellular trafficking of antisense and siRNA oligonucleotides. *Bioconjug Chem*, 23 (2012) 147-157.

[63] N Dias and CA Stein. Antisense oligonucleotides: Basic concepts and mechanisms. *Molecular Cancer Therapeutics*, 1 (2002) 347-355.

[64] RS Geary, BF Baker, and ST Crooke. Clinical and preclinical pharmacokinetics and pharmacodynamics of mipomersen (kynamro): A second-generation antisense oligonucleotide inhibitor of apolipoprotein B. *Clin Pharmacokinet*, 54 (2015) 133-146.

[65] T Coelho, D Adams, A Silva, P Lozeron, PN Hawkins, T Mant, J Perez, J Chiesa, et al. Safety and efficacy of RNAi therapy for transthyretin amyloidosis. *N Engl J Med*, 369 (2013) 819-829.

[66] A Aigner. MicroRNAs (mirnas) in cancer invasion and metastasis: Therapeutic approaches based on metastasis-related mirnas. *J Mol Med*, (2011).

[67] W Xue, JE Dahlman, T Tammela, OF Khan, S Sood, A Dave, W Cai, LM Chirino, et al. Small RNA combination therapy for lung cancer. *Proc Natl Acad Sci U S A*, 111 (2014) E3553-3561.

[68] DS Schwarz, H Ding, L Kennington, JT Moore, J Schelter, J Burchard, PS Linsley, N Aronin, et al. Designing siRNA that distinguish between genes that differ by a single nucleotide. *PLoS Genet*, 2 (2006) e140.

[69] SI Pai, Y-Y Lin, B Macaes, A Meneshian, C-F Hung, and T-C Wu. Prospects of RNA interference therapy for cancer. *Gene Ther*, 13 (2006) 464-477.

[70] J Tabernero, GI Shapiro, PM LoRusso, A Cervantes, GK Schwartz, GJ Weiss, L Paz-Ares, DC Cho, et al. First-in-humans trial of an RNA interference therapeutic targeting VEGF and KSP in cancer patients with liver involvement. *Cancer Discov*, 3 (2013) 406-417.

[71] L He, X He, LP Lim, E de Stanchina, Z Xuan, Y Liang, W Xue, L Zender, et al. A microRNA component of the p53 tumour suppressor network. *Nature*, 447 (2007) 1130-1134.

[72] L He, JM Thomson, MT Hemann, E Hernando-Monge, D Mu, S Goodson, S Powers, C Cordon-Cardo, et al. A microRNA polycistron as a potential human oncogene. *Nature*, 435 (2005) 828-833.

[73] BJ Reinhart, FJ Slack, M Basson, AE Pasquinelli, JC Bettinger, AE Rougvie, HR Horvitz, and G Ruvkun. The 21-nucleotide let-7 RNA regulates developmental timing in Caenorhabditis elegans. *Nature*, 403 (2000) 901-906.

[74] AG Bader, D Brown, and M Winkler. The promise of microRNA replacement therapy. *Cancer Res*, 70 (2010) 7027-7030.

[75] DE Root, N Hacohen, WC Hahn, ES Lander, and DM Sabatini. Genome-scale loss-of-function screening with a lentiviral RNAi library. *Nat Methods*, 3 (2006) 715-719.

[76] HW Cheung, GS Cowley, BA Weir, JS Boehm, S Rusin, JA Scott, A East, LD Ali, et al. Systematic investigation of genetic vulnerabilities across cancer cell lines reveals lineage-specific dependencies in ovarian cancer. *Proc Natl Acad Sci U S A*, 108 (2011) 12372-12377.

[77] L Zender, W Xue, J Zuber, CP Semighini, A Krasnitz, B Ma, P Zender, S Kubicka, et al. An oncogenomics-based *in vivo* RNAi screen identifies tumor suppressors in liver cancer. *Cell*, 135 (2008) 852-864.

[78] S Chen, NE Sanjana, K Zheng, O Shalem, K Lee, X Shi, DA Scott, J Song, et al. Genome-wide CRISPR screen in a mouse model of tumor growth and metastasis. *Cell*, 160 (2015) 1246-1260.

[79] MH Porteus and D Baltimore. Chimeric nucleases stimulate gene targeting in human cells. *Science*, 300 (2003) 763.

[80] M Christian, T Cermak, EL Doyle, C Schmidt, F Zhang, A Hummel, AJ Bogdanove, and DF Voytas. Targeting DNA double-strand breaks with TAL effector nucleases. *Genetics*, 186 (2010) 757-761.

[81] P Horvath and R Barrangou. CRISPR/Cas, the immune system of bacteria and archaea. *Science*, 327 (2010) 167-170.

[82] M Jinek, K Chylinski, I Fonfara, M Hauer, JA Doudna, and E Charpentier. A programmable dual-RNA–guided DNA endonuclease in adaptive bacterial immunity. *Science*, 337 (2012) 816-821.

[83] JA Doudna and E Charpentier. Genome editing. The new frontier of genome engineering with CRISPR-Cas9. *Science*, 346 (2014) 1258096.

[84] PD Hsu, DA Scott, JA Weinstein, FA Ran, S Konermann, V Agarwala, Y Li, EJ Fine, et al. DNA targeting specificity of RNA-guided Cas9 nucleases. *Nat Biotechnol*, 31 (2013) 827-832.

[85] B Shen, W Zhang, J Zhang, J Zhou, J Wang, L Chen, L Wang, A Hodgkins, et al. Efficient genome modification by CRISPR-Cas9 nickase with minimal off-target effects. *Nat Meth*, 11 (2014) 399-402.

[86] FA Ran, PD Hsu, CY Lin, JS Gootenberg, S Konermann, A Trevino, DA Scott, A Inoue, et al. Double nicking by RNA-guided CRISPR Cas9 for enhanced genome editing specificity. *Cell*, 154 (2013).

[87] B Zetsche, SE Volz, and F Zhang. A split-Cas9 architecture for inducible genome editing and transcription modulation. *Nat Biotechnol*, 33 (2015) 139-142.

[88] AV Wright, SH Sternberg, DW Taylor, BT Staahl, JA Bardales, JE Kornfeld, and JA Doudna. Rational design of a split-Cas9 enzyme complex. *Proc Natl Acad Sci U S A*, 112 (2015) 2984-2989.

[89] ML Maeder, SJ Linder, VM Cascio, Y Fu, QH Ho, and JK Joung. CRISPR RNA-guided activation of endogenous human genes. *Nat Methods*, 10 (2013) 977-979.

[90] F Xie, L Ye, JC Chang, AI Beyer, J Wang, MO Muench, and YW Kan. Seamless gene correction of beta-thalassemia mutations in patient-specific iPSCs using CRISPR/Cas9 and piggybac. *Genome Res*, 24 (2014) 1526-1533.

[91] G Schwank, BK Koo, V Sasselli, JF Dekkers, I Heo, T Demircan, N Sasaki, S Boymans, et al. Functional repair of CFTR by CRISPR/Cas9 in intestinal stem cell organoids of cystic fibrosis patients. *Cell Stem Cell*, 13 (2013) 653-658.

[92] W Xue, S Chen, H Yin, T Tammela, T Papagiannakopoulos, NS Joshi, W Cai, G Yang, et al. CRISPR-mediated direct mutation of cancer genes in the mouse liver. *Nature*, 514 (2014) 380-384.

[93] KA Whitehead, R Langer, and DG Anderson. Knocking down barriers: Advances in siRNA delivery. *Nat Rev Drug Discov*, 8 (2009) 129-138.

[94] K Knop, R Hoogenboom, D Fischer, and US Schubert. Poly(ethylene glycol) in drug delivery: Pros and cons as well as potential alternatives. *Angew Chem Int Ed Engl*, 49 (2010) 6288-6308.

[95] BM Koeppen, BA Stanton. Renal physiology. Mosby, 2001.

[96] JE Zuckerman, CHJ Choi, H Han, and ME Davis. Polycation-siRNA nanoparticles can disassemble at the kidney glomerular basement membrane. *Proc Natl Acad Sci U S A*, 109 (2012) 3137-3142.

[97] A Schroeder, DA Heller, MM Winslow, JE Dahlman, GW Pratt, R Langer, T Jacks, and DG Anderson. Treating metastatic cancer with nanotechnology. *Nat Rev Cancer*, 12 (2012) 39-50.

[98] CV Pecot, GA Calin, RL Coleman, G Lopez-Berestein, and AK Sood. RNA interference in the clinic: Challenges and future directions. *Nat Rev Cancer*, 11 (2011) 59-67.

[99] J-H Park, G von Maltzahn, L Zhang, AM Derfus, D Simberg, TJ Harris, E Ruoslahti, SN Bhatia, et al. Systematic surface engineering of magnetic nanoworms for *in vivo* tumor targeting. *Small*, 5 (2009) 694-700.

[100] VP Chauhan, T Stylianopoulos, Y Boucher, and RK Jain. Delivery of molecular and nanoscale medicine to tumors: Transport barriers and strategies. *Annual Review of Chemical and Biomolecular Engineering*, 2 (2011) 281-298.

[101] H Hashizume, P Baluk, S Morikawa, JW McLean, G Thurston, S Roberge, RK Jain, and DM McDonald. Openings between defective endothelial cells explain tumor vessel leakiness. *Am J Pathol*, 156 (2000) 1363-1380.

[102] W Arap, R Pasqualini, and E Ruoslahti. Cancer treatment by targeted drug delivery to tumor vasculature in a mouse model. *Science*, 279 (1998) 377-380.

[103] RK Jain and T Stylianopoulos. Delivering nanomedicine to solid tumors. *Nat Rev Clin Oncol*, 7 (2010) 653-664.

[104] LD Leserman, J Barbet, F Kourilsky, and JN Weinstein. Targeting to cells of fluorescent liposomes covalently coupled with monoclonal antibody or protein A. *Nature*, 288 (1980) 602-604.

[105] DB Kirpotin, DC Drummond, Y Shao, MR Shalaby, K Hong, UB Nielsen, JD Marks, CC Benz, et al. Antibody targeting of long-circulating lipidic nanoparticles does not increase tumor localization but does increase internalization in animal models. *Cancer Res*, 66 (2006) 6732-6740.

[106] F Gu, L Zhang, BA Teply, N Mann, A Wang, AF Radovic-Moreno, R Langer, and OC Farokhzad. Precise engineering of targeted nanoparticles by using self-assembled biointegrated block copolymers. *Proc Natl Acad Sci U S A*, 105 (2008) 2586-2591.

[107] SE Lupold, BJ Hicke, Y Lin, and DS Coffey. Identification and characterization of nuclease-stabilized RNA molecules that bind human prostate cancer cells via the prostate-specific membrane antigen. *Cancer Res*, 62 (2002) 4029-4033.

[108] CP Graff and KD Wittrup. Theoretical analysis of antibody targeting of tumor spheroids: Importance of dosage for penetration, and affinity for retention. *Cancer Res*, 63 (2003) 1288-1296.

[109] T Saga, RD Neumann, T Heya, J Sato, S Kinuya, N Le, CH Paik, and JN Weinstein. Targeting cancer micrometastases with monoclonal antibodies: A binding-site barrier. *Proc Natl Acad Sci U S A*, 92 (1995) 8999-9003.

[110] O Feron. Tumor-penetrating peptides: A shift from magic bullets to magic guns. *Sci Transl Med*, 2 (2010) 34ps26.

[111] DW Bartlett, H Su, IJ Hildebrandt, WA Weber, and ME Davis. Impact of tumor-specific targeting on the biodistribution and efficacy of siRNA nanoparticles measured by multimodality *in vivo* imaging. *Proc Natl Acad Sci U S A*, 104 (2007) 15549-15554.

[112] KC Gatter, G Brown, IS Trowbridge, RE Woolston, and DY Mason. Transferrin receptors in human tissues: Their distribution and possible clinical relevance. *J Clin Pathol*, 36 (1983) 539-545.

[113] R Sciot, G Verhoeven, P Van Eyken, J Cailleau, and VJ Desmet. Transferrin receptor expression in rat liver: Immunohistochemical and biochemical analysis of the effect of age and iron storage. *Hepatology*, 11 (1990) 416-427.

[114] F Curnis, A Sacchi, A Gasparri, R Longhi, A Bachi, C Doglioni, C Bordignon, C Traversari, et al. Isoaspartate-glycine-arginine: A new tumor vasculature-targeting motif. *Cancer Res*, 68 (2008) 7073-7082.

[115] T Teesalu, KN Sugahara, VR Kotamraju, and E Ruoslahti. C-end rule peptides mediate neuropilin-1-dependent cell, vascular, and tissue penetration. *Proc Natl Acad Sci U S A*, 106 (2009) 16157-16162.

[116] KN Sugahara, T Teesalu, PP Karmali, VR Kotamraju, L Agemy, OM Girard, D Hanahan, RF Mattrey, et al. Tissue-penetrating delivery of compounds and nanoparticles into tumors. *Cancer Cell*, 16 (2009) 510-520.

[117] V Fogal, L Zhang, S Krajewski, and E Ruoslahti. Mitochondrial/cell-surface protein p32/gC1qR as a molecular target in tumor cells and tumor stroma. *Cancer Res*, 68 (2008) 7210-7218.

[118] G von Maltzahn, Y Ren, J-H Park, D-H Min, VR Kotamraju, J Jayakumar, V Fogal, MJ Sailor, et al. *In vivo* tumor cell targeting with "click" nanoparticles. *Bioconjug Chem*, 19 (2008) 1570-1578.

[119] KN Sugahara, T Teesalu, PP Karmali, VR Kotamraju, L Agemy, DR Greenwald, and E Ruoslahti. Coadministration of a tumor-penetrating peptide enhances the efficacy of cancer drugs. *Science*, 328 (2010) 1031-1035.

[120] Y Akashi, T Oda, Y Ohara, R Miyamoto, T Kurokawa, S Hashimoto, T Enomoto, K Yamada, et al. Anticancer effects of gemcitabine are enhanced by co-administered iRGD peptide in murine pancreatic cancer models that overexpressed neuropilin-1. *Br J Cancer*, 110 (2014) 1481-1487.

[121] CE Thomas, A Ehrhardt, and MA Kay. Progress and problems with the use of viral vectors for gene therapy. *Nat Rev Genet*, 4 (2003) 346-358.

[122] AC Hunter. Molecular hurdles in polyfectin design and mechanistic background to polycation induced cytotoxicity. *Adv Drug Deliv Rev*, 58 (2006) 1523-1531.

[123] J Elmén, M Lindow, S Schütz, M Lawrence, A Petri, S Obad, M Lindholm, M Hedtjärn, et al. Lna-mediated microRNA silencing in non-human primates. *Nature*, 452 (2008) 896-899.

[124] JB Lee, J Hong, DK Bonner, Z Poon, and PT Hammond. Self-assembled RNA interference microsponges for efficient siRNA delivery. *Nat Mater*, 11 (2012) 316-322.

[125] NM Snead, JR Escamilla-Powers, JJ Rossi, and AP McCaffrey. 5[prime] unlocked nucleic acid modification improves siRNA targeting. *Mol Ther Nucleic Acids*, 2 (2013) e103.

[126] AL Jackson, J Burchard, D Leake, A Reynolds, J Schelter, J Guo, JM Johnson, L Lim, et al. Position-specific chemical modification of sirnas reduces “off-target” transcript silencing. *RNA*, 12 (2006) 1197-1205.

[127] A Akinc, M Goldberg, J Qin, JR Dorkin, C Gamba-Vitalo, M Maier, KN Jayaprakash, M Jayaraman, et al. Development of lipidoid-siRNA formulations for systemic delivery to the liver. *Mol Ther*, 17 (2009) 872-879.

[128] JE Dahlman, C Barnes, O Khan, A Thiriot, S Jhunjunwala, TE Shaw, Y Xing, HB Sager, et al. *In vivo* endothelial siRNA delivery using polymeric nanoparticles with low molecular weight. *Nat Nanotechnol*, (2014).

[129] JI Cutler, E Auyeung, and CA Mirkin. Spherical nucleic acids. *J Am Chem Soc*, 134 (2012) 1376-1391.

[130] H Lee, AK Lytton-Jean, Y Chen, KT Love, AI Park, ED Karagiannis, A Sehgal, W Querbes, et al. Molecularly self-assembled nucleic acid nanoparticles for targeted *in vivo* siRNA delivery. *Nat Nanotechnol*, 7 (2012) 389-393.

[131] O Boussif, F Lezoualc'h, MA Zanta, MD Mergny, D Scherman, B Demeneix, and JP Behr. A versatile vector for gene and oligonucleotide transfer into cells in culture and *in vivo*: Polyethylenimine. *Proc Natl Acad Sci U S A*, 92 (1995) 7297-7301.

[132] ME Davis, JE Zuckerman, CHJ Choi, D Seligson, A Tolcher, CA Alabi, Y Yen, JD Heidel, et al. Evidence of RNAi in humans from systemically administered siRNA via targeted nanoparticles. *Nature*, 464 (2010) 1067-1070.

[133] A Agrawal, D-H Min, N Singh, H Zhu, A Birjiniuk, G von Maltzahn, TJ Harris, D Xing, et al. Functional delivery of siRNA in mice using dendriworms. *ACS Nano*, 3 (2009) 2495-2504.

[134] S Matsuda, K Keiser, JK Nair, K Charisse, RM Manoharan, P Kretschmer, CG Peng, VKi A, et al. siRNA conjugates carrying sequentially assembled trivalent N-Acetylgalactosamine linked through nucleosides elicit robust gene silencing *in vivo* in hepatocytes. *ACS Chem Biol*, (2015).

[135] S Fawell, J Seery, Y Daikh, C Moore, LL Chen, B Pepinsky, and J Barsoum. Tat-mediated delivery of heterologous proteins into cells. *Proc Natl Acad Sci U S A*, 91 (1994) 664-668.

[136] MT Sciortino, B Taddeo, APW Poon, A Mastino, and B Roizman. Of the three tegument proteins that package mRNA in herpes simplex virions, one (VP22) transports the mrna to uninfected cells for expression prior to viral infection. *Proc Natl Acad Sci U S A*, 99 (2002) 8318-8323.

[137] S Futaki, T Suzuki, W Ohashi, T Yagami, S Tanaka, K Ueda, and Y Sugiura. Arginine-rich peptides. An abundant source of membrane-permeable peptides having potential as carriers for intracellular protein delivery. *J Biol Chem*, 276 (2001) 5836-5840.

[138] P Kumar, H-S Ban, S-S Kim, H Wu, T Pearson, DL Greiner, A Laouar, J Yao, et al. T cell-specific siRNA delivery suppresses HIV-1 infection in humanized mice. *Cell*, 134 (2008) 577-586.

[139] Z Ma, J Li, F He, A Wilson, B Pitt, and S Li. Cationic lipids enhance siRNA-mediated interferon response in mice. *Biochem Biophys Res Commun*, 330 (2005) 755-759.

[140] M Pooga, C Kut, M Kihlmark, M Hällbrink, S Fernaeus, R Raid, T Land, E Hallberg, et al. Cellular translocation of proteins by transportan. *FASEB J*, 15 (2001) 1451-1453.

[141] U Soomets, M Lindgren, X Gallet, M Hällbrink, A Elmquist, L Balaspiri, M Zorko, M Pooga, et al. Deletion analogues of transportan. *Biochim Biophys Acta*, 1467 (2000) 165-176.

[142] D Derossi, AH Joliot, G Chassaing, and A Prochiantz. The third helix of the antennapedia homeodomain translocates through biological membranes. *J Biol Chem*, 269 (1994) 10444-10450.

[143] L Kurzawa, M Pellerano, and MC Morris. Pep and cady-mediated delivery of fluorescent peptides and proteins into living cells. *Biochim Biophys Acta*, 1798 (2010) 2274-2285.

[144] MC Morris, E Gros, G Aldrian-Herrada, M Choob, J Archdeacon, F Heitz, and G Divita. A non-covalent peptide-based carrier for *in vivo* delivery of DNA mimics. *Nucleic Acids Res*, 35 (2007) e49.

[145] Y Dong, KT Love, JR Dorkin, S Sirirungruang, Y Zhang, D Chen, RL Bogorad, H Yin, et al. Lipopeptide nanoparticles for potent and selective siRNA delivery in rodents and nonhuman primates. *Proc Natl Acad Sci U S A*, 111 (2014) 3955-3960.

[146] Alnylam Pharmaceuticals. Alnylam and collaborators present new clinical data for patisiran, an RNAi therapeutic targeting transthyretin (TTR) in development for the treatment of TTR-mediated amyloidosis (ATTR), 2014.

[147] X-B Xiong and A Lavasanifar. Traceable multifunctional micellar nanocarriers for cancer-targeted co-delivery of mdr-1 siRNA and doxorubicin. *ACS Nano*, 5 (2011) 5202-5213.

[148] Y Ren, S Hauert, JH Lo, and SN Bhatia. Identification and characterization of receptor-specific peptides for siRNA delivery. *ACS Nano*, 6 (2012) 8620-8631.

[149] Y Ren, HW Cheung, G von Maltzhan, A Agrawal, GS Cowley, BA Weir, JS Boehm, P Tamayo, et al. Targeted tumor-penetrating siRNA nanocomplexes for credentialing the ovarian cancer oncogene id4. *Sci Transl Med*, 4 (2012) 147ra112.

[150] M Jinek, F Jiang, DW Taylor, SH Sternberg, E Kaya, E Ma, C Anders, M Hauer, et al. Structures of Cas9 endonucleases reveal RNA-mediated conformational activation. *Science*, 343 (2014) 1247997.

[151] R Cheng, J Peng, Y Yan, P Cao, J Wang, C Qiu, L Tang, D Liu, et al. Efficient gene editing in adult mouse livers via adenoviral delivery of CRISPR/Cas9. *FEBS Letters*, 588 (2014) 3954-3958.

[152] E Senis, C Fatouros, S Grosse, E Wiedtke, D Niopek, AK Mueller, K Borner, and D Grimm. CRISPR/Cas9-mediated genome engineering: An adeno-associated viral (AAV) vector toolbox. *Biotechnol J*, 9 (2014) 1402-1412.

[153] S Ramakrishna, AB Kwaku Dad, J Beloor, R Gopalappa, SK Lee, and H Kim. Gene disruption by cell-penetrating peptide-mediated delivery of Cas9 protein and guide RNA. *Genome Res*, 24 (2014) 1020-1027.

[154] JA Zuris, DB Thompson, Y Shu, JP Guilinger, JL Bessen, JH Hu, ML Maeder, JK Joung, et al. Cationic lipid-mediated delivery of proteins enables efficient protein-based genome editing *in vitro* and *in vivo*. *Nat Biotechnol*, 33 (2015) 73-80.

[155] PJ Vanveldhuizen, M Zulfiqar, S Banerjee, R Cherian, NK Saxena, A Rabe, JB Thrasher, and SK Banerjee. Differential expression of neuropilin-1 in malignant and benign prostatic stromal tissue. *Oncol Rep*, 10 (2003) 1067-1071.

[156] U Yaqoob, S Cao, U Shergill, K Jagavelu, Z Geng, M Yin, TM de Assuncao, Y Cao, et al. Neuropilin-1 stimulates tumor growth by increasing fibronectin fibril assembly in the tumor microenvironment. *Cancer Res*, 72 (2012) 4047-4059.

[157] JS Wey, MJ Gray, F Fan, A Belcheva, MF McCarty, O Stoeltzing, R Somcio, W Liu, et al. Overexpression of neuropilin-1 promotes constitutive mapk signalling and chemoresistance in pancreatic cancer cells. *Br J Cancer*, 93 (2005) 233-241.

[158] Y Zhang, C Chen, Q Yao, and M Li. Zip4 upregulates the expression of neuropilin-1, vascular endothelial growth factor, and matrix metalloproteases in pancreatic cancer cell lines and xenografts. *Cancer Biol Ther*, 9 (2010) 236-242.

[159] H Zhu, ZY Liang, XY Ren, and TH Liu. Small interfering rnas targeting mutant K-ras inhibit human pancreatic carcinoma cells growth *in vitro* and *in vivo*. *Cancer Biol Ther*, 5 (2006) 1693-1698.

[160] E Zorde Khvalevsky, R Gabai, IH Rachmut, E Horwitz, Z Brunschwig, A Orbach, A Shemi, T Golan, et al. Mutant KRAS is a druggable target for pancreatic cancer. *Proceedings of the National Academy of Sciences*, 110 (2013) 20723-20728.

[161] A Singh, MF Sweeney, M Yu, A Burger, P Greninger, C Benes, DA Haber, and J Settleman. TAK1 (MAP3K7) inhibition promotes apoptosis in KRAS-dependent colon cancers. *Cell*, 148 (2012) 639-650.

[162] EL Deer, J Gonzalez-Hernandez, JD Coursen, JE Shea, J Ngatia, CL Scaife, MA Firpo, and SJ Mulvihill. Phenotype and genotype of pancreatic cancer cell lines. *Pancreas*, 39 (2010) 425-435.

[163] L Crombez, G Aldrian-Herrada, K Konate, QN Nguyen, GK McMaster, R Brasseur, F Heitz, and G Divita. A new potent secondary amphipathic cell-penetrating peptide for siRNA delivery into mammalian cells. *Mol Ther*, 17 (2008) 95-103.

[164] SL Ginn, IE Alexander, ML Edelstein, MR Abedi, and J Wixon. Gene therapy clinical trials worldwide to 2012 - an update. *J Gene Med*, 15 (2013) 65-77.

[165] A Sato, SW Choi, M Hirai, A Yamayoshi, R Moriyama, T Yamano, M Takagi, A Kano, et al. Polymer brush-stabilized polyplex for a siRNA carrier with long circulatory half-life. *J Control Release*, 122 (2007) 209-216.

[166] KT Love, KP Mahon, CG Levins, KA Whitehead, W Querbes, JR Dorkin, J Qin, W Cantley, et al. Lipid-like materials for low-dose, *in vivo* gene silencing. *Proc Natl Acad Sci U S A*, 107 (2010) 1864-1869.

[167] A Akinc, A Zumbuehl, M Goldberg, ES Leshchiner, V Busini, N Hossain, SA Bacallado, DN Nguyen, et al. A combinatorial library of lipid-like materials for delivery of RNAi therapeutics. *Nat Biotechnol*, 26 (2008) 561-569.

[168] A Malek, O Merkel, L Fink, F Czubayko, T Kissel, and A Aigner. *In vivo* pharmacokinetics, tissue distribution and underlying mechanisms of various PEI(-PEG)/siRNA complexes. *Toxicol Appl Pharmacol*, 236 (2009) 97-108.

[169] T Teesalu, KN Sugahara, and E Ruoslahti. Tumor-penetrating peptides. *Front Oncol*, 3 (2013) 216.

[170] KY Lin, EJ Kwon, JH Lo, and SN Bhatia. Drug-induced amplification of nanoparticle targeting to tumors. *Nano Today*, 9 (2014) 550-559.

[171] J-H Park, G von Maltzahn, MJ Xu, V Fogal, VR Kotamraju, E Ruoslahti, SN Bhatia, and MJ Sailor. Cooperative nanomaterial system to sensitize, target, and treat tumors. *Proceedings of the National Academy of Sciences*, 107 (2010) 981-986.

[172] M Uchida, H Kosuge, M Terashima, DA Willits, LO Liepold, MJ Young, MV McConnell, and T Douglas. Protein cage nanoparticles bearing the LyP-1 peptide for enhanced imaging of macrophage-rich vascular lesions. *ACS Nano*, 5 (2011) 2493-2502.

[173] JW Seo, H Baek, LM Mahakian, J Kusunose, J Hamzah, E Ruoslahti, and KW Ferrara. 64cu-labeled LyP-1-dendrimer for PET-CT imaging of atherosclerotic plaque. *Bioconjugate Chemistry*, 25 (2014) 231-239.

[174] DW Pack, AS Hoffman, S Pun, and PS Stayton. Design and development of polymers for gene delivery. *Nat Rev Drug Discov*, 4 (2005) 581-593.

[175] A Aied, U Greiser, A Pandit, and W Wang. Polymer gene delivery: Overcoming the obstacles. *Drug Discov Today*, 18 (2013) 1090-1098.

[176] JV Jokerst, T Lobovkina, RN Zare, and SS Gambhir. Nanoparticle pegylation for imaging and therapy. *Nanomedicine (Lond)*, 6 (2011) 715-728.

[177] KY Lin, JH Lo, N Consul, GA Kwong, and SN Bhatia. Self-titrating anticoagulant nanocomplexes that restore homeostatic regulation of the coagulation cascade. *ACS Nano*, 8 (2014) 8776-8785.

[178] G von Maltzahn, JH Park, A Agrawal, NK Bandaru, SK Das, MJ Sailor, and SN Bhatia. Computationally guided photothermal tumor therapy using long-circulating gold nanorod antennas. *Cancer Res*, 69 (2009) 3892-3900.

[179] S Mishra, P Webster, and ME Davis. Pegylation significantly affects cellular uptake and intracellular trafficking of non-viral gene delivery particles. *Eur J Cell Biol*, 83 (2004) 97-111.

[180] HS Qhattal, T Hye, A Alali, and X Liu. Hyaluronan polymer length, grafting density, and surface poly(ethylene glycol) coating influence *in vivo* circulation and tumor targeting of hyaluronan-grafted liposomes. *ACS Nano*, 8 (2014) 5423-5440.

[181] CE Nelson, JR Kintzing, A Hanna, JM Shannon, MK Gupta, and CL Duvall. Balancing cationic and hydrophobic content of pegylated siRNA polyplexes enhances endosome escape, stability, blood circulation time, and bioactivity *in vivo*. *ACS Nano*, 7 (2013) 8870-8880.

[182] S Gao, F Dagnaes-Hansen, EJ Nielsen, J Wengel, F Besenbacher, KA Howard, and J Kjems. The effect of chemical modification and nanoparticle formulation on stability and biodistribution of siRNA in mice. *Mol Ther*, 17 (2009) 1225-1233.

[183] M Srinivasarao, CV Galliford, and PS Low. Principles in the design of ligand-targeted cancer therapeutics and imaging agents. *Nat Rev Drug Discov*, 14 (2015) 203-219.

[184] TR Daniels, T Delgado, G Helguera, and ML Penichet. The transferrin receptor part II: Targeted delivery of therapeutic agents into cancer cells. *Clin Immunol*, 121 (2006) 159-176.

[185] A Akinc, W Querbes, S De, J Qin, M Frank-Kamenetsky, KN Jayaprakash, M Jayaraman, KG Rajeev, et al. Targeted delivery of RNAi therapeutics with endogenous and exogenous ligand-based mechanisms. *Mol Ther*, 18 (2010) 1357-1364.

[186] S Nie. Understanding and overcoming major barriers in cancer nanomedicine. *Nanomedicine (Lond)*, 5 (2010) 523-528.

[187] AM Alkilany, SR Abulateefeh, KK Mills, AI Bani Yaseen, MA Hamaly, HS Alkhatib, KM Aiedeh, and JW Stone. Colloidal stability of citrate and mercaptoacetic acid capped gold nanoparticles upon lyophilization: Effect of capping ligand attachment and type of cryoprotectants. *Langmuir*, 30 (2014) 13799-13808.

[188] JP Morton, P Timpson, SA Karim, RA Ridgway, D Athineos, B Doyle, NB Jamieson, KA Oien, et al. Mutant p53 drives metastasis and overcomes growth arrest/senescence in pancreatic cancer. *Proc Natl Acad Sci U S A*, 107 (2010) 246-251.

[189] PD Hsu, DA Scott, JA Weinstein, FA Ran, S Konermann, V Agarwala, Y Li, EJ Fine, et al. DNA targeting specificity of RNA-guided Cas9 nucleases. *Nat Biotech*, 31 (2013) 827-832.

[190] RJ Platt, S Chen, Y Zhou, MJ Yim, L Swiech, HR Kempton, JE Dahlman, O Parnas, et al. CRISPR-Cas9 knockin mice for genome editing and cancer modeling. *Cell*, 159 (2014) 440-455.

[191] D Rajotte, W Arap, M Hagedorn, E Koivunen, R Pasqualini, and E Ruoslahti. Molecular heterogeneity of the vascular endothelium revealed by *in vivo* phage display. *The Journal of Clinical Investigation*, 102 (1998) 430-437.

[192] P Laakkonen and K Vuorinen. Homing peptides as targeted delivery vehicles. *Integrative Biology*, 2 (2010) 326-337.

[193] MC Morris, J Depollier, J Mery, F Heitz, and G Divita. A peptide carrier for the delivery of biologically active proteins into mammalian cells. *Nat Biotech*, 19 (2001) 1173-1176.

[194] LE Jao, SR Wente, and W Chen. Efficient multiplex biallelic zebrafish genome editing using a CRISPR nuclease system. *Proc Natl Acad Sci U S A*, 110 (2013) 13904-13909.

[195] PW Rothemund. Folding DNA to create nanoscale shapes and patterns. *Nature*, 440 (2006) 297-302.

[196] Y Ke, LL Ong, W Sun, J Song, M Dong, WM Shih, and P Yin. DNA brick crystals with prescribed depths. *Nat Chem*, 6 (2014) 994-1002.

[197] B Wei, M Dai, and P Yin. Complex shapes self-assembled from single-stranded DNA tiles. *Nature*, 485 (2012) 623-626.

[198] GM Church, Y Gao, and S Kosuri. Next-generation digital information storage in DNA. *Science*, 337 (2012) 1628.

[199] TJ Harris, G von Maltzahn, ME Lord, JH Park, A Agrawal, DH Min, MJ Sailor, and SN Bhatia. Protease-triggered unveiling of bioactive nanoparticles. *Small*, 4 (2008) 1307-1312.

[200] GA Kwong, G von Maltzahn, G Murugappan, O Abudayyeh, S Mo, IA Papayannopoulos, DY Sverdlov, SB Liu, et al. Mass-encoded synthetic biomarkers for multiplexed urinary monitoring of disease. *Nat Biotechnol*, 31 (2013) 63-70.

[201] AD Warren, GA Kwong, DK Wood, KY Lin, and SN Bhatia. Point-of-care diagnostics for noncommunicable diseases using synthetic urinary biomarkers and paper microfluidics. *Proc Natl Acad Sci U S A*, 111 (2014) 3671-3676.

[202] JH Lo, G von Maltzahn, J Douglass, JH Park, MJ Sailor, E Ruoslahti, and SN Bhatia. Nanoparticle amplification photothermal unveiling of cryptic collagen binding sites. *J Mater Chem B Mater Biol Med*, 1 (2013) 5235-5240.

[203] P Diagaradjane, A Shetty, JC Wang, AM Elliott, J Schwartz, S Shentu, HC Park, A Deorukhkar, et al. Modulation of *in vivo* tumor radiation response via gold nanoshell-mediated vascular-focused hyperthermia: Characterizing an integrated antihypoxic and localized vascular disrupting targeting strategy. *Nano Lett*, 8 (2008) 1492-1500.

[204] DK Kirui, C Celia, R Molinaro, SS Bansal, D Cosco, M Fresta, H Shen, and M Ferrari. Mild hyperthermia enhances transport of liposomal gemcitabine and improves *in vivo* therapeutic response. *Advanced Healthcare Materials*, (2015).

[205] DK Chatterjee, P Diagaradjane, and S Krishnan. Nanoparticle-mediated hyperthermia in cancer therapy. *Ther Deliv*, 2 (2011) 1001-1014.

[206] AF Bagley, R Scherz-Shouval, PA Galie, AQ Zhang, J Wyckoff, L Whitesell, CS Chen, S Lindquist, SN Bhatia. Endothelial thermotolerance impairs nanoparticle transport in tumors. *Cancer Research* (2015).

[207] S Maluta, M Schaffer, F Pioli, S Dall'oglio, S Pasetto, PM Schaffer, B Weber, and MG Giri. Regional hyperthermia combined with chemoradiotherapy in primary or recurrent locally advanced pancreatic cancer : An open-label comparative cohort trial. *Strahlenther Onkol*, 187 (2011) 619-625.

Chapter 8: Appendix [^]

8.1 Preliminary results

8.1.1 mRNA delivery

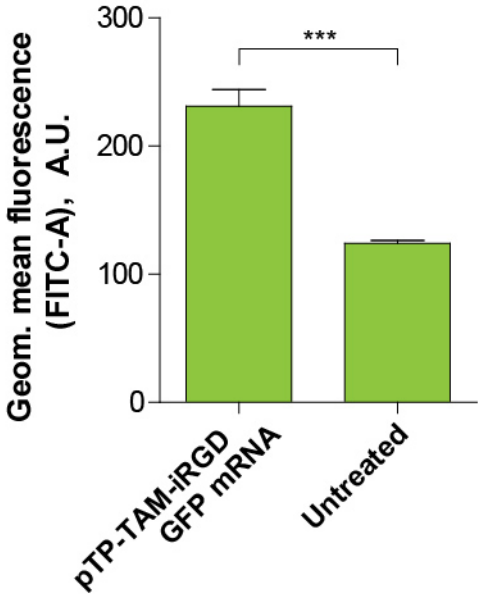

Fig. 8-1: mRNA delivery with tandem peptides. Average geometric mean fluorescence of cells 24 hours after transfection with GFP mRNA compared to untreated controls. Statistical significance determined by two-tailed t-test; ***: $p < 0.001$.

Method: MIA PaCa-2 cells were plated at 2,500 cells per well in a 96-well plate, 24 hours prior to dosing. Cells were transfected with tandem peptide-mRNA complexes at 1.5 μM pTP-TAM-iRGD encapsulating 0.5 μg of GFP mRNA per well (100 μL total in Opti-MEM, ~3 nM mRNA). After 3 hours, transfection solutions were supplemented with 100 μL of DMEM + 20% fetal bovine serum. Cells were trypsinized after 24 hours and analyzed by flow cytometry on a Becton Dickinson LSR-II HTS flow cytometer. Data were analyzed in Flow-Jo.

8.1.2 Pancreatic targeting

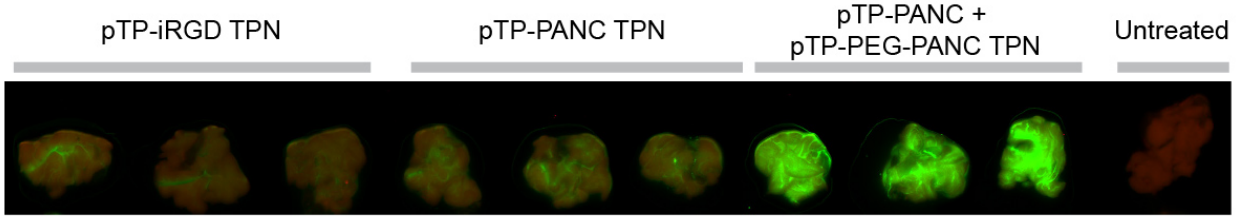

Figure 8-2: pTP-SWCEPGWCR delivery to the pancreas. Delivery of VivoTag-S750-labeled siRNA (green) to healthy pancreata of mice by pTP-iRGD (left), pTP-PANC (SWCEPGWCR) (center), or PEGylated pTP-PANC TPNs (right). Delivery by PEGylated pTP-PANC TPNs exceeded that of pTP-iRGD particles by ~5-fold.

Method:
pTP-SWCEPGWCR ("pTP-PANC") peptide (full sequence: palmitoyl-GWTLNSAGYLLGKINLKALAALAKKILGGKKKKGGSWCEPGWCR) was synthesized by CPC Scientific. Four hydrophilic residues were added to the linker between the two peptide domains to improve solubility in aqueous solutions, given the hydrophobic character of the targeting peptide. pTP-PEG-SWCEPGWCR was synthesized as described in Section 3.4, replacing azidoacetyl-LyP-1 with azidoacetyl-SWCEPGWCR. For biodistribution studies, Swiss Webster mice were injected intravenously with 10:0:1 pTP-iRGD:pTP-PEG-iRGD:VivoTag-S750-siRNA or 10:0:1 or 10:10:1 pTP-PANC:pTP-PEG-PANC:VivoTag-S750-siRNA at 0.5 nmol total siRNA dose in 100 μL D5W (5% D-glucose solution). Mice were sacrificed after 3 hours, and pancreata were removed upon necropsy and imaged on a LI-COR Odyssey near-infrared scanner.

8.1.3 microRNA delivery

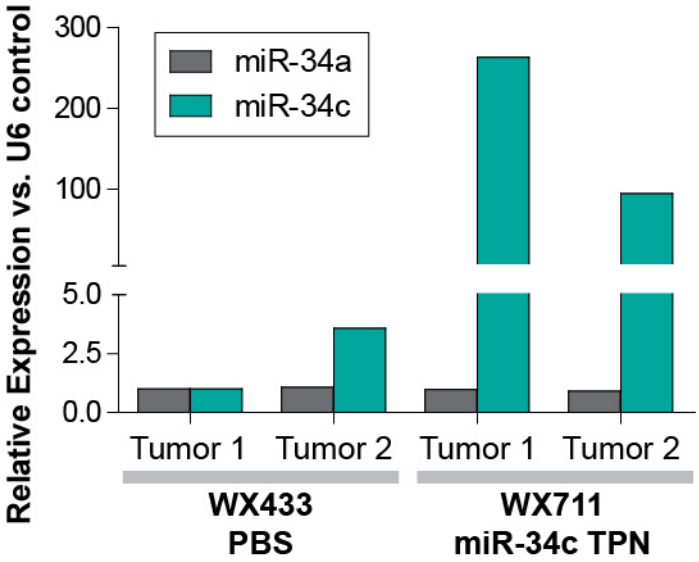

Figure 8-3: microRNA delivery in vivo. Delivery of pro-apoptotic microRNA-34c to genetically-engineered mouse models of lung cancer; mouse WX433 was treated with PBS while WX711 was treated with miR-34c TPNs.

Method:
KP mice ($Kras^{LSL\text{-}G12D}$;$p53^{fl/fl}$) with lung tumors induced by intratracheally-administered lentiviruses delivering Cre recombinase and GFP were dosed with either 100 μL PBS or mTP-LyP1 TPNs, comprised of 20:1 peptide:microRNA-34c for a total dose of 1 mg/kg microRNA (GE Dharmacon miRIDIAN microRNA mimic). After 24 hours, tumors were selectively harvested and separated from healthy lung tissue by dissection under a fluorescent dissection microscope. Samples were homogenized and microRNA was quantified using the Applied Biosciences Taqman miRNA qPCR assay and commercially-available hairpin primers (Life Technologies). microRNA-34c and microRNA-34a levels were quantified relative to a U6 microRNA control.

8.2 Contributions from colleagues and collaborators.

I certify that the written content of this thesis is my own original work, and except where cited otherwise, I have striven to create my own artwork and presentations of the data. It goes without saying that many of the concepts and experiments contained within could not possibly have been executed without the help of many collaborators and labmates, hence the use of "we" rather than "I" throughout the thesis. Furthermore, I would like to specifically give credit for the following:

Chapter 2: Angela Zhang performed the experiments in panels Figure 2-3A and Figure 2-4E, and helped with the experiments in Figure 2-5.

Chapter 3: This chapter is adapted from a recently submitted manuscript co-authored by Ester Kwon and myself. Ester Kwon conceived of the chemical syntheses for modular PEG strategies as presented here, improving considerably upon preliminary experiments I performed demonstrating that random PEGylation of peptide at lysine residues improved particle stability. Ester also helped with experiments presented in Figure 3-2 (materials), Figure 3-3 (particle formation), Figure 3-5B, and Figure 3-6A-C, and wholly performed the experiment shown in Figure 3-5C. Angela Zhang helped with Figure 3-2 and Figure 3-4.

Chapter 4: Mandar Muzumdar bred and raised the GEM mouse models, used particularly in Fig. 4-6B. Jeffrey Wyckoff performed intravital fluorescence microscopy for Figure 4-6C. Angela Zhang performed the blinded tumor measurements presented in Figure 4-6D. Dong-Soo Yun performed the TEM imaging in Fig. 4-1D.

Chapter 5: David Canner created or provided all FRT-based cell lines and designed and synthesized guide RNAs, templates, and primer sets pertaining to Figures 5-2, 5-3, and 5-4. He additionally performed the qPCR analysis presented in Fig. 5-3.

I would also like to give credit to the Koch Institute Core Facilities, whose instrumentation and staff were essential to this work. Particularly, these experiments would not be possible without the Flow Cytometry Core, Biopolymers & Proteomics Core (peptide synthesis, HPLC, lyophilization, mass spectrometry), Nanoparticle Materials Core (TEM, high-throughput DLS), Microscopy Core (intravital imaging), Animal Imaging and Preclinical Testing Core (IVIS and CT), and Histology Core (sample sectioning and staining).

8.3 Curriculum Vitae

Education

Massachusetts Institute of Technology, Cambridge, MA, September 2010-June 2015
Division of Health Sciences & Technology
Candidate for PhD in Medical Engineering/Medical Physics Program. GPA 5.0/5.0.

Harvard Medical School, Boston, MA, July 2008-present
Candidate for MD as part of Medical Scientist Training Program (MD-PhD)

Massachusetts Institute of Technology, Cambridge, MA, September 2004-June 2008
B.S. in Biological Engineering, 2008 and B.S. in Music, 2008. GPA: 5.0/5.0.

Chapel Hill High School, Chapel Hill, NC, August 2001-June 2004
Graduated 5th in class of 380, June 2004. Weighted GPA: 5.2. Unweighted GPA: 4.0/4.0.

Research Experience

S. N. Bhatia Lab, HST, Koch Institute for Cancer Research at MIT, Cambridge, MA. *PhD candidate*
Feb. 2008 – Oct. 2008 (rotation during medical school), Sept. 2010 – Present (graduate student)

- Designed and characterized iRGD-targeted tumor-penetrating nanocomplexes for delivery of siRNA to pancreatic cancer. With post-doctoral researcher Ester Kwon and undergraduate research assistant Angela Zhang, systematically compared modular strategies for nanocomplex stabilization, identifying formulations that retain function while improving particle stability and pharmacokinetics. Presently testing stabilized iRGD nanocomplexes as delivery vehicles for therapeutic siRNA in animal models of pancreatic cancer. *Manuscript on modular stabilization strategies has been submitted; a second on siRNA delivery to PDAC in preparation.*
- Adapted tandem peptide technology for targeted delivery of CRISPR/Cas9 reagents, to allow selective gene editing. The end goal of this project is to create a platform for systemic delivery of pancreas-targeted CRISPR/Cas9 nanocomplexes in order to create sporadic animal models of pancreatic cancer with known genotypes.
- Helped to design and characterize nanoparticle self-titrating anticoagulants (nanoSTATs), where anticoagulant release from the particles is triggered by cleavage of the particle by activated thrombin, thus acting as a negative feedback loop for regulating inappropriate thrombin activity. Particular focus on kinetic studies *in vitro* to quantify the process of unveiling anticoagulant function as well as safety profiling *in vivo*. *Published (see Article 4).*
- Studied new tumor-targeted bacteria and bacterially-derived minicells, with particular focus on working with post-doctoral fellow Tal Danino on animal studies to demonstrate the feasibility and behavior of quorum-sensing synthetic biology circuits in the tumor environment. *Published (see Article 7).*

- Investigated and validated a paradigm for stigmergic communication between nanoparticles, for the purpose of targeted amplification of tumor therapy with graduate student Geoffrey von Maltzahn. Demonstrated how irradiated gold nanorod particles can initially interact with and modify tumor extracellular matrix in order to provide amplified recruitment of targeted secondary particles. Such signaling schemes could help minimize off-target side effects associated with cancer chemotherapy. *Published (see Article 6).*

J. P. Vacanti Lab, Center for Regenerative Medicine at MGH, Boston, MA. *Researcher*
January 2009 – August 2009 (rotation during medical school)

- Developed and tested a tissue-engineered blood gas exchange device that allows gas exchange across a cellularized ultra-thin collagen membrane, an important step towards creating functional tissue engineered artificial lungs. The project's team included a surgical research fellow and mechanical engineer. Devices with optimal channel depth, membrane thickness, gas exchange length, and blood flow rate showed highly efficient oxygen and carbon dioxide gas transfer. *This project and related work have been published as two separate manuscripts (see Articles 5 and 10).*

B. P. Engelward Lab, Dept. of Biological Engineering, MIT, Cambridge, MA**.** *Researcher & Animator*
February 2005 – December 2007 (undergraduate)

- Helped design a miniaturized, multiplexed device for rapid and automated analysis of the single-cell gel electrophoresis (comet) assay. An improved assay would reduce variability and increase throughput, enabling its use as a toxicology screen and for investigating the kinetics of DNA repair.
- Created animated videos to elucidate key DNA repair mechanisms, integrating dynamic graphics and scientific literature; published as part of a review article (see Article 11). Also created 3D animations of the same processes for the MIT Museum and the MIT Open Labware project for educational purposes.

Publications

Articles

1. **Lo JH***, Kwon EJ*, Zhang AQ, Singhal P, Bhatia SN. Modular strategies for stabilization of self-assembled nanoparticles. *Submitted*.
2. Kwon EJ, **Lo JH**, Bhatia SN. Smart nanosystems: Bio-inspired technologies that interact with the host environment. *Submitted*.
3. Lin KY, Kwon EJ, **Lo JH**, Bhatia SN. Drug-induced amplification of nanoparticle targeting to tumors. *Nano Today*. 2014 Sep 1; 9(5): 550-559.
4. Lin KY, **Lo JH**, Consul N, Kwong GA, Bhatia SN. Self-titrating anticoagulant nanocomplexes that restore homeostatic regulation of the coagulation cascade. *ACS Nano*. 2014 Sep 23; 8(9):8776-85.

5. **Lo JH**, Bassett EK, Penson EJ, Hoganson DM, Vacanti JP. Gas transfer in cellularized collagen-membrane lung assist devices, *Accepted at Tissue Engineering Part A*.
6. **Lo JH***, von Maltzahn G*, Douglass J, Park J-H, Sailor MJ, Ruoslahti E, Bhatia SN. Nanoparticle amplification via photothermal unveiling of cryptic collagen binding sites. *Journal of Materials Chemistry B*, 2013; 1, 5235-5240.
7. Danino T, **Lo J**, Prindle A, Hasty J, Bhatia SN. *In vivo* gene expression dynamics of tumor-targeted bacteria. *ACS Synthetic Biology.* 2012 Oct 19; 1(10): 465-470.
8. Ren Y, Hauert S, **Lo JH**, Bhatia SN. Identification and characterization of receptor-specific peptides for siRNA delivery. *ACS Nano*. 2012 Oct 23; 6(10):8620-31.
9. Ren Y, Cheung HW, von Maltzahn G, Agrawal A, Cowley GS, Weir BA, Boehm JS, Wong TC, Subramanian A, Gopal S, Tamayo P, Mesirov J, Drapkin R, Root DE, **Lo JH**, Fogal V, Ruohslahti E, Hahn WC, Bhatia SN. Targeted tumor-penetrating siRNA nanocomplexes for credentialing the ovarian cancer oncogene ID4. *Science Translational Medicine*. 2012 Aug 15; 4(147):147ra112.
10. Bassett EK, Hoganson DM, **Lo JH**, Penson EJ, Vacanti JP. Influence of Vascular Network Design on Gas Transfer in Lung Assist Device Technology. *ASAIO*, 2011 Nov-Dec; 57(6):533-8.
11. Helleday T, **Lo J**, van Gent DC, Engelward BP. DNA double-strand break repair: From mechanistic understanding to cancer treatment. *DNA Repair*. 2007 Jul 1;6(7):923-35..

Note: asterisk (*) indicates equal contribution to the manuscript.

Book Chapters

Justin Lo, "Respiratory Pathophysiology," in *First Aid: Organ Systems, 2nd ed*., Senior Authors Tao Le and Kendall Krause. McGraw-Hill Medical, 2011 Sep 16.

Selected Presentations

1. **Lo, JH**, Kwon, EJ, Muzumdar, MD, Ren Y, Jacks T. "Tumor-penetrating nanocomplexes for siRNA delivery to pancreatic cancer." Oral Presentation. *Biomedical Engineering Society Annual Meeting*. San Antonio, TX, 2014 Oct 25.
2. **Lo, JH**. "Targeting nucleic acids for pancreatic cancer: disease modeling and therapy." Oral Presentation. *Koch Institute Annual Retreat.* North Falmouth, MA, 2014 Nov 3.

Patent

Lin, KY, Kwong, GA, **Lo, JH**, and Bhatia, SN. U.S. Patent Application No. 14/298,317, "Stimulus Responsive Nanocomplexes and Methods of Use Thereof," filed June 6, 2014.

Teaching, Mentoring, and Advising

Teaching Assistant for HST.500: Frontiers in Biomedical Science, Spring 2014.

Research Mentor for Undergraduates (MIT Undergraduate Research Opportunities Program):
Felicia Hsu, Spring 2013-Fall 2014.
Angela Zhang, Summer 2014-Spring 2015.

Mentor for MIT Medical Student Mentorship program, advising pre-medical students

Teaching Assistant for DNA module of 20.309J: Biological Instrumentation and Measurement, Fall 2007.
Tutor for 5.111: Principles of Chemical Science, Fall 2005.
Resident Advisor for Vanderbilt Hall at Harvard Medical School, 2009-2010.

Awards and Honors

BMES Graduate Student Award for Outstanding Achievement in a Research and Design Project, October 2014
Ludwig Fellowship for Metastasis Research, 2011-2012
Tau Beta Pi Engineering Society, inducted Spring 2006.
Sigma Xi Scientific Research Society, inducted Spring 2008.
Phi Beta Kappa Society, inducted Spring 2008.
Philip Loew Award (2007) for creative accomplishment in music composition.

Skills

2D & 3D Art and Animation: Adobe Flash, Illustrator, Photoshop, 3D Studio Max, Swift 3D.
Programming: MATLAB, Python, Actionscript 2.0 & 3.0 (Flash), HTML, PHP.

Personal Activities

Longwood Symphony Orchestra, 2008-present. *Associate Concertmaster and Membership Committee Member*.
First violinist; concertmaster Summer 2009 and Fall 2010. The orchestra gives quarterly performances to benefit medical causes and also gives chamber music performances in hospital settings for patients.

Chamber Music Society at Harvard Medical School, 2008-present. *President* (2012-2013), *Co-President* (2013-2014), *Community Outreach Chair* (2014-2015).
Member of piano quintet and string quartet. Performing at regular concerts as well as organizing and performing at fundraising and community outreach events.

Dudley House Orchestra, 2011-2014. *Principal Second Violin*.

Biomedical Engineering Society at MIT, 2004-2008
President (2007-2008), Vice President & Treasurer (2006-2007), Secretary (2005-2006)

American Red Cross, 2006-2008
Disaster Action Team Member (2006-2007) and Blood Drive Volunteer Coordinator (2007-2008)